Inês Sofia Duarte Flores

Licenciatura em Bioquímica

Iron storage and regulation at a molecular level

Dissertação para obtenção do Grau de Mestre em Bioquímica

Orientador: Prof. Doutor Pedro António de Brito Tavares, Professor Auxiliar, FCT-UNL
Co-orientador: Prof. Doutora Maria Alice Santos Pereira, Professor Auxiliar, FCT-UNL

Júri:

Presidente: Prof. Doutor Ricardo Ramos Franco Tavares
Arguente(s): Prof. Doutora Maria Cristina de Oliveira Costa
Vogal(ais): Prof. Doutor Pedro António de Brito Tavares

FACULDADE DE CIÊNCIAS E TECNOLOGIA
UNIVERSIDADE NOVA DE LISBOA

Inês Sofia Duarte Flores

Licenciatura em Bioquímica

Iron storage and regulation at a molecular level

Dissertação para obtenção do Grau de Mestre em Bioquímica

Orientador: Prof. Doutor Pedro António de Brito Tavares,
Professor Auxiliar, FCT-UNL

Co-orientador: Prof. Doutor Maria Alice Santos Pereira,
Professor Auxiliar, FCT-UNL

Setembro 2015

Iron storage and regulation at a molecular level

Agradecimentos

São vários os agradecimentos e não existem palavras suficientes que consigam mostrar o papel importante de todas as pessoas, que foram e são importantes na minha vida pessoal e consequentemente profissional.

Agradeço a todos os que contribuiram para a minha formação e para o desenvolvimento das minhas capacidades profissionais, desde os professores até colegas. Um obrigada especial ao Doutor Pedro Tavares e à Doutora Alice Pereira, que para além de terem sido meus professores foram também meus orientadores, antes e durante esta dissertação. Obrigada por realmente me orientarem neste precurso profissional, pela oportunidade, por acreditaram nas minhas capacidades e por todo o tempo e esforços gastos.

Porque sou alguém de fé agradeço a Deus por realmente tudo, porque tu me susténs. Agradeço à minha familia, especialmente aos meus Pais, ao meu irmão e aos meus avós, que tantos sacrifícios fizeram para que eu pudesse seguir o meu sonho.

Agradeço ao meu noivo Ismael Marques que tanto suportou e sacrificou sem nunca se queixar. Por estares sempre comigo para o quer que seja, nos bons e maus momentos.

Também aos meus colegas, que acima de tudo são meus amigos (Inês Almeida, João Silva, Ana Diniz, Mariana Oliveira e Aline Viensiscki). Partilhamos não só uma profissão mas também uma grande amizade.

Agradeço aos meus amigos que em todas as alturas, mesmo quando eu não posso dar tanta atenção quanto merecem, sempre se preocupam comigo. Obrigada Nádia e Isaac Marques, Raquel e Gonçalo Paiva, Sara e Tiago Falcoeiras, Susana Calado, Miguel Rodrigues, Silvia Biscaia, Sofia Alberto, João e Andy Vieira, Cláudia Vieira, Jónatas e Sónia Luzia e Lucía Rodriguez.

Sem nunca esquecer, também um agradecimento especial à equipa do Laboratório de Biofísica Molecular, que me ajudaram e partilharam o seu conhecimento (Doutora Cristina Timóteo, Doutor Filipe Folgosa, Doutora Cristina Cordas, Daniela Penas, Alexandra Loupas e Nídia Almeida).

Mais uma vez repito, estas palavras não são suficientes para traduzir a dimensão do meu agradecimento.

Obrigada!

Abstract

Iron is an essential element for the proper functioning of the metabolic network in a living system. However, it is also toxic in physiological conditions. Apart from precipitation it can damage and compromise cellular macromolecules by Fenton reactions. Thus, ferritins, hollow spherical proteins, comes to solve this problem by storing iron in its inner cavity. Dps (DNA-binding protein in starved cells), focused in this study, has a detoxifying function, protecting DNA from ROS.

The reaction catalyzed by ferritins can be divided in the following stages: iron intake, oxidation, storage and release. The latter is the least explored and known function of this protein.

The *M. hydrocarbonoclasticus* WrbA flavoprotein, present in the same genome, was used as a *P. nauticas* Dps redox partner, to reduced and release iron from the iron core. Mössbauer spectroscopy was used to investigate the kinetics properties of WrbA(FMN):NADH:Dps in anaerobic conditions. To determine kinetic parameters it was needed to acquire spectra for different reaction times. The iron release for wild-type, Q14E and Δ15 Dps variants follow a first-order kinetic, with rate constants very similar.

Was also explored a more inexpensive and faster kinetic assay based on the *o*-phenanthroline method, monitored by Visible spectroscopy. The result showed that the three Dps variants have no significant difference regarding the kinetic profile obtained, but rate constants were significantly lower than those obtained by Mössbauer spectroscopy probed kinetic measurements. Phenanthroline might cause an inhibitor effect and in order to understand that effect, the kinetic assays were repeated in the absence of phenanthroline.

Using bioinformatic tools (docking, modeling and others), was possible to conclude that exist conserved amino acid (G43, L74, P78 e W149) in Dps that appear to participate and are in the electron transfer pathway.

Keywords: Dps, iron release, Mössbauer, UV-Visible spectroscopy, o-phenanthroline assay, docking, modeling, bioinformatic, WrbA

Resumo

O ferro é um elemento essencial para o bom funcionamento da rede metabólica de um ser vivo. No entanto, também é tóxico em condições fisiológicas. Para além de precipitar, pode também danificar e comprometer as macromoléculas constituintes das células através de reações de Fenton. Assim, as ferritinas, proteínas esféricas ocas, vêm colmatar este problema ao armazenar ferro nas suas cavidades. Este presente estudo, centra-se no desempenho e funcionamento da Dps (DNA-binding protein), que, ao contrário das maxi-ferritinas têm a sua função direccionada para a protecção do DNA contra as ROS.

O funcionamento das ferritinas pode ser dividido em várias etapas: entrada de ferro, oxidação, nucleação e saída de ferro. Esta última é a menos explorada e conhecida.

A flavoproteina WrbA de *M. hydrocarbonoclasticus* foi usada como parceiro redox da Dps de *P. nauticas* para o estudo do passo de libertação de ferro. Como tal, foram realizados estudos cinéticos por espectroscopia de Mössbauer numa mistura reacional de WrbA(FMN):NADH:Dps em condições anaeróbias. Para determinar parâmetros cinéticos, foi necessária a aquisição de espectros em diferentes tempos reacionais. A libertação de ferro da Dps wild-type e mutantes (Q14E e Δ15) segue uma cinética de primeira ordem com constantes de velocidade muito semelhantes.

Para além disso foi desenvolvido um ensaio cinético mais barato e rápido baseado no teste de determinação de ferro por formação de complexo o-fenantrolina. Os resultados não mostraram diferenças significativas no perfil cinético entre a Dps wild-type e mutantes. Não obstante, as constantes cinéticas calculadas neste ensaio são significativamente inferiores às obtidas através dos ensaios de espetroscopia de Mössbauer. Verifica-se que a presença de fenantrolina causa um efeito inibitório na cinética.

Com recurso a ferramentas bioinformáticas (docking, modelação e outros), foi possível concluir que existem aminoácidos conservados na Dps que podem participar e que estão no caminho de transferência eletrónica para libertação de ferro.

Keywords: Dps, libertação de ferro, espectroscopia de Mössbauer, espetroscopia UV-Visível, ensaio de quantificação de o-fenantrolina, docking, modelação, bioinformática, WrbA

Table of contents

List of figures

List of tables

Abbreviations

A	Alanine
ATP	Adenosine triphosphate
Bfr	Bacterioferritin
bp	Base pairs
D	Aspartate
DEAE	Diethylaminoethyl cellulose
DFB	3,3'-Difluorobenzaldazine
DNA	Deoxyribonucleic Acid
Dps	DNA-binding protein in starved cells
Dps(wt)	Wild-type Dps
E	Glutamic acid
E.	*Escherichia*
FeSid	Iron-siderophore complex
Flv	Flavoprotein
FMN	Flavin mononucleotide
FOC	Ferroxidase center
Ftn	Bacterial ferritin
G	Glycine
GMQE	Global model quality estimation
GTP	Guanine triphosphate
H	Histidine
HMM	Hidden Markov Model
HPLC	High performance liquid chromatography
I	Isoleucine
IPTG	Isopropyl β-D-1-thiogalactopyranoside
K	Lysine
L	Leucine
L.	*Listeria*
LB	Luria-Bertani
LMW	Low molecular weight
Mers	monomers
mRNA	Messenger RNA
MRI	Magnetic Ressonance Imaging
MWCO	Molecular weight cut-off
N	Asparagine
NADH	Nicotinamide adenine dinucleotide
NADPH	Nicotinamide adenine dinucliotide phosphate
OD	Optical Density
P	Proline
P.	Pseudomonas
PDB	Protein data bank
PFam	Protein families
Phen	o-phenanthroline
Prob	Probability
PSA	Ammonium persulfate
PSI-BLAST	Position- specific iterative basic local alignment search tool

Q	Glutamine
R	Arginine
ROS	Reactive oxygen species
S	Serine
SS	Secondary structure matching
SDS-PAGE	Sodium dodecyl polyacrylamide gem electrophoresis
SMART	Simple modular architecture research tool
T	Threonine
TEMED	Tetramethylethylenediamine
UV	Ultraviolet
V	Valine
Vdw+elec	Van der walls and electrostatic
W	Tryptophan
WrbA	Tryptophan [W] repressor binding protein
Wt	Wild-type
Phen	o-phenanthroline

1. Introduction

1.1 Metal elements in biological systems

Homeostasis, i.e. the balance of energy flow in and out of an open system, is essential for the survival of a living system.[1] Furthermore, the chemical elements that are used in a whole range of cross-linked reactions that constitute the metabolism must be bioavailable.[2]

In particular, metallic elements can participate in a series of metabolic reactions for the following biological functions:[3],[1],[4]

i) Charge carriers: Propagation of nervous impulses; one of the examples of this particular function, is triggered by the diffusion of inorganic ions through the membrane of neurons;[5]
ii) Electron transfer: Some metal elements have multiple oxidation states, which make possible a molecule to be redox-active;[3]
iii) Structural function: Metal ions may provide stability in protein structures, decreasing the effect of chaotropic agents.[6] An example is the zinc finger protein motif, in which one or more coordinated metal are responsible for the protein structure stabilization;[7]
iv) Catalytic function: Many proteins require metallic elements to fulfill his function;[8]

Among the various important metals that participate in biological reactions, like zinc, copper, molybdenum, cobalt, vanadium and others, iron is the most abundant.[3]

1.1.1 Iron chemistry and properties

There are two main reasons that make iron so suitable for biological use. In first place, it is the fourth element most abundant in earth crust (5%)[9] and, thus, theoretically the abundance and availability is no restrain. Also, this metal can adopt different spins and redox states[10] within a range of -300 to +700 mV, depending on the ligands and environment[11],[12] (figure 1). This versatility turns out to be a very important characteristic for a good prosthetic group.

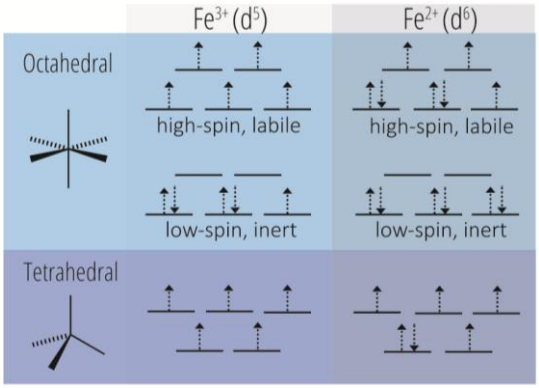

Figure 1 - Spin, geometric and redox state of iron coordination complexes. Adapted from reference [13].

Table 1 - Predominant redox states in physiological conditions. Adapted from reference [14].

	Coordination number, Geometry	Preferred ligands	Functions and examples
Fe^{2+} (d^6) / Fe^{3+} (d^5)	4, Tetrahedral	S-Tiolate	Electron transfer, Nitrogen fixation in nitrogenases
Fe^{2+} (d^6) / Fe^{3+} (d^5)	8, Octahedral	O-Carboxylate, alkolide, oxide, phenolate	Electron transfer in oxidases

These two properties permits iron, in a local ambient like a protein pocket, to adopt the redox potential, geometry or spin state necessary to proper biological function.[12]

As shown in table 1, both iron states have preferred ligands. Accordingly to the hard-soft acid and base theory, Fe^{3+} (hard metal ion) have a tendency to react with hard ligands and Fe^{2+} (medium metal ion) can bind to soft and hard ligands.[15] In a protein, it is natural that the metal ion reacts with the amino acids side-chains that contain these preferred chemical groups. In figure 2, the common amino acids that may be more reactive to Fe^{3+} and Fe^{2+} are represented.[16]

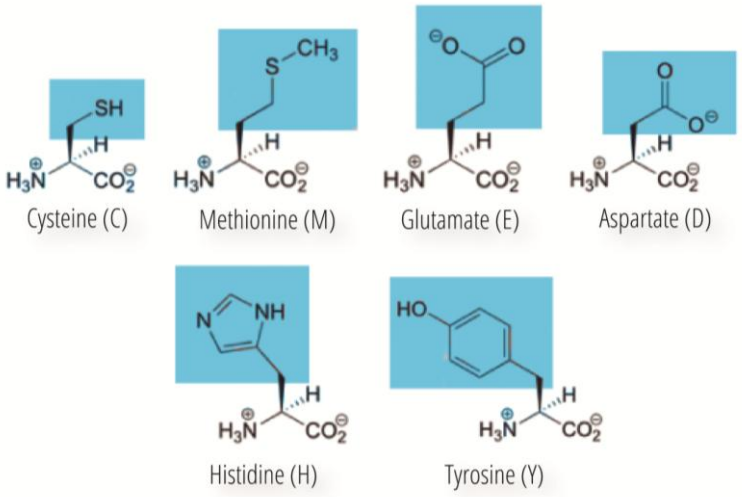

Figure 2 – Amino acids with high affinity side-chains for iron ions**.**

Despite all these favorable properties, in physiological medium, iron can be very toxic and limited.[10] At pH=7, two main redox states - Fe^{2+} and Fe^{3+}- with a solubility of ~10^{-1} M and 10^{-18} M, respectively, can exist.[12] The ferric insoluble form (Fe^{3+}), in presence of water, frequently associates into μ-oxo ferric species.[3] The more soluble ferrous form (Fe^{2+}) is still able to react. However, Fe^{2+} ion can react with molecular oxygen and hydrogen peroxide (product of the incomplete reduction of O_2) through Fenton reactions (eq. 1), forming Fe^{3+} and oxygen reactive species (ROS). This phenomenon, known by oxidative stress, is devastating, since ROS damage biomacromolecules, compromising the cell integrity.[12],[17]

$$Fe^{2+} + H_2O_2 \rightarrow Fe^{3+} + OH^{\bullet} \qquad \text{(eq. 1)}$$

$$O_2^{\bullet -} + Fe^{3+} \rightarrow O_2 + Fe^{2+} \qquad \text{(eq. 2)}$$

$$H_2O_2 + O_2^{\bullet -} \rightarrow OH^{\bullet} + O_2 \qquad \text{(eq. 3)}$$

1.2 Iron metabolism regulation in bacteria

1.2.1 Iron entry into the cell

However, before used inside the cell, specifically in gram– bacteria, iron has to pass through two independent steps (figure 3):[18], [19]

i) Transport across the external membrane: The general strategy for Fe^{3+} ions uptake is the synthesis of siderophores that are released to the medium in order to chelate the metal. The complex FeSid are uptaked by a transmembranar transporter.

ii) Iron release into the cytoplasm: The prevailing system for the Fe^{3+} siderophores, heme and iron transport to the cytoplasm, are the ATP-dependent transmembranar complexes. Fe^{2+} ions are transported by several transmembranar transporters (figure 3). The most common is the Feo system, an operon of three genes feoA, feoB, feoC and a Fe^{2+}-Fur regulated promotor upstream of FeoA. FeoB is a protein with a GTPase domain and is essential for Fe^{2+} transport. Fe^{3+} can be released from siderophores and reduced to the Fe^{2+} form. Due to the stability of FeSid complexes, the iron release reaction is an enzymatic process.

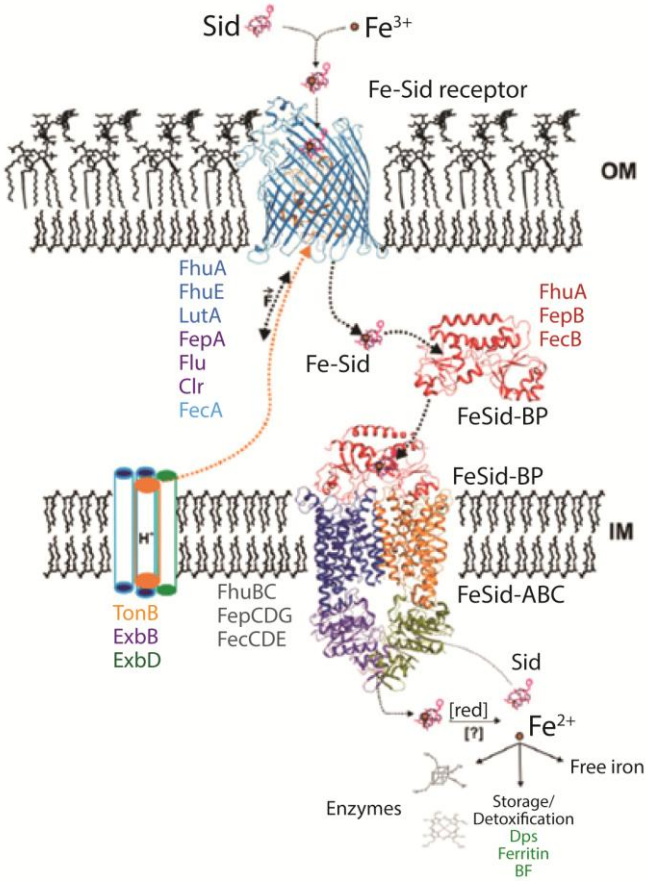

Figure 3- Iron uptake by a gram– bacterial cell. Figure adapted from reference [19].

This general mechanism permits an uptake of sufficient iron, 10^5 –10^6 iron atoms per bacterial cell, for incorporation into cofactors, and biological processes.[19] In the cytoplasm, to

overcome the toxicity and low availability of unneeded iron, living systems have to evolve mechanisms to sequester iron and liberate only when required.[10] The proteins from the ferritin family have two main functions. First, serving as iron sink, storing iron in a nonreactive site until it is necessary, and thus time avoiding loss of available iron ions. The second function, dependent of the first, is saving macromolecules from damage by oxidative stress, avoiding the occurrence of Fenton reaction.[20],[21]

1.2.2 The ferritin family

The ferritin-related family (IPR012347) belongs to the ferritin-like superfamily. This family of proteins nanocages produces biocompatible ferrihydrated nanoparticles and based on their subunit composition are classified as maxi- or mini- ferritins.[22] Superparamagnetic iron oxide nanoparticles have been a great contribution to health biotechnology, for example as contrast agents in MRI or in chemotherapy.[23] As such, some research groups have been studying and using ferritins for the production of biocompatible nanoparticles for these applications.

Maxi-ferritins have 24 subunits (of about 20 kDa) and an internal diameter of 6-8 Å, capable of storing more than 4000 Fe atoms. Mini-ferritins, however, are smaller (12 subunits and an internal cavity of 4-5 Å) and thus have less storage capacity (< 500 Fe atoms).[22],[24]

In prokaryotes, there are two maxi-ferritins: Bacterial ferritin (Ftn) and the heme-containing bacterioferritin (Bfr). The mini- ferritin, also called Dps, will be described in more detail later. *Escherichia (E.) coli* is a typical organism where these three ferritins co-exist. Most of prokaryotes have one or two of these three ferritins with different specialized functions. Actually, each type of ferritin can have different specific function in different organisms. For example, while in *E. coli* Ftn is the main source of iron, in *Neirserria gonorrhoeae* Bfr serves as main iron storage protein.[25]

In eukaryotes, maxi-ferritin are quite different from those found in prokaryotes.[22] Different types of subunits combine and co-assemble to form the nanocavity. In animals, ferritins have a catalytic active heavy-type subunit and a ferroxidase inactive light-type.[26] Until today, eukaryotic mini-ferritin was not reported.

1.3 DNA binding protein from starved cells (Dps)

First described by Almiron et. Al, the *E. coli* Dps, highly expressed in starving conditions, *in vivo* and *in vitro,* was shown to bind DNA protecting it from chemical damage.[24],[27] Later in 1997, Martinez and Kolter demonstrated an increase of cell survival (and a decrease in DNA breaks) when Dps is expressed *in vivo*.[28]

The crystallographic structure of Dps from *E.coli* was reported in 1998.[29] Aside some variations, Dps structures have a ferritin-like structure, proving to be ferritin related (figure 4). Each Dps monomer have essentially the same 4-helix bundle fold and a hollow sphere

multimeric organization. Some authors proposed that mini-ferritins resulted from the evolution of maxi-ferritins in order to become adapted to more versatile functions.[24],[30]

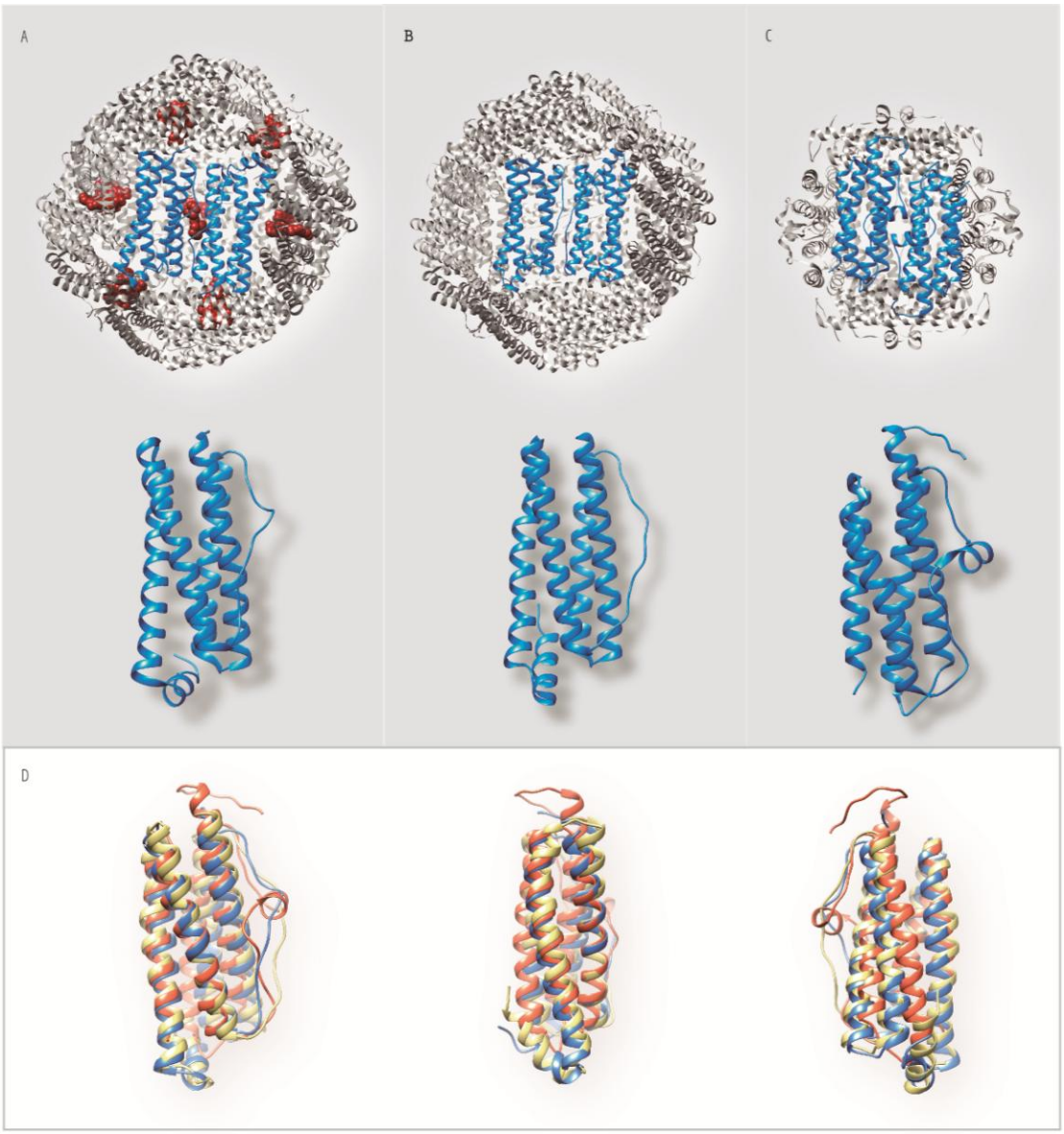

Figure 4 – Tridimensional structures of *E. coli* ferritins proteins. Top panel: Protein nanocavities with dimers in blue and heme group in red and respective monomers. Crystal structures of **A)** Bfr (PDB: 2Y3Q); **B)** Ftn (PDB: 1EUM); **C)** Dps (PDB: 1L8H); **D)** Structural superposition of Bfr (blue), Ftn (yellow) and Dps (orange) monomers.

As figure 4 shows, 12 Dps monomers are assembled in a 23 (tetrahedral) symmetry. Each monomer has different interfaces with the neighbor subunits resulting in a spherical structure with a hollow cavity. This architect arrangement allows the communication from the outside to the inside (nanocavity) of the protein through channels with a three and two-fold symmetry axes.[29],[30] Contrarily to maxi-ferritins, Dps monomers do not have a small helix (helix E in maxi-ferritins) in the N-terminal region and neither a C-tail (figure 4D). These tails are responsible for the formation of the 4-fold channels present in Bfr and Ftn, resulting in a smaller quaternary structure. Also, the 4-fold channels in maxi-ferritins are replaced by type II 3-fold channels.[29] The 3 types of pores in Dps are represented in figure 5. The ferritin-like 3-fold type

I channel is more acidic while type II is more hydrophobic.[31],[32] Besides, the small helixes in the middle of the long loops, also not present in maxi-ferritins, are responsible for establishing interaction inter-monomers in 2-fold channels.

Figure 5- From left to right, 2-fold, 3-fold (type II) and 3-fold (type I) Dps channels. Protein structure data from reference [33].

1.3.1 Dps function

Recently, Ping et al described a new and rare function in Dps, the synthesis and degradation of amino-acyl glutamines, although attributing as principal function the protection of macromolecules, especially DNA, in oxidative stress, starving, heat-shock, pH alterations or osmotic pressure conditions.[32],[34],[35] In fact, this protein is involved in the survival of pathogenic bacteria like *Bacteroid fragilis* in a host environment to overcome the oxygen toxicity of the host.[36]

How can Dps fulfill these functions?

i) Ferroxidase activity: Such as all other ferritins, Dps can oxidize free ferrous iron in solution and store it in its cavity so that Fenton reaction cannot take place;[35], [37], [38]

ii) Peroxidase activity: Hydrogen peroxide is a more efficient substrate in iron oxidation than oxygen. Dps can detoxify both reagents of Fenton reaction without ROS formation (eq. 1);[39],[40]

iii) Physical and chemical shielding of DNA: This mechanism can occur in synergy of Dps self-aggregation and DNA condensation.[41] Dps self-aggregation result in a crystal lattice of three adjacent dodecamers forming a hole lined by the N-termini.[42],[43] This will be the driving force to DNA condensation. The flexible N-terminal, observed in *E. coli* Dps, is crucial for the Dps-DNA co-crystallization, through lysine binding with no apparent specificity.[27],[28],[43],[44] Arnold proposed the hypothesis that Dps acts by distance with DNA charge transport.[45] This study revealed that ferrous iron-loaded Dps, but not apo-Dps or ferric iron-loaded Dps, can protect DNA from oxidative damage. However, some Dps proteins are not able to bind DNA.[24],[30]

1.3.2 Regulation of Dps expression

Dps is predominantly expressed in the stationary phase of *E. coli* growth, corresponding up to 2% of the cell proteome.[19] At this growth phase, the microorganism is in intense competition of nutrients, i.e. in starving conditions, once more vulnerable to adverse events like oxidative stress, needing machinery to protect all types of macromolecules.[27] *E. coli* Dps vary from 600 copies on exponential phase to 180 000 in stationary stage.[46]

Iron limitation, chelators and molecules of FeSid up regulate the Dps expression at any growth phase.[47],[48] However, at transcriptional level, the control at stationary phase is up regulated by σ^s transcription initiation factor that recognized the promotor. At the exponential phase, H_2O_2 regulates the OxyR that, in turn, activates the σ^{70}-RNA polymerase initiating the transcription of Dps mRNA.[46],[49]

In *E. coli* down-regulation during exponential phase can occur by proteolysis or by repression through H-NH to the promotor, preventing σ^{70} recognition.[50],[51] To block the σ^s promotor complex formation in the stationary phase, Fis binds to the promoter in the exponential phase.[51]

1.3.3 Dynamics of iron in Dps

The overall process can be divided in the following steps: Iron uptake, iron oxidation, nucleation and iron exit.

1.3.3.1 Iron uptake

It has been proposed that iron translocation in ferritins inside the hollow protein sphere occurs through the 3-fold channels. In most Dps, the preferential pathway is the 3-fold type I channels.[19]

The X-ray structure of iron loaded *Listeria* (*L*.) *inoccua* Dps provided important outcomes about the iron entry through these pores.[52],[31] Iron ions are guided through the funnel shaped channel by the electrostatic gradient. This gradient is formed by D121, D126 and D130 residues located along the surface (figure 6A). Since these channels are tapered, the negative charges become more concentrated in the inner side of the channel. Bellapadrona *et al* studied the effect of this three aspartate residues in the iron uptake process.[52] D130, situated in the most interior and narrow region of the channel, has 80 % of conservation in Dps proteins. The mutation on this residue decreases the ferroxidation reaction rate. Mutation of residues D121 or D126 does not affect the uptake process. However, the triple mutant has a drastic effect, which suggests a cooperative effect of these three negative carboxylate residues.

Later, two hexa-hydrated iron complexes aligned along the 3-fold type I channels were observed by Pesek.[48] These complexes resemble the one formed in solution (figure 6B). The water molecule shell interacts with E132, D131, Q138, D139 and E143 side-chain amino acids

exposed in the channel surface. It has been speculated that E132 and D139 have the role of guiding these complexes to the cavity; the aspartate residue also constrains the diffusion of iron, by stripping off the water molecules, so that iron can enter “naked” for subsequent oxidation.

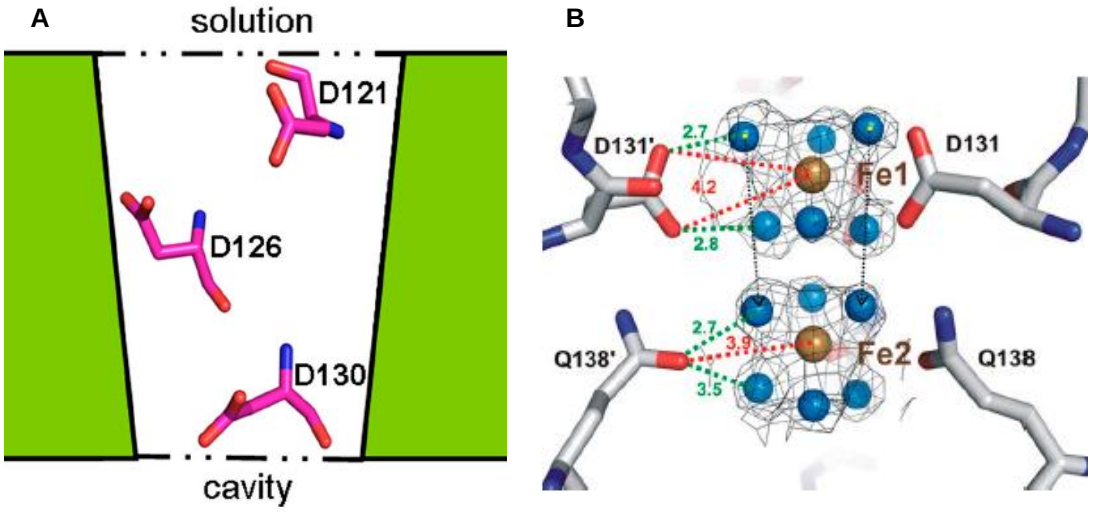

Figure 6 – 3-fold channels as a pathway of iron uptake. **A)** Aspartate residues aligned through the *L. innocua* Dps 3-fold type I channel; **B)** Experimental observation of iron-water complexes. Figures from references [52] and [48], respectively.

A different pathway for the entry of iron was observed in DpsA from *H. salinarum*, through the hydrophobic 3-fold channels.[48] Three iron translocation sites were seen the crystallographic structure. The T1 site, most outside, is at a distance of 20 Å of the iron oxidation sites and binds Fe^{2+} ions via E171 and D172 residues. A cluster of 6 amino acids (E13, E15, D18, E167, E71 and D173) acts as electrostatic guide. At the second site, T2, iron is coordinated by E56, E86 and H168 side-chains. Site T3 (H164 and Q86), situated at 7 Å from the iron oxidation site, weakly interacts with the metal.

Only in *H. salinarum* was reported his iron pathway (figure7). Maybe, a hydrophobic route has become preferable upon the restrict hydration resulted from the high salt concentrations faced by this enzyme. Also, the distance between the iron oxidation centers is 8 Å for T3 type II channel and 1nm for the second hydrated iron complex in type I channels.

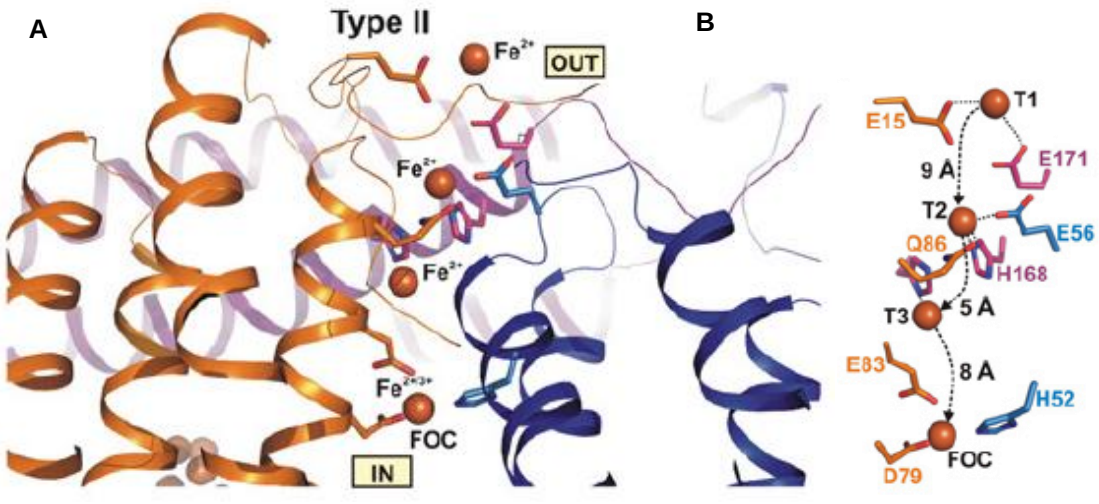

Figure 7 - Iron entry to the ferroxidase center of DpsA from *H. salinarum* via a 3-fold type II channel. **A)** Three subunits are colored in orange, blue and magenta. Iron ions in the channel are in the ferrous state, and can be Fe^{2+} or Fe^{3+} in the FOC. **B)** A schematic representation of the iron pathway. Both figures from reference [19].

1.3.3.2 Ferroxidase activity

After iron translocation through the pores, ferrous ions are oxidized at the ferroxidase centers (FOCs).[19] In Dps these centers are localized in the two-fold interface of monomers with the exception of the proteins from. *Lactococcus (L.) lactis* and *L. sulfobos* are exceptions in which the catalytic centers are located in the middle of the four-helix bundle monomers.[44],[53] Each dimer interface has 2 catalytic centers. A typical FOC is bimetallic.

The oxidation of Fe^{2+} to Fe^{3+} can occur with H_2O_2 or O_2 as oxidant. Although O_2 can be used, the reaction is slower. The two reactions are represented in the following equations:[30]

$$2Fe^{2+} + P_z \rightarrow [Fe_2 - P]^{z+2} + 2H^+$$

$$[Fe_2 - P]^{z+2} + H_2O_2 + H_2O \rightarrow [Fe_2O_2(OH) - P]^z + 3H^+$$

$$2Fe^{2+} + H_2O_2 + 2H_2O \rightarrow 2FeOOH + 4H^+$$

$$[Fe_2 - P]^{z+2} + {}^1/_2\,O_2 + H_2O \rightarrow [Fe_2(OH)_2 - P]^z + 2H^+$$

$$4Fe^{2+} + O_2 + 8H_2O \rightarrow 8FeOOH + 8H^+$$

The two ferrous ions bind to the ferroxidase center and are oxidized producing a diferric μ-oxo bridged (FeOOH) species. Iron atoms are coordinated by histidine and carboxylate residues. However one, usually designated by site A, has a higher affinity for iron, once that has a histidine not present in site B.[19],[30] Site B were not visible in all Dps. In *L. innocua* Dps, site A was firstly discovered, the iron atom was coordinated to H31, H43, D47, G62 and D58.[31] The site B was confirmed experimentally in DpsA.[54]

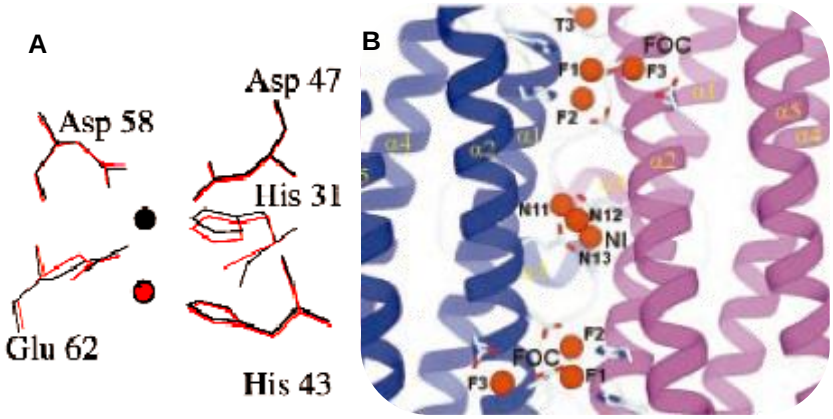

Figure 8- Bimetallic ferroxidase centers. **A)** Site A from *L. Innocua*. The iron atoms are coordinated to D58 and G62 from one subunit and D47, H31, H43 from another. The di-iron binding site A was modeled and is shown at red. **B)** View from the inside of the Dps of site A and B. Figures from references [31] and [19], respectively.

1.3.3.3 Nucleation and core formation

Mineralization is explained by the crystal growth mechanism, in which nucleation is the first step of mineralization that consists in the formation of initial small iron clusters that become auto-catalytic increasing in size.[55]

Two different types of nuclei were observed in *H. salinarum* DpsA, one located at the 2-fold axis and a second at the 3-fold axis at approximately 12-13 Å of FOCs.[54]

Negatively charged residues in the FOC vicinity might facilitate iron oxide nucleation. *L. innocua* Dps residues E44 and D47 at two-fold symmetry axis have been proposed to be involved in nucleation.[31]

The mineralization process is also dependent of the electrostatic gradient of pores. On the study of Bellapadrona, previously described, the mutation of the aspartate residue also resulted in the alteration of size distribution of iron core.[52]

The iron cores of ferritins and Dps proteins have superparamagnetic properties. A native core, i.e. the core of purified protein, contains only tens of atoms with different phosphate ratios. The smallest native core analyzed so far contains only 16 iron atoms with a phosphate/Fe ratio of 0.7.[56] The *in vitro* cores are formed by addition of iron to the protein and have more well-ordered crystalline state and higher phosphate content. This disorder makes iron more readily usable.[53]

1.3.3.4 Iron exit

This phase of Dps and ferritin function is the less known and explored. There are still many questions. Most described studies are from mammalian and prokaryotic ferritins.[57]–[59] Iron release has been neglected in scientific research; however has an important role and

application for medical biotechnology, for example in chelation therapy for iron overdosage or even in nanodrugs and nanomaterial design.

Great number of experimental procedures used for iron release used a reducing agent, such as NADH/FMN and chelators. In 1980, Crichton shows that different chelators lead to different results, but all are efficient in iron liberation studies in human ferritins *in vitro*.[60] This was also verified in Dps, at uptake profiles for DFB and sulfoxine.[61] In fact, some evidences suggest that chelators can entry to the cavity and liberate the iron there stored.[62], [63]

The presence of biological ferritin unfolders inside the cell that would modulate the iron exit channels has been postulated.[57] Unfolding of hydrophobic zones at 3-fold channels in 24-mers mammalian ferritins results in small differences in the iron exit profile. Pores structure modifications can be induced by narrow variation of urea concentration or by mutation of conserved amino acids at the surrounding area. These 3-fold pores resemble those found in Dps, specially the type I. Despite not proved, this type of 3-fold pores can be an iron exit pathway. Due to their hydrophobic character and shorter radius, type II channel may have a major role in iron entry.[64]

In Dps the iron release curves depend on the shape and size of iron cores.[52] The iron release process can be divided into two different phases. The first is the reducing of ferric ions at the core surface. In the second phase iron is removed from the bulk mineral.

NADH and acid ascorbic are the most studied ferritin redox partners. A physiological redox partner still not clearly identified.

2 . Aims

As mentioned before, the iron release process is the less explored reaction of ferritins' function. This present study is focused about the identification of a putative physiological redox partners of Dps and to unveil this function, specifically about the role of WrbA. This protein is coded by the *wrba* gene expressed in the stationary phase *E. coli* cells under the regulation of σ^S factor (described in section 1.3.2).[65] It is a NADH:Quinone reductase that binds a FMN cofactor to 3 subunits of a tetramer (each tetramer has 4 pockets for FMN and NADH ligation) (figure 9).[66], [67] As mentioned before the FMN/NADH system is used for iron release experimental studies from ferritins and because WrbA flavoprotein was proposed to be involved in bacterial stress defense mechanisms we postulated that this protein could participate in iron release from Dps.

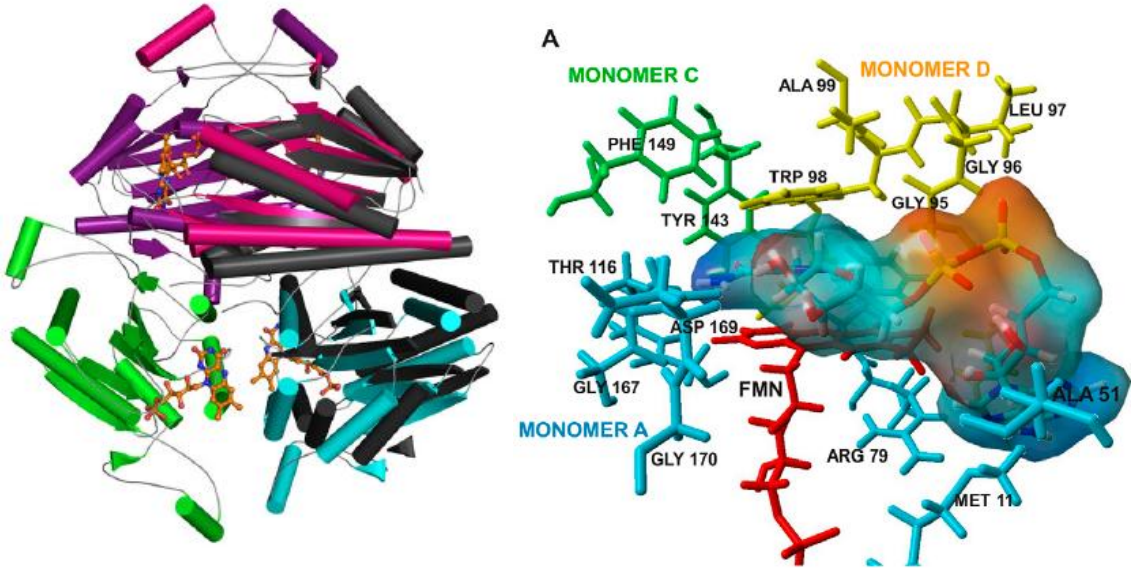

Figure 9 – Structural representation of flavoprotein WrbA. **A)** Tridimensional structure of *E. coli* WrbA with the FMN groups represented as stick and balls. The apo-WrbA monomers are represented in blue, green, purple and pink; holo-WrbA in green, purple, and grey. **B)** Representation of FMN/NADH binding pocket. FMN is represented in red and WrbA monomers are in green, blue and yellow. NADH is depicted as a skeletal model with a translucent electrostatic potential surface shaded from red (negative charge) to blue (positive charge). Figures from reference [66], [67], respectively.

Previous Mössbauer kinetic studies, Almeida revealed that the WrbA/NADH/FMN system has the ability to remove iron from the *Pseudomonas (P.) nautica* Dps core.[68] One aim of this thesis is to develop a faster and inexpensive kinetic assay to test iron release from ferritins. This novel kinetic assay is based on the chelators' assay commonly used, utilizing the chelator *o*-phenanthroline.

In parallel, the putative WrbA-Dps complex formation was rationalized by applying bioinformatic tools. For this, a literature search was done and a list of readily available software

packages was compiled. Choice of which software to use was made based on calculation capabilities and assessment of end user usability. It was also an aim of this study to compare the used software packages regarding usability, reproducibility and performance when analyzing our multimeric, cofactor containing protein-protein complexes.

Once optimized with wild-type Dps, this characterization will be repeated with a Dps mutant (Dps Q14E and DpsΔ15) in order to infer about the role of specific protein regions in Dps important in iron exit or electron entry pathways.

In summary, we aim to answer the following questions:

- Is it possible to identify relevant amino acid residues with an active role in iron release?
- Is it possible to obtain a plausible hypothesis for the interactions of these complex proteins?
- What are the best/more relevant point mutations that can be done to obtain further information about the iron release mechanism?
- What are the possibilities to establish a reliable and less expensive kinetic assay, replacing the current Mössbauer methodology?

3 . Experimental Procedure

3.1 Protein overexpression production

3.1.1 Plasmid preparation

E. coli NZY5γ and BL21(DE3) Nzytech competent cells were transformed with pET21c-Dps(wt) plasmid, harboring the gene coding for *P. nautica* Dps (sequence at annex 8.1), for subsequent plasmid purification and protein production, respectively, following the Nzytech protocol (annex 8.2).[69],[70] The genotypes of these cells are presented in annex 8.2.

Briefly, the appropriate amount of pET21c-Dps(wt) was added to competent cells and kept on ice for 30 min. After a heat shock of 40 seconds of at 42 ^{o}C in a heating bath (50-60 Hz Grant Instruments Cambridge Ltda.), cells suspensions were kept on ice for 2 min. Liquid LB medium (Nzytech) was added for cellular growth during 2 h at 42 ^{o}C at 225 rpm (Ovan Incubator OPAQ I10-OE+ACOP Ref. 10000-01056). Transformation controls were treated in parallel.

The transformation suspensions, including controls, were plated on LB/Agar (Nzytech) plates with 100 µg/mL of ampicillin (Nzytech). All plates were incubated overnight at 37 ^{o}C.

A single *E. coli* NZ5γ transformant colony was used to inoculate 5 mL of LB medium (Nzytech) with 100 µg/mL ampicillin and incubated with vigorous shaking at 36 ^{o}C for 22 hours for plasmid isolation and purification.

Plasmid DNA was purified using the low copy number plasmid NZYMiniprep Kit protocol (annex 8.3).[71] The efficiency of the plasmid purification was evaluated by agarose gel electrophoresis, as described in annex 8.4.

Plasmid minipreps were quantified by UV spectroscopy using a molar extinction coefficient at 280 nm of 0.02 µg/mL/cm.

The same protocol was used to produce WrbA flavoprotein[68] from *Marinobacter hydrocarbonoclasticus* coded by MARHY3073 gene and Dps variants (Dps15 and DpsQ14E).

3.1.2 Cellular growth

Cellular growth and protein purification were performed using a protocol established by the Molecular Biophysics group.

First, a pre-inoculum of 5 mL (triplicates) LB medium containing ampicillin (100 µg/mL) were inoculated with single *E. coli* BL21(DE3) transformant. After incubation at 37 ^{o}C with 220 rpm shaking for 8 h, 1 mL pre-inoculum was added to two 100 mL LB-ampicillin (100 µg/mL)

medium, incubated for 9 h in the same conditions and used to inoculate 1 L of LB-ampicillin (100 µg/mL) (10 mL of inoculum).

Cell growth, at 37 ^{o}C, 220 rpm, was monitored measuring the OD at 600 nm. Gene expression was induced with 0.5 mM of IPTG at an $OD_{600\ nm}$ of approximately 0.5. After 3 hours of induction, cells were harvested by centrifugation on a Hermle Z36HK centrifuge at 11 000 *g* at 10 ºC for 10 min. The resulting pellets were suspended in 10 mM Tris-HCl pH=7.6 buffer and stored at −80 ^{o}C.

Proteins expression was evaluated by SDS-PAGE (protocol in annex 8.5) of aliquots collected at time zero and 3 h of induction.

3.1.3 Protein isolation and purification

To facilitate cell lysis, the membrane of the bacterial cells was embrittled with cycles of freeze-thaw.

Disruption of cell membranes was made with cycles of 3 min of sonication with a Ultrasonic homogenizer (LABSONIC M Sartorius Stedim Biotech) at 100% of amplitude on ice followed by 30 sec of cooling on ice. DNase I (Roche) was added to reduce viscosity. The suspension was centrifuged to remove cell debris at 10 000 *g* (Hermle Z36HK LaborTechnik centrifuge) for 15 min at 10 ^{o}C; the supernatant was subsequently ultracentrifuged (Optima LE-80K with a 70Ti rotor, Beckam) at 207 870 g to obtain the soluble protein fraction.

The soluble fraction was dialyzed in 12-14 kDa MWCO membranes (Visking, Medicell International, Ltd) against 10 mM Tris-HCl pH 7.6 buffer, at 4 ^{o}C, overnight. The dialyzed crude extract was centrifuged at 11 000 *g* for 15 min at 4 ^{o}C before purification. Aliquots of each fractionated fraction were collected to evaluate the efficiency of the isolation process by SDS-PAGE.

The dialyzed soluble fraction was filtered with a 25 mm syringe filter (0.45 µm polyethersulfone membrane, VWR International) and loaded into a DEAE-Sepharose Fast Flow column (2.6 x 30 cm, GE Healthcare Life Sciences) coupled to a ÄKTA Prime Plus chromatography system (GE Healthcare Life Sciences), pre-equilibrated with 10 mM Tris-HCl pH 7.6 buffer (buffer A). After washing the column (with buffer A), elution of bound proteins was made with a discontinuous linear gradient of NaCl (0 to 500 mM) with buffer B (10 mM Tris-HCl pH=7.6, 200 mM NaCl), at 5 mL/min. 12 mL fractions were collected and analyzed by SDS-PAGE and tested for catalase.

The less pure fractions were injected into a size exclusion Superdex 200 column (1.6 x 49 cm, GE Healthcare Life Sciences), using a flow rate of 1.5 mL/min and collecting 2 mL fractions. Elution was made with buffer B.

When judged necessary, a third chromatographic step was used to further purify the protein on a Resource Q column (6 mL, GE Healthcare Life Sciences) and following the same procedure used for the first step. The chromatographic separation was performed at a flow rate of 1 mL/min; fractions of 2 mL were collected.

Pure fractions were concentrated in ultrafiltration cells, 30 kDa MWCO Vivaspin (of 6 or 70 mL, Sartorius).

The catalase test was used to verify the presence of any trace of catalase that will interfere with subsequent kinetic studies. For such, 3 drops of 30% hydrogen peroxide was added to small aliquots of protein fraction. If release of O_2 is observed, the fraction is contaminated with catalase.

Pure Dps fractions were dialyzed against 200 mM MOPS pH 7.0 buffer, 200 mM NaCl and kept at −80 ^{o}C.

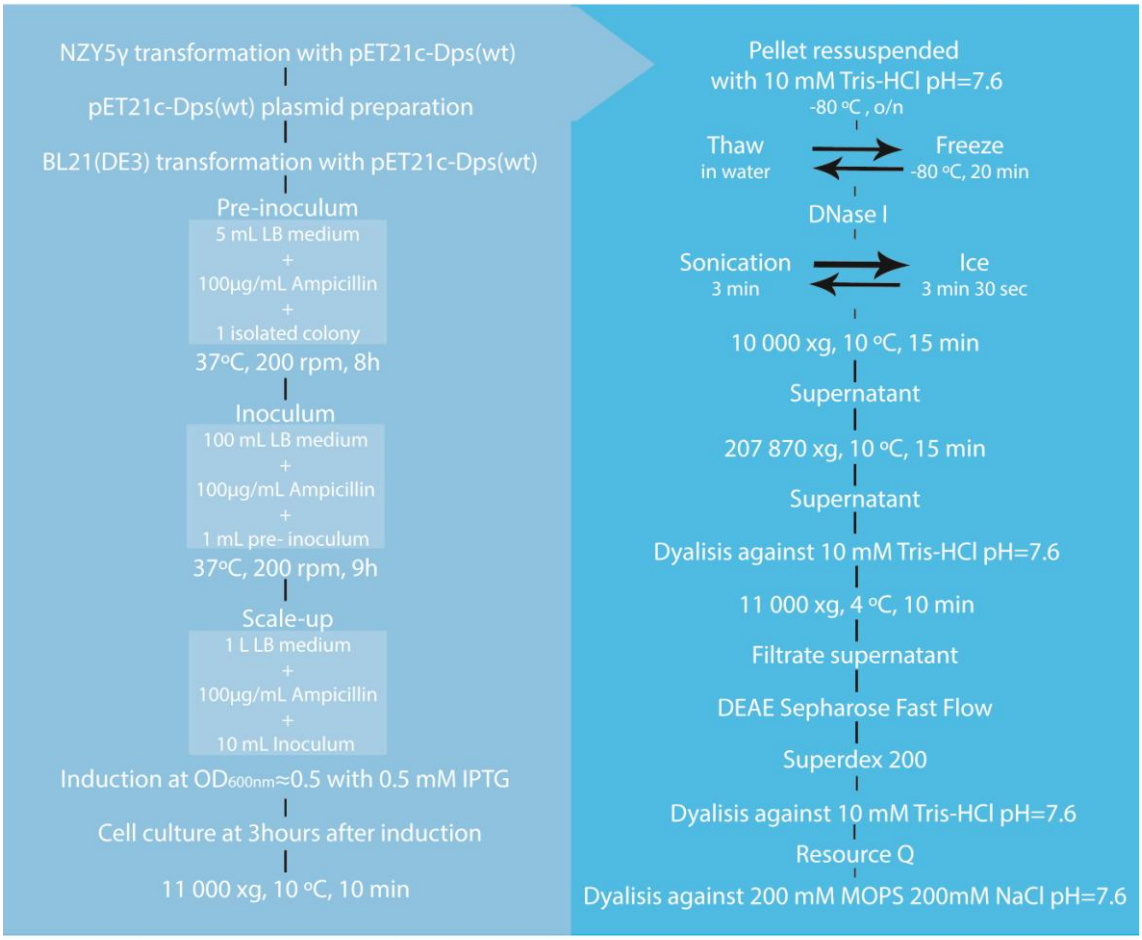

Figure 10 – Schematic representation of the experimental procedure used for protein production.

WrbA flavoprotein and Dps mutants were kindly provided by Almeida N. [68] and Penas D., respectively.

3.2 Kinetic studies

3.2.1 Iron-loaded Dps samples preparation

For the iron release studies, Dps had to be previously loaded with iron. The iron solution was quantified by the *o*-phenanthroline method, based on the formation of a colored Fe^{2+}(*o*-phen)$_3$ complex (called ferroin). This complex has an intense orange color and a molar extinction coefficient at 510 nm of 11.2 $mM^{-1}cm^{-1}$.

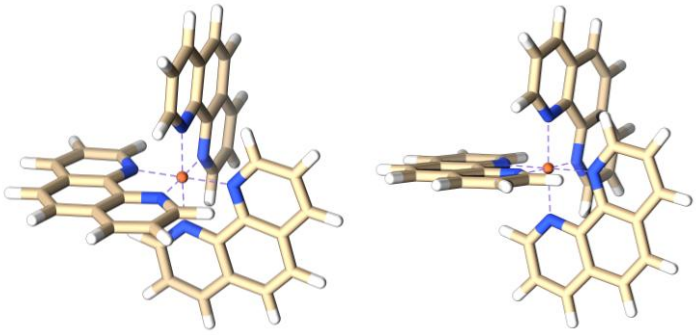

Figure 11- Structure of the ferroin complex (created in ChemDraw® Professional v.14).

The calibration curve was produced using a Iron atomic absorption standard solution (Sigma-Aldrich) at 0.01 mg/mL. The composition of all samples, standard and iron solution of unknown concentration, are presented on table 2. After reduction with 10% hydroxylamine hydrochloride samples were quantified (eq. 9 and 10).

Table 2 – Composition of samples for iron determination by the *o*-phenanthroline method.

Sample	1	2	3	4	5	6	7	8	9	10	11
Iron standard solution 0.01 mg/mL (µL)	0	40	80	160	200	240	300	400			
Iron solution to be quantified (µL)									50	100	150
dH_2O (µL)	500	460	420	340	300	260	200	100	450	400	350
10% hydroxylamine hydrochloride (µL)	80										
Vortex											
0.3% phenanthroline (µL)	80										
dH_2O (µL)	340										
Measure absorbance at 510 nm											

$$4Fe^{3+} + 2NH_2OH \cdot HCl \rightarrow 4Fe^{2+} + N_2O + 4H^+ + H_2O \qquad \text{(eq. 9)}$$

$$Fe^{2+} + 3C_{12}H_8N_2 \rightarrow Fe^{2+}(C_{12}H_8N_2)_3 \qquad \text{(eq. 10)}$$

Protein preparations and NADH were quantified by UV-Visible spectroscopy using a Thermo Scientific Evolution 300BB spectrometer. The molar extinction coefficients are presented in table 3.

Table 3- Molar extinction coefficients in $M^{-1}cm^{-1}$.

Dps wild-type	$\varepsilon_{280\ nm} = 2.93 \times 10^5$
Dps Δ15 / Dps Q14E	$\varepsilon_{280\ nm} = 2.57 \times 10^5$
WrbA	$\varepsilon_{280\ nm} = 1.9 \times 10^4$
NADH	$\varepsilon_{339\ nm} = 6220$

The ^{57}Fe solution used in the preparation of holo-Dps for Mössbauer analysis was dissolved in sulfur acid with stirring in an anaerobic chamber (MBraun Labmaster) and diluted with milli-Q water at pH 2.8. Holo-Dps with 144 Fe/protein was prepared in a headspace sealed microliter conic vials (Wheaton) by the 6 successive additions of 24 Fe(II)/protein aliquots. Samples were left to incubate for 5 days, oxygenated 2-3 times per day and stored at 4 ^{o}C.

The same procedure was followed for the preparation of iron-loaded Dps samples used in the UV-Visible spectroscopic study, with the exception of iron solution, which was replaced by a $^{56}Fe_3SO_4$.

3.2.2 Kinetic studies of release of iron from Dps

3.2.2.1 Mössbauer spectroscopy

The Mössbauer spectroscopy is based on the resonant emission or absorption of gamma energy associated to level energy transition of nuclei in atoms. However, this resonance is prevented by the recoil of the atoms. To overcome this obstacle, Mössbauer discovered that, if the atoms are in a solid matrix, the recoil and the Doppler energies are low enough to observe resonance, since now the nucleus is fixed in a matrix.

The Mössbauer experiment consists in an isotope at an excited sate and an absorber that is the sample to study. The absorber contains the isotope from the same type of source. The gamma rays emitted by the nuclei source pass to the absorber where it may be partially absorbed. To modify the energy of gamma rays emitted, the isotope source is moving relative to the absorbance. The resonance absorbance is observed when the gamma rays energy is equal to the energy of the level energy transition. A Mössbauer spectrum is a plot of gamma ray relative absorption against the velocity of the source movement.

Calibration is made by spectra records of an iron foil at room temperature with different driver velocities (4-12 mms^{-1}). The results are computed and analyzed at WMOSS© v 1.51 (See co.) software.

All the Mossbauer samples were prepared in an MBraun Labmaster anaerobic chamber (<4 ppm O_2). All solutions were degassed with vacuum and argon cycles before placing inside the chamber.

The reaction time scale was previously assessed by a former Master student.[68] Mössbauer samples were prepared by addition of WrbA (15.897 µM Dps: 190.68 µM WrbA) to 144 ^{57}Fe/protein loaded Dps wild-type samples of 5x molar excess of NADH (2.289 mM 57Fe: 11.445 mM NADH). The same was proceeded for Dps variants DpsΔ15 and Dps Q14E. However for these, Dps protein concentrations were 16.71 µM and 17.44 µM, respectively. The WrbA and NADH added to Dps mutant samples were accordingly to the same proportions of the WT samples, i.e WrbA 12 times Dps and NADH 5 times iron concentration.

The iron release reaction was initiated by the addition of the flavoprotein WrbA (12 WrbA/Dps) and stopped by freezing samples in liquid nitrogen after 2, 12, 20, 30, 50, 100 and 200 min. Mössbauer spectra were recorded at 10 K and 80 K.

3.2.2.2 UV-Visible spectroscopy

Based in the *o*-phenanthroline assay (described before) for iron quantification, a kinetic assay was developed for the detection of iron release from Dps and mimicking the Mössbauer samples.

Reaction mixtures were prepared in a septum-sealed quartz cuvette with optical path length of 2 cm. The chelator *o*-phenanthroline (10 Phen/Fe in Dps) was included to $^{57}Fe_2SO_3$ iron loaded Dps with 5 and 12 times molar excess of NADH and WrbA, respectively. Such as in the Mössbauer samples, reaction was started by the addition of the WrbA protein and followed by continuous acquisition of spectrums over time. Special attention was made to keep the sample in anaerobic conditions. All spectra were recorded with a Thermo Evolution 300BB spectrometer between 300 and 600 nm.

3.3 Bioinformatic study

3.3.1 Modeling Flavoprotein

Protein modeling has been drawn up in response to the inability to obtain protein structures, when experimental means are not available. The basic idea is to predict the unknown tridimensional structure of a protein based in know structure of homologous relatives. Why homologous relatives? Great evolutive changes are not favorable if protein loses important functions and properties. As such, within a protein family, mutations will normally not affect protein structure and the close relatives tend to have the same structure. Figure 12 shows the relation that exists between the number of aligned residues with the template protein and the percentage of identity for safe modeling.

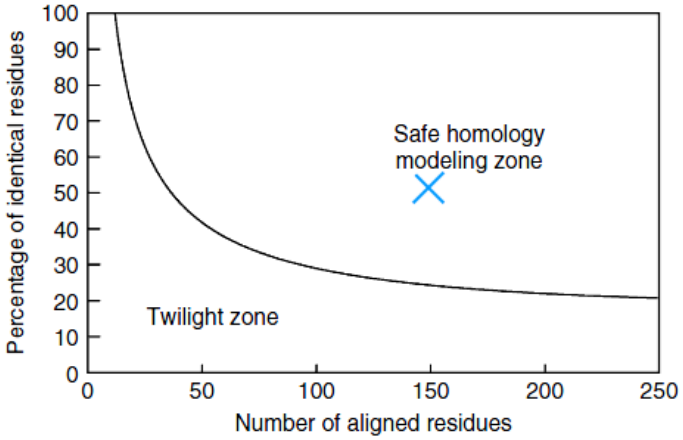

Figure 12- The two zones of sequence alignments. Two sequences are practically guaranteed to fold into the same structure if their length and percentage sequence identity fall into the region marked as ‘‘safe.’’ An example of two sequences with 150 amino acids, 50% of which are identical, is shown (cross). Figure from reference [72].

Homology modeling comprises the steps:

1. Find the best template
2. Align the template with the protein sequence
3. Create the backbone structure
4. Model loops
5. Model side-chains
6. Optimize
7. Validate

For the study of the interaction between Dps(wt) and WrbA it was necessary to request protein modeling tools to predict flavoprotein tridimensional structure. Seven different webservers provide models based in parent templates (table 4). All these servers search and select the best template from a database and use it to predict the 3D structure for the protein of interest. Two of the used servers can also perform *ab initio* modeling.

Table 4- Modeling servers.

Webserver	Type of modeling	Website
3D Jigsaw	Homology	http://bmm.crick.ac.uk/~3djigsaw/
Modeller	Homology	http://toolkit.tuebingen.mpg.de/hhpred/
M4T v. 3.0	Homology	http://manaslu.aecom.yu.edu/M4T/
Phyre 2	Homology + *ab initio*	http://www.sbg.bio.ic.ac.uk/phyre2/
Robetta	Homology + *ab initio*	http://robetta.bakerlab.org/
Swiss model	Homology	http://swissmodel.expasy.org/

The amino acid sequence used in the query was the following:

MAKILVLYYSMYGHIETMANTVAEGARGVNGADVVVKRVPETMADEAFLNAG
GKADQGAPVADPKELADYDAIIFGTPTRFGNMAGQMRTFLDQTGGLWAEGKL
HGKVGSVFTSTGTGGGQEQTITSFWTTLAHHGMVLVPLGYGIPEFFDISEVNG
GTPYGASTIAGGDGSRQPSEKELAIARFQGEHVAELAIKLHG

3.3.1.1 3D Jigsaw

3D Jigsaw server[73]–[75] looks for homologous in PFam[76], PDB[77] and non-redunctant templates database[78]. In iterative mode, the algorithm split the query sequences into domains and attributes a score accordingly to the template coverage in the query sequence.

After selecting the best template, the alignment can be corrected before submitting the modeling job. For the WrbA the alignment was not corrected.

3.3.1.2 Modeller/HHPred

This method is based on HMM (Hidden Markov model based profiles) profile comparison.[79] HMM profiles have information about the frequency of insertion and deletion that reflect how important each position is for defining other member of the protein family. By using both HMM profiles and iterative PSI-BLAST[80] alignment in uniprot[81], non-reduncted, HHpred, PFAM and SMART databases,[82] this algorithm become more conventional for predicting 3D structure from more distance related parents.[83],[84],[77]

The templates with more score were chosen in order to be modeled by Modeller program. This is one of the most popular programs for protein comparative modeling. Constrains, like Cα-Cα distances, bond lengths, main-chain and side-chain dihedral angles, are formulated in order to find the parameters that maximize the total probability density obtained by combining all constraints.

3.3.1.3 M4T version 3.0

M4T is the Multiple Mapping Method with Multiple Templates, i.e., uses an iterative implementation of the alignment method named Multiple Mapping Method (MMM).[85]–[87] But before, the templates are searched by a PSI-BLAST alignment in PDB database. Then the results are iterative clustered. The cluster with high score is used as template and submitted to a sequence-to-structure alignment method that optimally combines alternatively aligned regions according to their fit in the structural environment of the template structure. Models are build using Modeller program.

3.3.1.4 Phyre2

Phyre2 server searches (PSI-BLAST alignment) for a WrbA sequence in the PDB database.[88] Then generate a HMM profile from the aligned sequences and compare to HMM profiles of known structures database. This process can generate 3D models with templates with lower identity.

3.3.1.5 Robetta

Robetta server provides *ab initio* and comparative models.[89]–[91] The server uses Ginzu protocol that identifies templates and predicts the domain regions that are aligned to PDB templates with reasonable confidence. The comparative models are built from templates detected and aligned by HHSearch/HHpred[92], RaptorX[93] and Sparks-X[94] programs. When domains don't have a PDB homolog to serve as template, one is modeled with the Rosetta *de novo* protocol.

3.3.1.6 Swiss model

For the WrbA modeling was used the Swiss model server in fully automated mode.[95]–[97] The requested templates are identified by the homology modeling pipeline based on BLAST and HHBlits[98]. The templates ranked according to their estimated quality are selected and modeled using PROMOD-II[99] and Modeller.

All the steps (Template selection, Model building and Structure quality evaluation) are executed and can be invoked in the Workspace.

3.3.2 Model results evaluation

The best models obtained from each server were selected to be ranked according to SFCheck server [100],[101] results.

SFCheck server evaluates:

i) **Atomic Clashes:** unfavorable interactions where atoms are too close together
ii) **Peptide Linkage:** C-N bonds distance that outlier outside the accepted range for the peptide bond (1.30-1.45).
iii) **Covalent Geometry:** Bond angles that outlie outside the standard values.
iv) **Chirality Error:** detect chiral center with wrong chirality.
v) **Phi/Psi torsion angles:** identifies phi/psi torsion in forbidden region of Ramachandran plot.

The models approved by this server were submitted at SAVES v.4 server[102] for a more detailed validation. It runs the following programs:

i) **PROCHECK**[103]**:** Analyze the stereochemical quality residue-by-residue and the overall structure geometry.
ii) **WHAT Check**[104]**:** Does intensive checking of many stereochemical parameters of the residues.
iii) **ERRAT**[105]**:** Analyze the statistics of non-bonded interactions between different atoms types and compares with statistics from highly refined structures.
iv) **VERIFY 3D**[106],[107]**:** Assign a structural class on amino acid sequence (alpha, beta, loop, polar, nonpolar, etc) and compare the results to good structures.

v) **PROVE**[108]**:** Calculate a statistical Z-score deviation from highly resolved (2.0 Å or better) and refine (R-factor of 0.2 or better) PDB-deposited structures.

vi) **Ramachandran Plot:** Produce a interactive Ramachandran plot.

Also the QMEAN score of the pass models are generated by the Swiss Model QMEAN server for quality model estimation.[109],[110]

3.3.3 Model Refining

The WbrA model was minimized in UCSF Chimera v.1.10.1[111]. This tool moves the system toward a local minimum without crossing energy barriers.[112] The minimizing procedure have the following default parameters:

Steepest descent steps (default 100)

Steepest descent step size (Å) (default 0.02)

Conjugate gradient steps (default 10)

Conjugate gradient step size (Å) (default 0.02)

Update interval (default 10)

Fixed atoms -**none** (default)

However, Chimera calls first the Dockprep tools to perform the following tasks:

i) **AddH** to add hydrogens. This step also considers H-bonds and Histidine, Glutamic acid, Aspartic acid, Lysine and Cysteine was protonated based on residue name.

ii) **Add Charge** to associate atoms with partial charges and other force field parameters. Standard residues parameters were assigned from AMBER ff14SB force fields.[113]

3.3.4 Docking

Docking is basically modeling the quaternary structure, i.e. predict the orientation and interaction of the macromolecular complex as it would occur in a living organism. It is assumed that the contacts occur at the surface by non-covalent bonds. All docking processes can be resumed in three stages: search, filter and score.

Docking result must be integrated to data from mutagenesis, cross-linking, spectroscopy, reaction mechanism, active sites or machine learning.

3.3.4.1 Dps and WrbA interaction

Protein-protein docking is still a challenge in the bioinformatics world. Most of the user-friendly softwares programs have difficulties in performing a docking with large proteins, because of the large amount of information and number of variables. So, ClusPro protein-protein docking server was used for this docking study.[114]–[117] This server uses various

functions to calculate and score the docking, balanced, electrostatic favored, hydrophobic favored and Van der walls + electrostatic (vdw+elec) (annex 8.7).

3.3.5 Additional Bioinformatic tools

Two bioinformatics tools, Predict protein and Consurf, were assessed in order to find complementary structural information about Dps. The services provided by these tools are described in the next table.

Table 5- Additional bioinformatics tools description

Predict Protein	Prediction for: SS, Solvent accessibility, effect of point mutation, gene onthology, subcellular location, binding sites, disulphide bridges and cysteine bonds.	http://www.predictprotein.org/
ConSurf	Identification of conservated aminoacids by surface-mapping of phylogenetic information	http://consurf.tau.ac.il/

4 . Results and Discussion

4.1 Plasmid preparation

The efficiency of the plasmid isolation and purification was evaluated by electrophoresis in an agarose gel. The electrophoresis profile (figure 13) a major band with higher mobility corresponding to the supercoiled form of the DNA allowing the progression of the work; two minor bands are also present attributed to different conformations of DNA.

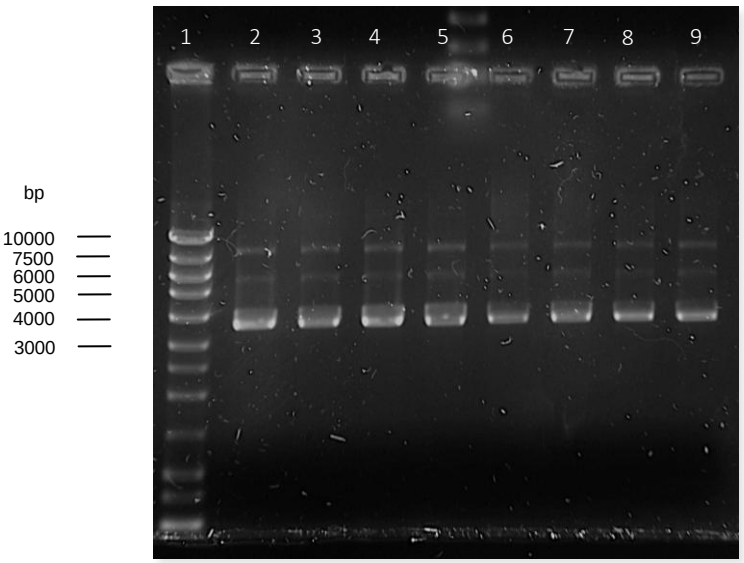

Figure 13 - Electrophoresis analysis of pET21c-Dps(wt) minipreps in agarose gel. **Lane 1-** NZYDNA Ladder III (Nzytech) Molecular weight marker.[118] **Lane 2-5)** pET21c-Dps(wt) more concentrated (was applied 3µL of plasmid) and **Lane 6-9)** less concentrated samples (was applied 3µL of plasmid).

Transformation of *E. coli* BL21(DE3) competent cells with the previous plasmid DNA was successful. Isolated transformants were observed in the LB-ampicillin-agar plates. No colonies were detected on the negative control plate showing no contamination.

4.2 Overproduction of Dps(wt)

The growth curve of *E. coli* cells harboring the pET21c-Dps(wt) expression vector for Dps production is presented on figure 14. After 3 h and 30 min, the expression of Dps encoding gene was induced with IPTG at an OD_{600nm} of 0.53.

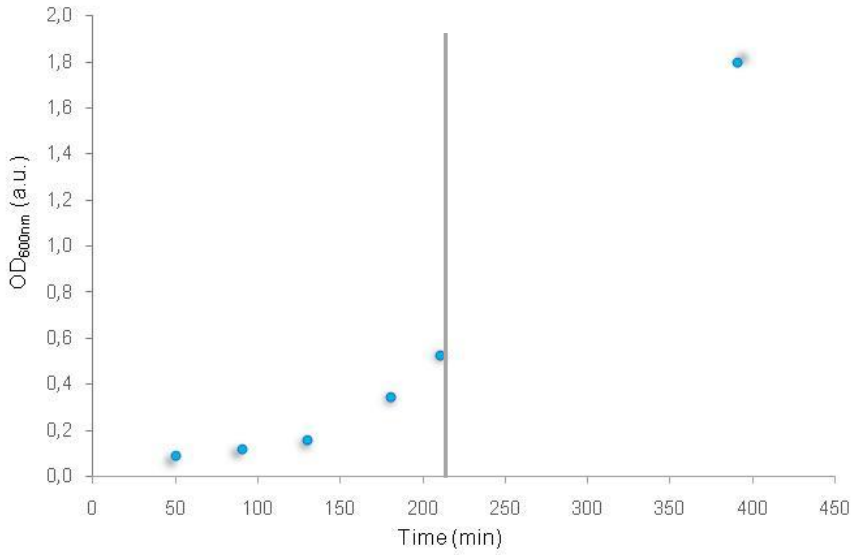

Figure 14 - Growth curve of *E. coli* BL21(DE3) harboring the pET21c-Dps(wt) expression vector. The vertical line indicates the time of induction with 0.5 mM IPTG.

The protein expression profile along the growth curve, assessed by SDS-PAGE, is shown in figure 15. The gel reveals an intensive band with an apparent molecular mass around 18 kDa due to the high level of production of Dps (lane 3). The presence of a very intense band in the supernatant of the ultracentrifugation step confirms the production of the protein in a soluble form (lane 6).

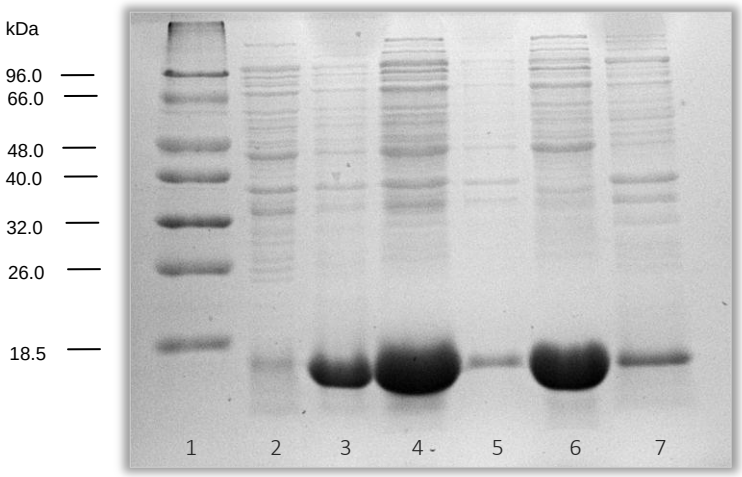

Figure 15 - SDS-PAGE analysis of the production of Dps in *E. coli* BL21(DE3). **Lane 1** - LMW protein weight Marker (Nzytech);[119] **lanes 2 and 3** - Protein profile at t=0 h and after 3 h of induction of gene expression with 0.5 mM IPTG, respectively; **Lanes 4 and 5** - Supernatant and pellet, respectively, from the low speed centrifugation; **Lanes 6 and 7 -** Supernatant and pellet from the ultracentrifugation.

Under the tested experimental conditions, 2.3 g of wet cells were obtained per liter of culture.

4.3 From cell lysis to purification of Dps

The purification of Dps protein was accomplished using 3 chromatographic steps of a weak anionic exchanger, size exclusion and strong anionic exchanger, in this sequence. Typical elution profiles of each column are presented in figures 16 to 18.

In the first chromatographic step, with a DEAE-Sepharose column, adsorbed proteins were eluted with a discontinued linear gradient of 10 mM Tris-HCl pH 7.6 with NaCl (figure 16). Dps containing fraction were eluted between 210 and 265 mM of NaCl (i.e. 42% to 53% of elution buffer), pooled and loaded into a Superdex 200 column (figure 17). The most impure fractions from were further purified in a third step using the buffer system of the first chromatographic column (figure 18). Pure Dps was eluted from the Q-resource column between 104 mM and 144 mM of NaCl (52-72% of elution buffer).

All collected fractions were analyzed by SDS-PAGE for purity assessment and tested for catalase.

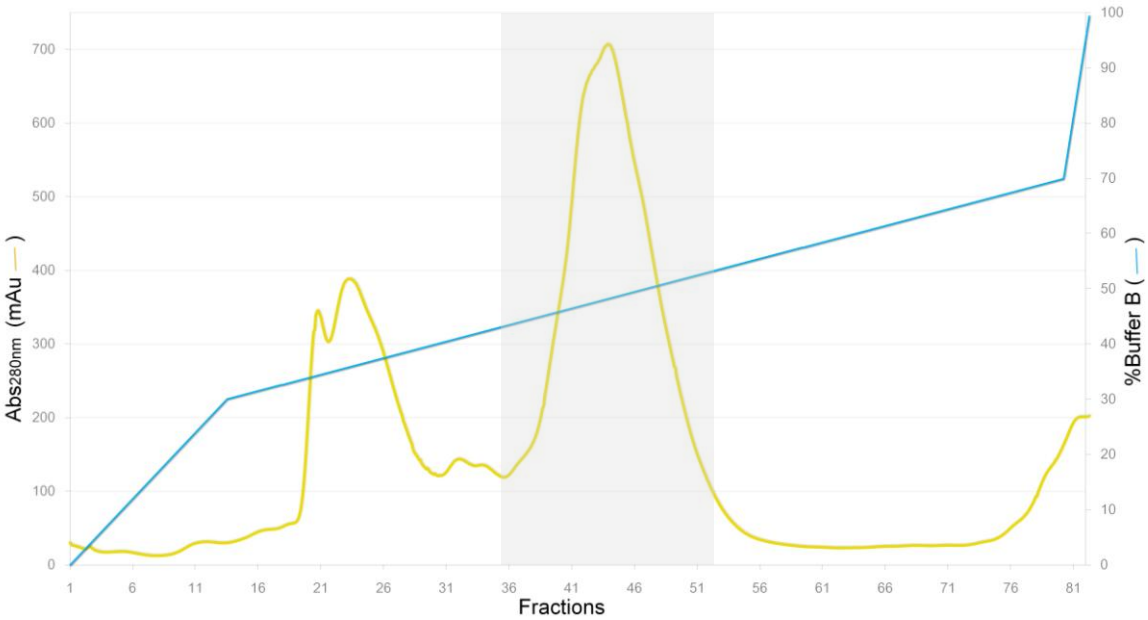

Figure 16 - Elution profile of DEAE-Sepharose FF column (2.6 x 30 cm) used as the first purification step of Dps(wt). Elution was performed with 10 mM Tris-HCl pH 7.6 with NaCl (Buffer B) at a flow rate of 5 mL/min. 12 mL samples were collected. The zone marked at grey corresponds to the Dps elution.

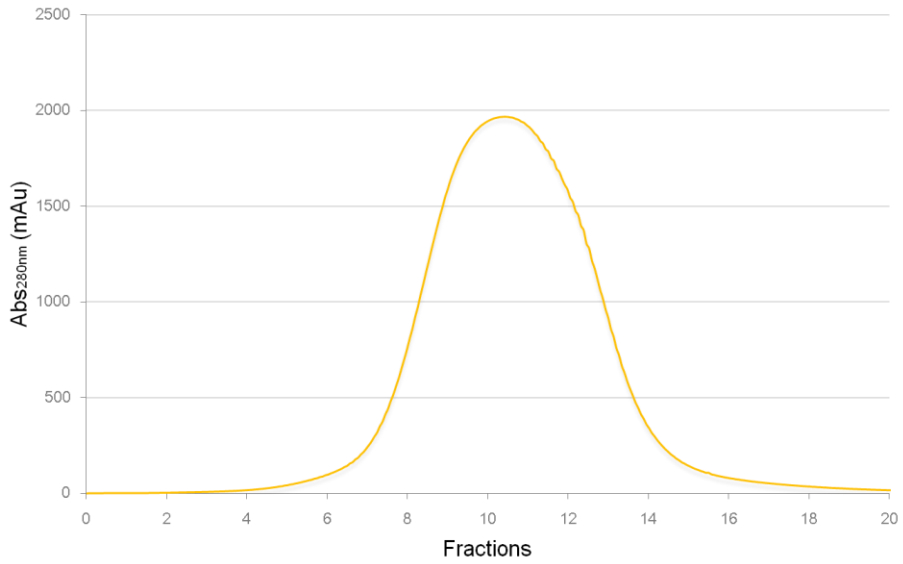

Figure 17 - Elution profile of the gel filtration Superdex 200 column (1.6 x 49 cm) used as the 2nd purification step of Dps(wt). Proteins were eluted with 10 mM Tris-HCl pH 7.6 with NaCl at a flow rate of 1.5 mL/min. Fractions were collected in 2 mL.

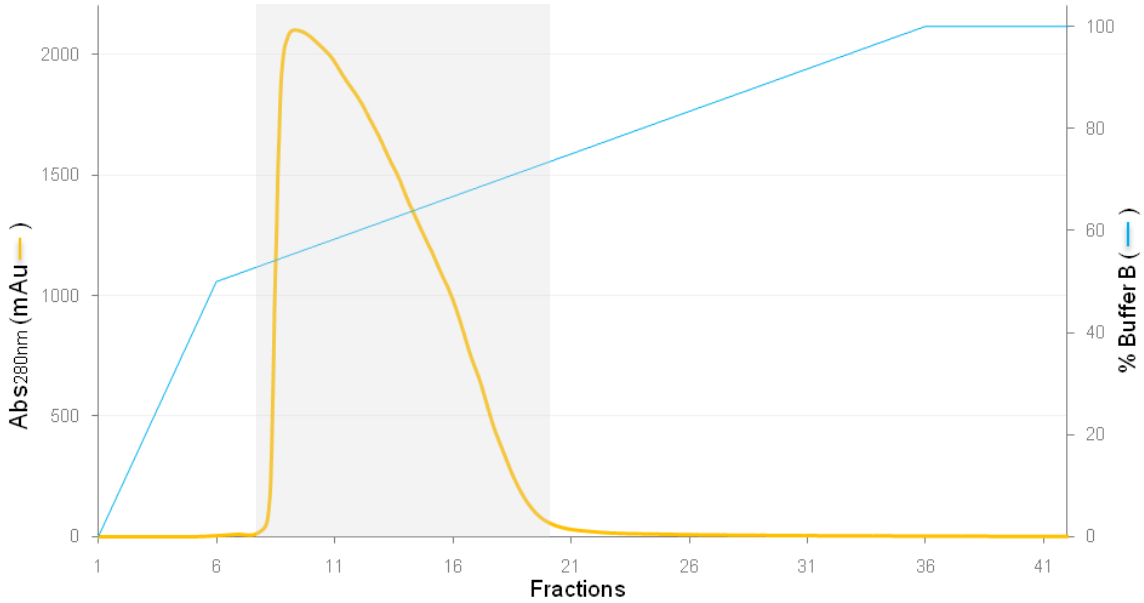

Figure 18 - Elution profile of the 3rd purification step on a Q-Resource column (6 mL) of Dps(wt). Elution was performed with 10 mM Tris-HCl pH 7.6 with NaCl (Buffer B) at a flow rate of 1 mL/min. 2 mL samples were collected. The zone marked at grey corresponds to the Dps elution.

Three final pooled fractions were obtained and assessed by SDS-PAGE as can been seen in figure 18: a pure (at 110.47 μM), an impure (at 329 μM), and an almost pure fraction containing traces of catalase (at 124.45 μM). The chromatographic steps were effective so that catalase is no longer present.

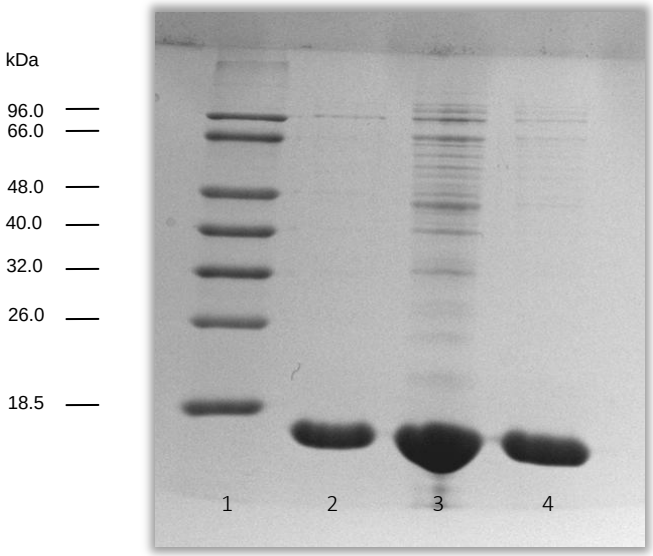

Figure 19 – Purity assessment of final pooled fractions during purification of Dps(wt). **Lane 1** – LMW protein marker (Nzytech);[119] **Lane 2 and 3** – Pure and impure Dps fractions, respectively, obtained after 3 chromatographic steps; **Lane 4** – Dps fraction with a trace of catalase. For all was applied 0.5 µL of protein.

As referred before, presence of catalase was assessed by the addition of hydrogen peroxide. In the following figure (figure 20), a typical example of fractions with and without catalase is presented. As can been seen, when catalase is present, this protein catalyze the formation of O_2 (gas) and H_2O using H_2O_2 as substrate.

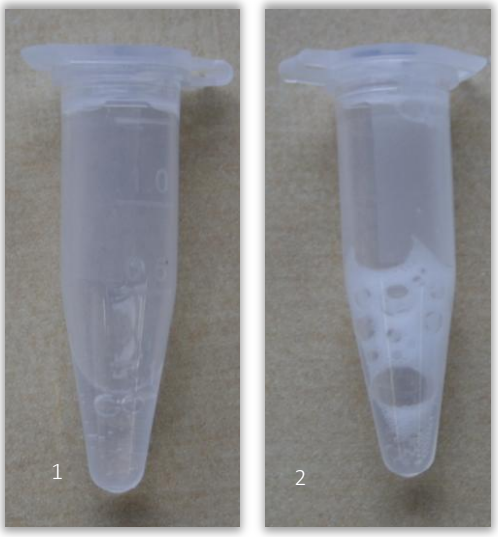

Figure 20 – A typical catalase test. **1 -** Negative result; **2-** Positive result.

Since hydrogen peroxide was not a substrate in the kinetic assays, the presence of traces of catalase will not be a problem, and thus was used for the following experiments.

4.4 Modeling WrbA

4.4.1 3DJigsaw

Results of the search in Pfam indicate that our target sequence matches the NADPH-dependent FMN reductase (pf03358.10). The PFam alignment result has 60% identity and an e-value of $6x10^{-56}$. Five structural templates from PDB search were selected to model.

Table 6- Best templates from alignment in 3DJigsaw.

Model	Template	Alignment
1	2r97_A	**Query sequence:** residues 2 to 199 **%Seq.Identity:** 78 **%Secondary-Structure Matching:** 100 **bit-score:** 6.2602
2	2r96_A	**Query sequence:** residues 2 to 199 **%Seq.Identity:** 78 **%Secondary-Structure Matching:** 100 **bit-score:** 6.22959
3	2r96_C	**Query sequence:** residues 2 to 199 **%Seq.Identity:** 78 **%Secondary-Structure Matching:** 100 **bit-score:** 6.21939
4	2r97_C	**Query sequence:** residues 2 to 199 **%Seq.Identity:** 78 **%Secondary-Structure Matching:** 100 **bit-score:** 6.32632
5	2rg1_A	**Query sequence:** residues 2 to 198 **%Seq.Identity:** 81 **%Secondary-Structure Matching:** 100 **bit-score:** 6.41317

4.4.2 HHPred/Modeller

The top four PDB structures obtained from HHPpred analysis were selected to be used as templates for modeling. The multiple alignment of the 4 templates with the query serves as input for Modeller.

Table 7- Templates select for multiple alignment in Modeller.

Hit	1	2	3	4
Protein	Flavoprotein WrbA	NADP(H) desidrogenase (quinone)	Trp repressor binding protein WrbA	Trp repressor binding protein WrbA
Prob	100	100	100	100
E-value	3.3×10^{-47}	3.3×10^{-42}	1×10^{-40}	2.7×10^{-40}
P-value	9.2×10^{-47}	1×10^{-46}	2.9×10^{-45}	7.6×10^{-45}
Score	255.4	255.2	247.2	244.9
SS	21.1	18.9	19.7	17.7
Cols	197	199	195	191
Template	1-197	2-205	5-200	4-202
HMM	197	207	200	211

The model generated was evaluated in the Modeller server by VERIFY_3D, SOLVX and ANNOLEA. Using VERIFY_3D, none of the residues of the protein sequence has a negative score.

4.4.3 M4T

M4T Server uses only one template. For that reason, flavoprotein WrbA (PDB: 3zho_A), with the top score according to HHPpred analysis, was used as template. The alignment of the template sequence do not covered the first aminoacid of the target sequence. The resulting model has a DOPE score of -21224.359375 and a z-score of -8.76.

4.4.4 Phyre2

For Phyre2 server used a *E.coli* flavoprotein WrbA (PDB:c3b6iB) with 77% identity and whose alignment covers the residues 2-199 of the query sequence. The template's probability to be homologous to the target, i.e. the confidence, is 100%. Thus, after excluding the first residue of the query sequence from the alignment, modeling by *ab initio* was performed.

4.4.5 Robetta

Ginzu protocol found a domain for modeling, 4la4A that span the whole query sequence. The confidence is 95.14%.

4.4.6 Swiss Model

The 4 hit template obtained by the alignment performed in the Swiss Model server were selected to model.

Table 8- Detailed results for the 4 best models.

Model	Template	Protein	Seq. Similarly	GMQE	QMEAN4	Coverage
1	3b6k.1.A	WrbA	0.54	0.96	-0.18	0.99 (2-199)
2	3b6m.1.A	WrbA	0.54	0.91	-0.88	0.99 (2-199)
3	2r97.1.A	WrbA	0.54	0.94	-1.61	0.99 (2-199)
4	2r97.1.B	WrbA	0.54	0.91	-1.61	0.99 (2-199)

4.5 Modeling validation

4.5.1 SFCheck

Since the different servers validate the models by different types of scores and in order to validate the models with the same methodology, two different servers were used to evaluate the best model. At first, SFCheck program was used for a first screening. Only 6 out of the 16 models screened show none of the errors referred at table 9.

Table 9- Resume of SFCheck results. (x) represents errors and (-) no errors. The red marks correspond to the models with no errors.

Server	Model	Atomic Clashes	Peptide Clashes	Covalent Geometry	Chirality error	Phi/ Psi torsion angles
3D Jigsaw	1	-	x	x	-	-
	2	-	x	x	x	-
	3	-	x	x	x	-
	4	-	x	x	x	-
Modeller	1	-	-	-	-	-
M4T	1	-	x	-	-	-
Phyre2	1	-	-	-	-	-
Robetta	1	-	-	-	-	-
	2	-	-	x	-	-
	3	-	-	x	-	-
	4	-	-	-	-	-
	5	-	-	-	-	-
Swiss model	1	-	-	x	-	-
	2	-	-	-	-	-
	3	-	-	x	-	-
	4	-	-	x	-	-

4.5.2 SAVES

For a more detailed analysis, the models that pass SFCheck screen were submitted to SAVES server. This server evaluates the quality of each model using a set of different scores.

Table 10- SAVES results. The meaning of WHATCHECK numbers are in annex 8.6.

Server	Model	PROVE (the percentage of buried outlier protein atoms of scored)	ERRAT (overall quality factor)	VERIFY 3D (residues with 3D-1D average score >0.2)	WHATCHECK	PROCHECK	QMEAN (z-score)
Modeller	1	3.5 %	85.340	87.44 %	E: 1.2.39.47.50 W:13.14.23.24.29. 30.31. 33.44.46.48.52.53	Failed	0.678 (-0.98)
Phyre2	1	4.9 %	75.916	91.96 %	E: 1.2.39.50 W:14.23.24.29.31. 33.44.46.48.49.52.53	Failed	0.646 (-1.32)
Robetta	1	1.9 %	96.859	93.97 %	E: 1.2.39.45.62 W:9.10.13.22.23.24.29.30. 31.33.53.54.57.57.64.65.	E:0 W:2 P:9	0.84 (0.91)
	4	1.7 %	97.379	89.95 %	E: 1.2.45.63 W:9.10.13.22.23.24.29.30. 31.33.46.53.54.55.57.58.65. 66.	E:0 W:3 P:8	0.829 (0.79)
	5	1.6 %	96.597	93.47 %	E: 1.2.45.62 W:9.10.13.22.23.24.29.30. 31.33.46.53.54.55.56.57.64. 65.	E:0 W:3 P:8	0.853 (1.05)
Swiss model	2	4.5 %	82.718	81.31 %	E: 1.2.45.62 W:14.23.24.29.30.31.33. 53.54.55.56.57.64.65.	E:0 W:2 P:9	0.823 (0.71)

The previous table resumes the SAVES output results. From all the scores, the Robetta models have proven to be of higher quality. PROCHECK results for HHPred/Modeller and Phyre2 failed because only are a monomeric structure. Only Swiss model and Robetta can perform a multimeric modeling.

4.5.3 Modeling results overview

The most common sources of errors in comparative modeling are:

- Incorrect choice of template
- Template alignment: The wrong alignment can result in incorrect secondary structure assigned for each amino acid. This problem can be diminished by using multiple or iterative alignments.
- Loop structure modeling: The loops are highly flexible regions, with higher RMSD values. This brings difficulties for structure determination. When loops can't be build based on the template, there are two alternatives. The first is looking up in the PDB database with known structures for loop with the same endpoints and the second is the *ab initio* building.
- Side-chain rotamers: The wrong rotamer attribution can result in wrong packing and unfavorable energetic regions. So generally, the servers use rotamer libraries with high resolution structures.

Each modeling server was capable to detect WrbA structure with high identity as template. Actually, 2r97, 3zho and 4laf, were at the top template hit in two different servers. HHPred/Modeller, Phyre2, Robetta and Swiss model servers build the best models for the WrbA protein. Once the template was correctly identified, differences in the models from table 10 may stem from other type of errors (for example at sequence alignment, threading and modeling loops and side-chains).

Interestingly, the Swiss model also uses the Modeller algorithm, which can contribute to the fact that these two servers had some of the best model results. Also, Phyre 2 and Robetta can perform comparative and *ab initio* modeling, so that the residues that can't be aligned with the template can be also modeled.

Robetta models were built based on the 4laf template (also used by modeler server with addition of other 3 templates). The 3 other templates may contribute to increase errors in the alignment target-template at Modeller server.

Many factors and variables can be responsible for the different score results, but Robetta models 4 and 5 were clearly the best templates. The reason for such fact can be because *ab initio* algorithm can participate in the model building, or/and the target-template alignment and threading is better than those performed by other servers. The two best models

were very similar. (figure 21). The most visible differences are in loops and chain- terminal modeling.

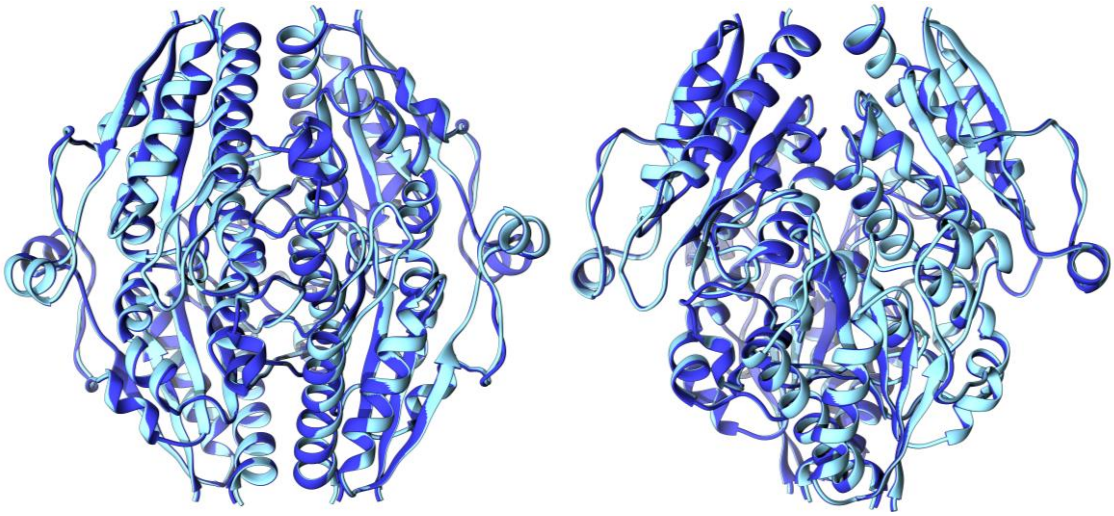

Figure 21- Overposition of Robetta models 4 and 5 of WrbA. Front view (right) and side view (left).

4.6 Docking Dps and WrbA

4.6.1 Dps and WrbA interaction

Since there is no experimental means available to study the structural interaction of these two proteins, bioinformatics comes to help look at this system more in an atomic point of view. The informatics tools used in this work are user-friendly, and the results are to be tested in laboratory. So, bioinformatic is used as an additional tool. By integrating different computational structural information, it is possible to infer and select a set of possible interaction in order to be tested in the laboratory. Also, it is the tool of choice to rationalize obtains results and help planning of future experiments.

Protein-protein docking has been a challenge in recent years. However, there are already some software packages for this purpose. These two proteins, Dps and WrbA, have very large dimensions, which makes the docking process more demanding. Nevertheless, the ClusPro server was able to calculate a set of proper results.

The output models are calculated and scored in 4 different functions, which differ in weight of electrostatic, hydrophobic and Van der walls forces (see functions at annex 8.7).

Dps and WrbA (model 4 and 5 of Robetta) were submitted in Cluspro server. The 5 best models for each type of score were analyzed. Briefly, it is shown in table 11 the common amino acids of each top 5 solution set. The monomers represented by color on table 11 correspond to the same shown in the three-dimensional representation of figure 22.

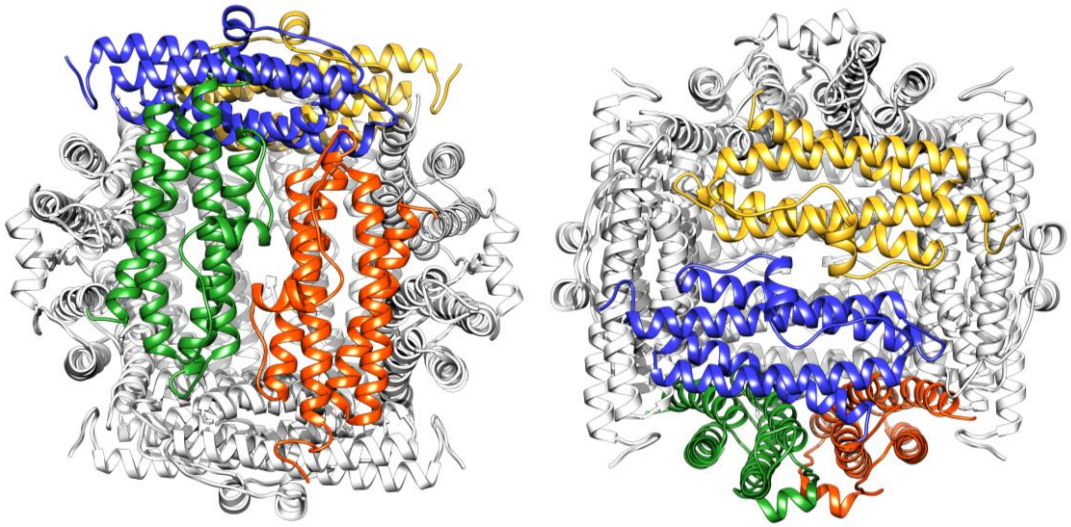

Figure 22- Spatial orientation of the monomers listed in table 11 by the respective color designation.

If we compare models with equivalent score functions, we conclude that exist some amino acids in common (shown in red at table 11). For an individual model, we also found common amino acids (highlighted residues at table 11). However, model 5 WrbA-Dps docking results obtained for vdw+elec score function is very different from all others. So, was also compared the model 5 results without those vdw+elec results (marked in bold).

Table 11- Common residues for each set of 5 best scored models. The red and highlighted amino acids correspond to the ones that remain in the same line and column, respectively. The ones at bold are those that remains in the same column ignoring the Van der walls +electrostatic result.

Score	Model 4 WrbA			Model 5 WrbA		
	Green	Orange	Blue	Green	Orange	Blue
Balanced	G2 K3 N4 F5 T10 Q14 G75 H76 R77	K42	E102 G105 E109 W149 R152 G156 G157	**N4 F5 T10** T13 **Q14 G75 H76 R77**	**K42**	D99 K101 E102 **G105** N106 **V108** W149 **R152** G156 **Q157**
Electrostatic	G2 K3 N4 F5	-	P92 E93 K95 V97 D99 E102 G105 E106 E109 R152 G157	**N4 F5 T10** T13 **Q14 G75 H76 R77**	**K42**	**G105 V108 R152 Q157**
Hydrophobic	K3 N4 F5 T10 N73	-	K101 E102 G105 N106 V108 R152 L155 G157	**N4 F5 T10 Q14** L74 **G75 H76 R77**	**K42**	D99 K101 E102 **G105 V108** W149 **R152** S153 L155 **Q157**
	Green	Orange	Blue	Dimer unit		
Van der Walls + Electrostatic (vdw+elec)	G2 K3 F5	-	E90 P92 E93 R94 D99 E102 N106 E109	R77 Q79 H80 A81 E93 K94 D96 V97		

From all marked amino acids of table 11, F5, E102, R152 and G157 are maintained as part of the interaction. It is also important to note that whenever the WrbA interacts with the monomer marked at orange in figure 22, the first 5 solutions have the K42 residue in common. Also, in the case of model 5, the only amino acid that the vdw+elec score function solutions have in common with each other is the R77 residue.

The balanced score function is the one that shows the most identical results between model 4 and model 5 of WrbA. As can be seen in figure 23, the overposition of the docking results is almost total.

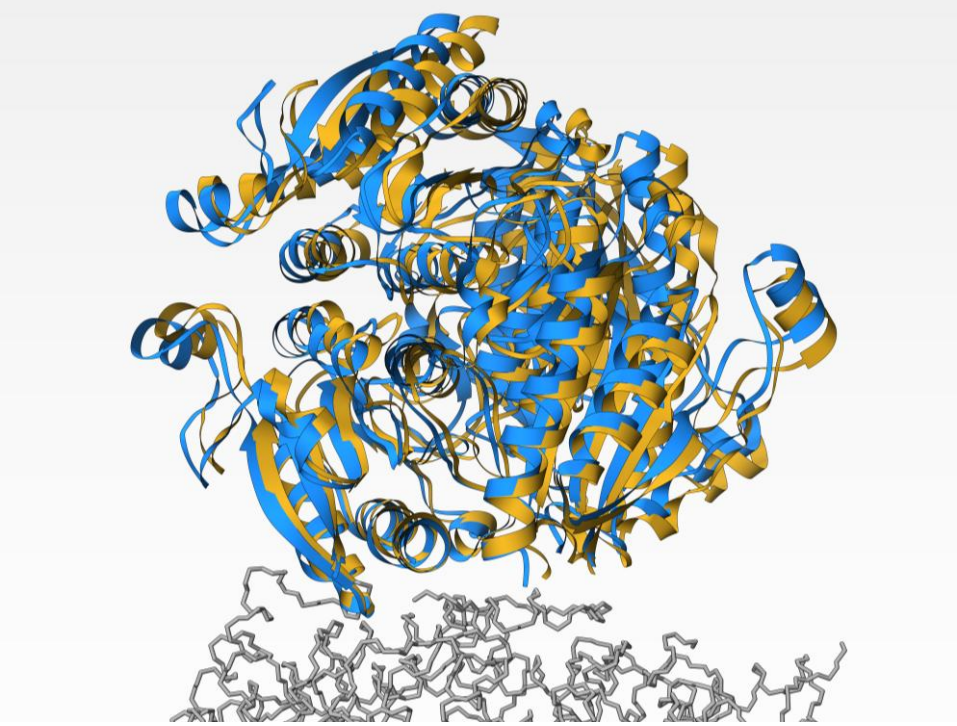

Figure 23- Overposition of Dps-WrbA docking result for model 4 (gold) and model 5 (blue) with best balanced score. The Dps chains backbone is represented at white.

In general, 2 types of solution should be considered. First, the interaction of WrbA with residues in the green, orange and blue monomers interface (figure 24). Second, shown in figure 25, is the vdw+elec docking results with model 5 is the WrbA localized in the interface of Dps dimers (2-fold channels).

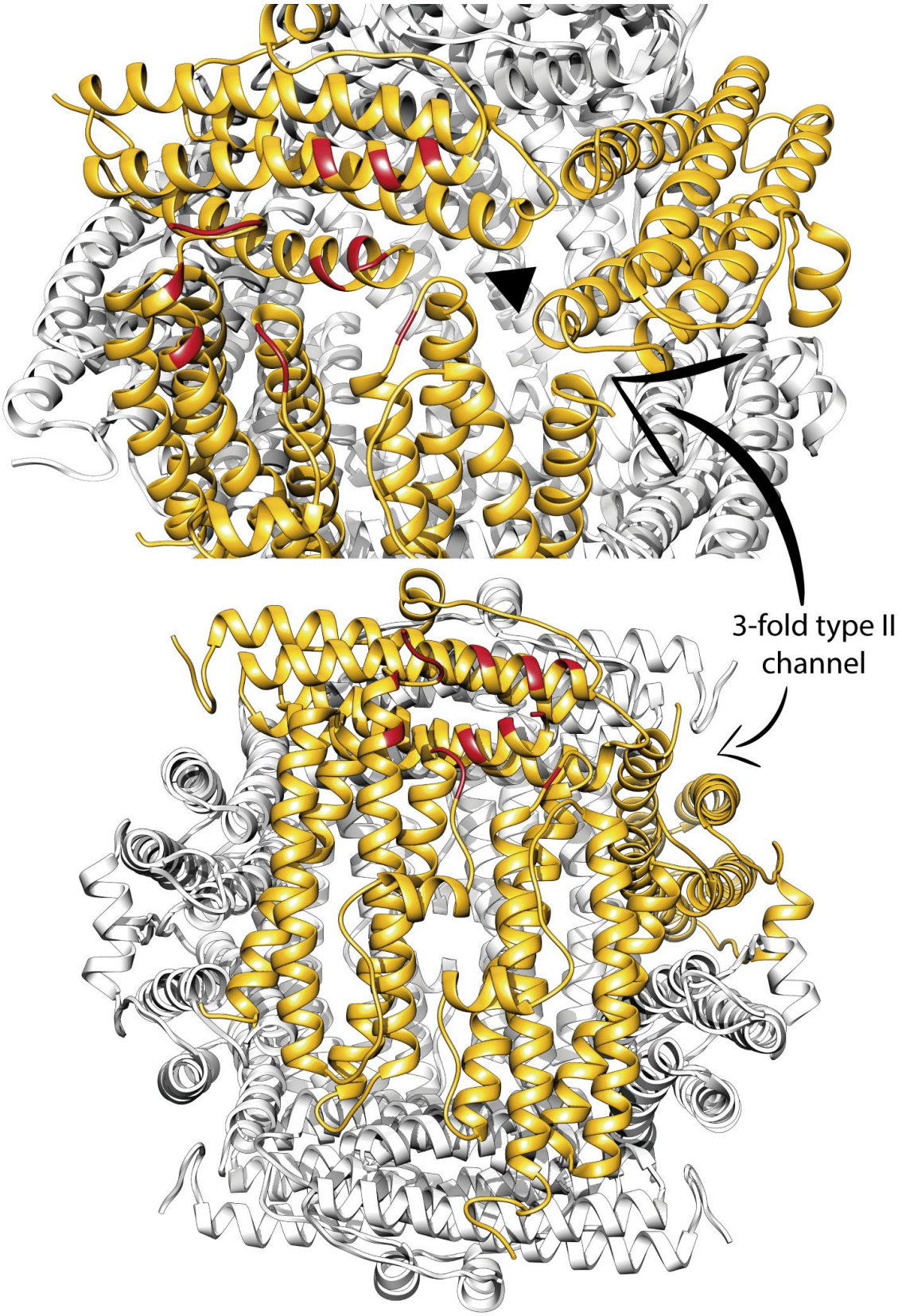

Figure 24 – Dps-WrbA docking result from Dps point-of-view. The gold monomers correspond to those at WrbA flavoprotein vicinity. The red residues are at less than 5 Å of WrbA protein.

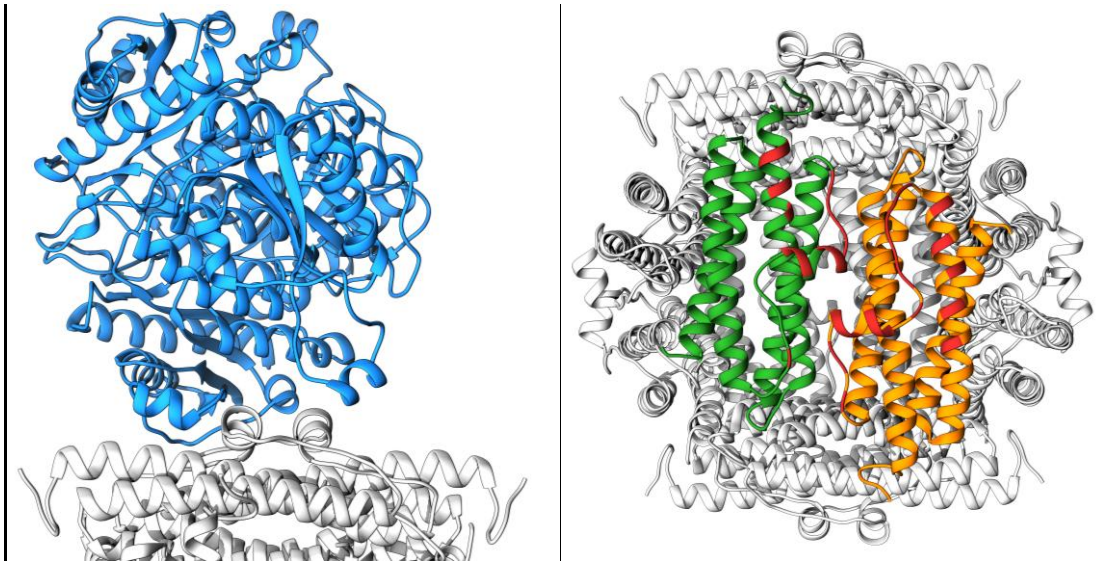

Figure 25 - Docking result of model5 and Dps with vdw+elec function scores. **Right-** Side-view of WrbA flavoprotein in the middle interface of a dimer. **Left-** Top view of the dimer close to Flavoprotein marked as green and orange. The residues at less than 5 Ä are at red.

In this hypothesis, the fact that the residues of the N-terminal appear responsible for the electron transfer with WrbA is quite interesting. As said in section 1.3.1, in some Dps proteins, the N-terminal has a role in the DNA co-crystallization. So, kinetic curves of iron uptake with WrbA(FMN) and NADH will be tested not only with Dps wild-type but also with DpsΔ15 and DpsQ14E.

Regarding docking results quality, they should be view as a way to rationalize and reduce the number of possible solutions. Actually, the Dps structure used for docking should have the iron nanoparticles inside. However, the structure was not available. Even so, the nanoparticles have total different properties and the interactions that actually occur between proteins might have a different nature and that might not be possible to compute by the docking software available.

4.7 Kinetic characterization

4.7.1 Iron loaded proteins

To study the kinetic process of iron release from Dps, the first step is to prepare the iron loaded proteins. Wild-type Dps, DpsΔ15 and DpsQ14E proteins were loaded with 144 irons/Dps (3.6 mM Fe/25 µM Dps) in aerobic conditions.

The ferrous iron solutions, either ^{56}Fe or ^{57}Fe, were quantified by the *o*-phenanthroline method. A typical example of an iron calibration curve is represented in figure 26.

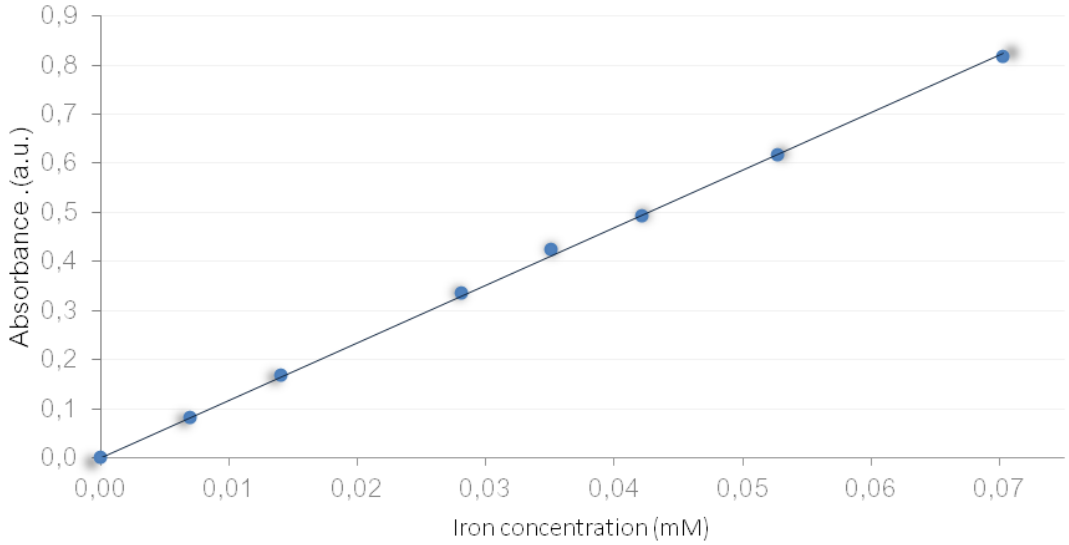

Figure 26 - Calibration curve with iron standard by the *o*-phenanthroline method. The equation of this curve, Y=11.738x (R^2=0.9995), was used to calculate the concentration of iron solution.

After successive additions of iron to Dps protein, samples were oxygenated two to three times per day, during 5 days to ensure all iron was in the ferric mineral form in the nanocavity. During the iron oxidation and storage reaction, an orange sediment was formed, characteristic of iron-loaded Dps that increased with reaction time (Figure 27).

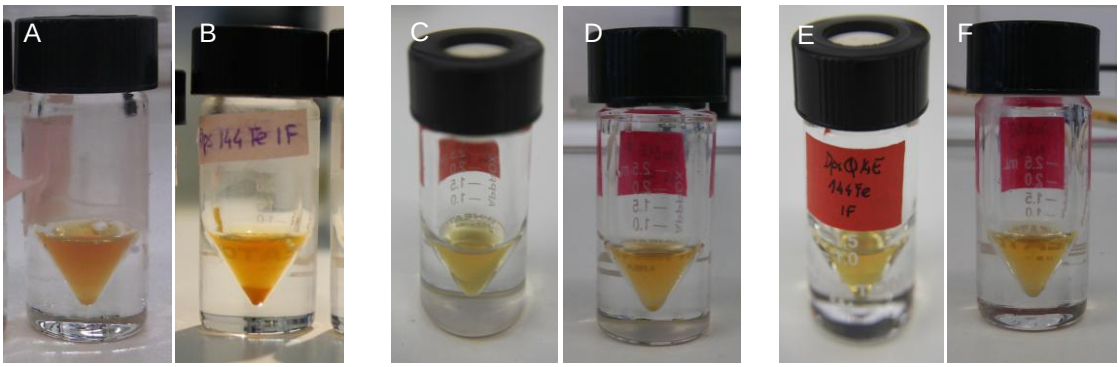

Figure 27 - Iron loaded (144 Fe/protein) of wild-type (A-B), Dps-Δ15 (C-D) and Dps-Q14E (E-F). **A, C, E)** after addition of Fe(II); **B, D, F)** after 5 days.

The iron loaded proteins were then used to prepare reaction mixtures to be analyzed by UV-Visible and Mössbauer spectroscopy to kinetically characterize the iron release process.

4.7.2 Kinetic characterization by Mössbauer spectroscopy

Mössbauer spectra acquired at 80 K in the absence of applied magnetic field, can give information about the oxidation state and on its electronic and magnetic states of the iron present in solution. So, there can be two iron states detected, Fe^{2+} and Fe^{3+}, which have

different electron configuration, $3d^6$ and $3d^5$ respectively. Acquisition at different reaction time points permits the quantification of iron species, ferric mineral in the Dps cavity and the ferrous iron released into solution by dissolution of the mineral by NADH and WrbA. The spectral evolution for Dps proteins, wild-type (WT samples), Dps-Δ15 (N15 samples) and Dps-Q14E (Q14E samples), are shown in figures 28 and 29.

In all proteins, the t=0 min spectrum, corresponding to the ferric mineral control species (prepared in the absence of WrbA), is a typical pure ferric core spectrum with a quadrupole doublet (δ= 0.47-0.48 mm/s and ΔE_Q= 0.6-1.11 mm/s). This result indicates that the experimental conditions used to prepare the iron loaded proteins were ideal to convert all Fe(II) into ferric mineral (spectra WT0, 15N0 and Q14E0 in figures 28 and 29). So all iron present in samples was inside the protein cavity and, consequently, by addition of WrbA and NADH release of ferrous iron from the mineral should be observed and easily quantified since this iron species exhibits very different Mössbauer parameters.

In fact, 2 min after the addition of holo-WrbA (FMN-WrbA) to the iron loaded Dps(wt) (144 Fe/Dps) in the presence of NADH, a ferrous doublet start to develop and increased with reaction time, which has characteristic absorption lines at -0.24 and 2.87 mm/s (with approximately δ= 1.27 mm/s and ΔE_Q= 3.28 mm/s). After 200 min all ferric mineral species was converted into ferrous species in solution. WrbA flavoprotein and NADH revealed to be a good redox partners for iron release from Dps. The iron present in the core decreased (confirmed by the disappearance of the ferric quadrupole doublet in the spectra). This happens because the iron in the core is reduced to ferrous iron that translocate through the Dps pore to the bulk solution. The same result was observed for all Dps proteins, wild-type and variants.

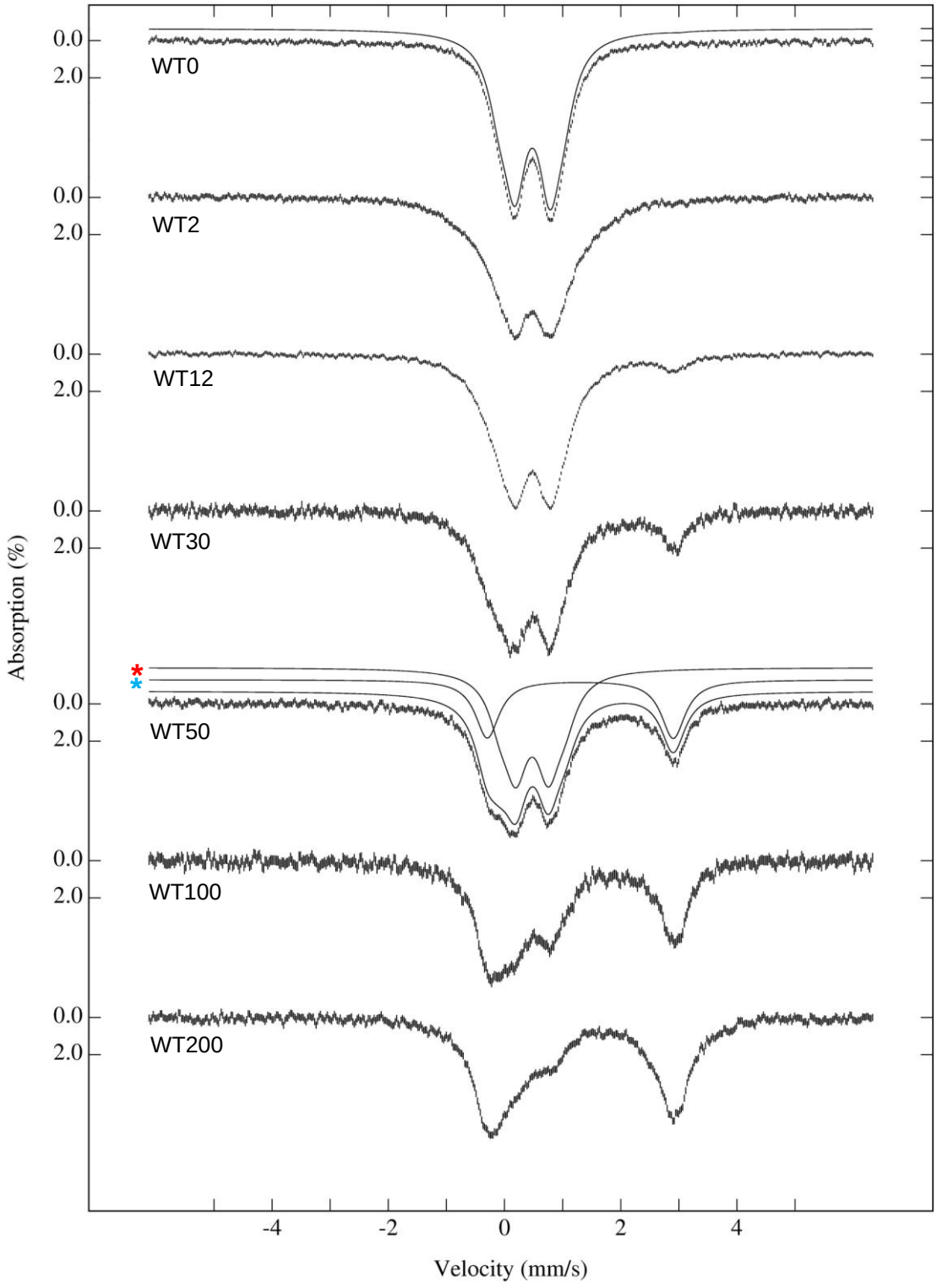

Figure 28 - Mössbauer spectra of Dps(wt) loaded with 144 ^{57}Fe/protein in anaerobic conditions. All spectra were recorded at 80 K in the absence of applied magnetic field. WT0 correspond to Dps reacted with NADH (positive mineral control). The others spectra were recorded after 2 (WT2), 12 (WT12), 30 (WT30), 50 (WT50), 100 (WT100) and 200 (WT200) minutes of adding WrbA flavoprotein. The quadrupole doublet of ferric core and ferrous iron simulation line, for WT50 sample, are indicated by (*) and (*), respectively. The total simulation line for WT0 and WT50 are represented by a full line above the respective spectra.

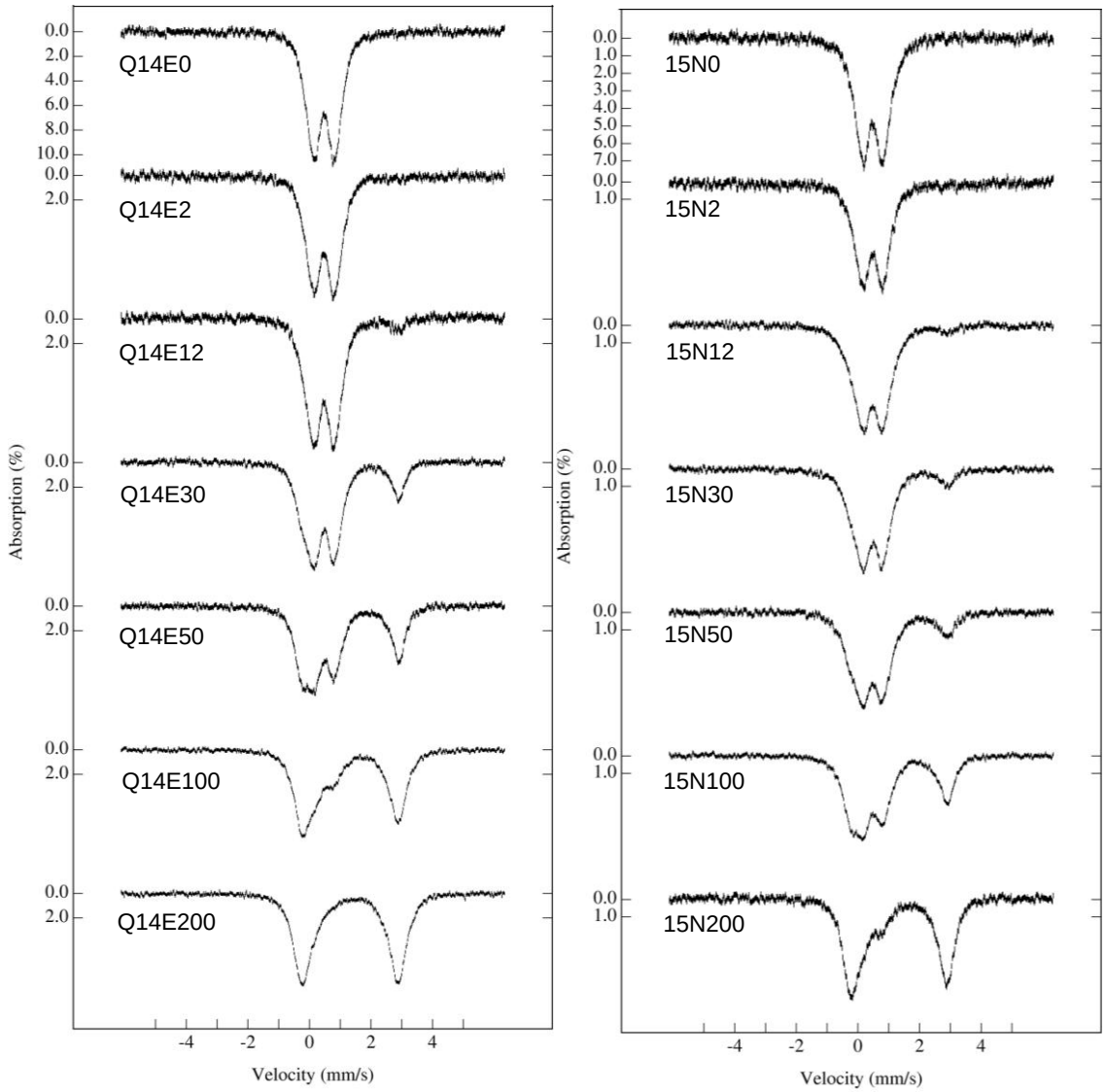

Figure 29 - Mössbauer spectra of Dps Q14E (right) and Δ15 (left) loaded with 144 ^{57}Fe/protein in anaerobic conditions. All spectra were recorded at 80K in absence of applied magnetic field. Q14E0 and 15N0 correspond to Dps reacted with NADH. The others spectra were recorded after 2 (Q14E2/15N2), 12 (Q14E12/15N12), 30 (Q14E30/15N30), 50 (Q14E50/15N50), 100 (Q14E100/15N100) and 200 (Q14E200/15N200) minutes of adding WrbA flavoprotein.

All spectra were analyzed using WMOSS© v. 2.51 (See Co.) software to quantify the ferric and ferrous species. The results are in annex 8.8. The percentage values of ferrous and ferric iron were used to calculate kinetic curves and constants. Figure 28 shows the obtained kinetics curves.

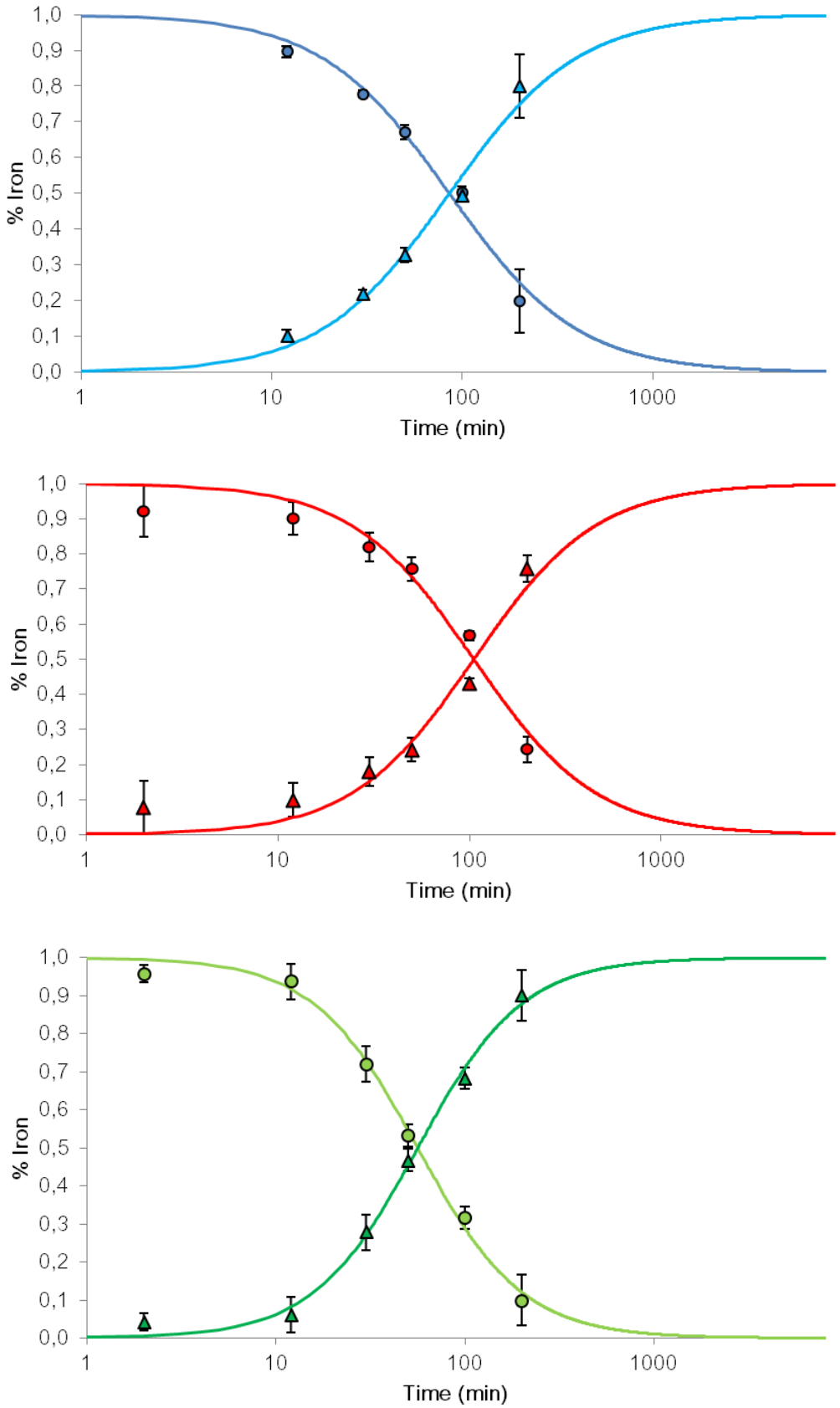

Figure 30 – Kinetic curves of iron release obtained from Mössbauer analysis. The circles represent the ferric species quantification while the triangles correspond to the ferrous. **A)** Dps(wt) sample **B)** Dps-Δ15 sample **C)** Dps-Q14E proteins. Curve fitting to a logistical function perform using Microsoft® Excel Solver tool.

Comparison of kinetic curves of all Dps proteins reveals that the half-time (50% of ferric and ferrous iron) of the process is different in all cases. The lowest half-time, 56 min, was obtained for Dps-Δ15, followed by the wild-type proteins with 86 min and Dps-Q14E with 105 min.

Previous experiments performed by Almeida with wild-type Dps revealed a first-order kinetic behavior.[68] The kinetic constant for iron release was obtained according to the following equation:

$$\ln\left(\frac{[A]}{[A_0]}\right) = -kt \quad \text{(eq. 11)}$$

where [A] is the substrate (ferric core) concentration at time *t* and $[A]_0$ the concentration at time zero.

Figure 29 displays linear representations of kinetic data for all Dps proteins allowing determination of kinetic constants. The kinetic constant obtained for wild-type Dps was 0.008 ± 0.0002 min^{-1}, very similar to the one determined before by Almeida of 0.011 ± 0.0003 min^{-1}.

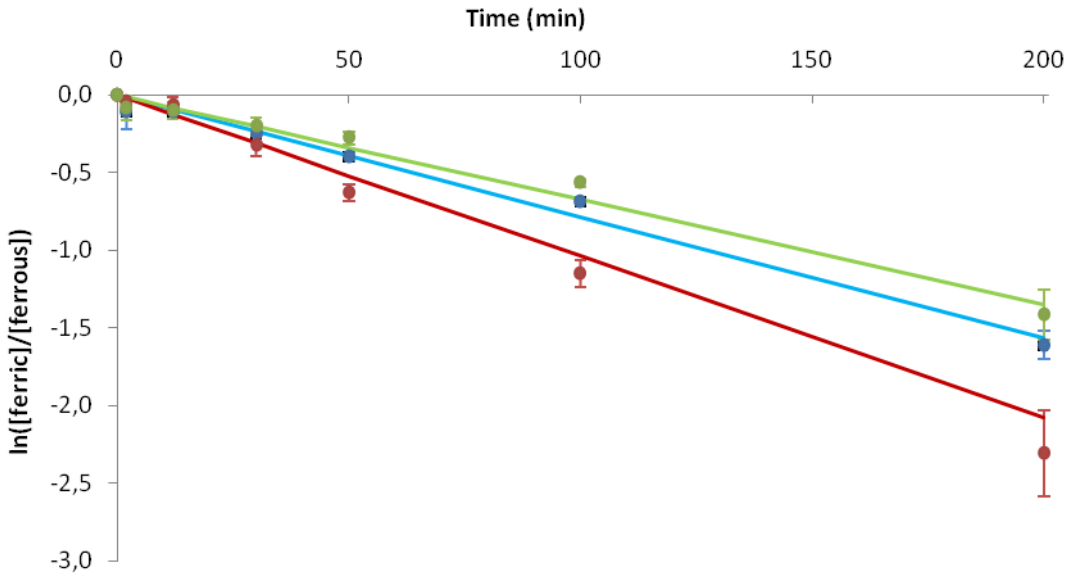

Figure 31- Kinetic results for WT (blue), N15 (red) and Q14E (green) samples. The regression lines have the following equations; **WT:** y= (-0.8 ± 0.02) x 10^{-2} x (R^2=0.992); **N15:** y=(-1.0 ± 0.03) x 10^{-2} x (R^2=0.993); **Q14E:** y= (-0.6 ± 0.02) x 10^{-2} x (R^2=0.989).

For the N15 sample, the constant obtained is 0.010 min^{-1} and the Q14E is 0.006 min^{-1}. Although among the mutants the value seems to have some difference, they are probably the same within the experimental errors. For example, WT values are very similar, especially N15 with the constant previously obtained. This variation may be caused by errors in reaction time,

because thawing and freezing cycles of each sample are not exactly the time for which the release reaction is stopped /resumed.

As result of some operational impediments, it was not possible to record the spectrum of the control samples. However, in wild-type Dps is known that NADH as itself is not able to start the iron release of Dps nanocavity in this setup conditions. The same need to be proven for mutant.

4.7.2 Kinetic characterization by optical spectroscopy

Mössbauer spectroscopy is an experimental technique with high accuracy. However, this requires large amounts of proteins and several hours of acquisition of each spectrum. Also, equipment maintenance is not straightforward and the necessary equipment has a relatively high cost. Therefore, to reduce these limitations, a new methodology to study the kinetics of iron release was developed, based on the iron quantification *o*-phenanthroline method and utilizing the experimental conditions used on the preparation of Mössbauer samples (replacing the ^{57}Fe solution by a $^{56}Fe_3SO_4$).

Control spectra of each component were characterized by UV-Visible spectroscopy (Figure 32).

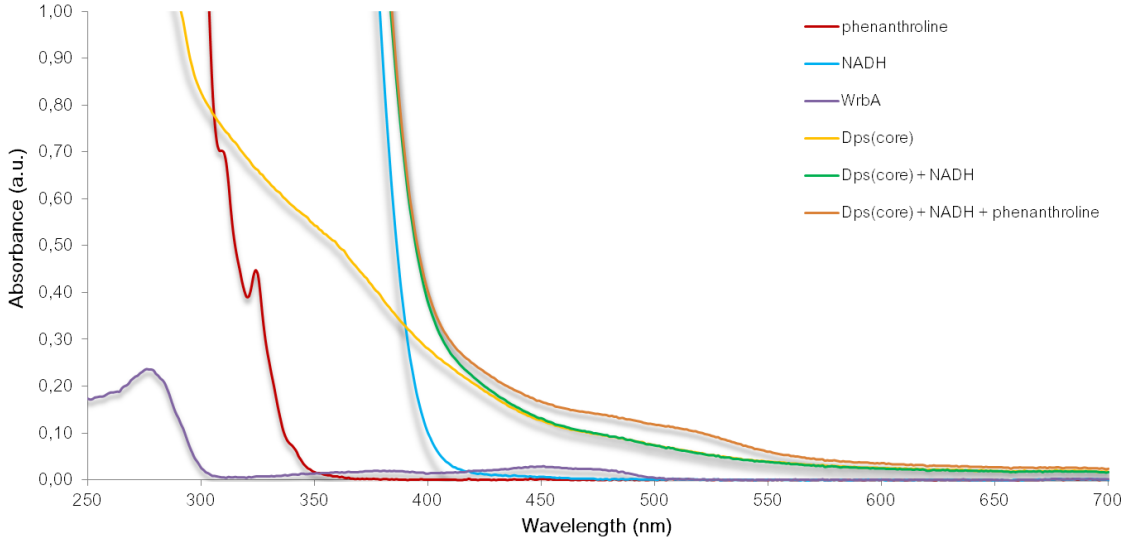

Figure 32 - UV-Visible spectra of the substrates of the anaerobic iron release reaction in Dps in 200 mM MOPS pH 7.6, 200 mM NaCl buffer. Iron-loaded Dps in yellow (0.5 µM), NADH in blue (0.3 mM), *o*-phenanthroline in red (0.3 mM) and WrbA in violet (12 µM); NADH reacted Dps (144 Fe/protein) in green and NADH- phenanthroline reacted Dps in brown.

The spectra observed for the solution Dps (core), in the presence of NADH and phenanthroline, doesn't match to the sum of the individual spectrum of each of the components. In fact, the sum of Dps spectra (core), NADH and phenanthroline should correspond to the Dps

(core) + NADH spectrum. The presence of a large absorption band between 450 and 550 nm, is attributed to the ferroin complex formed with residual iron, which is still in solution.

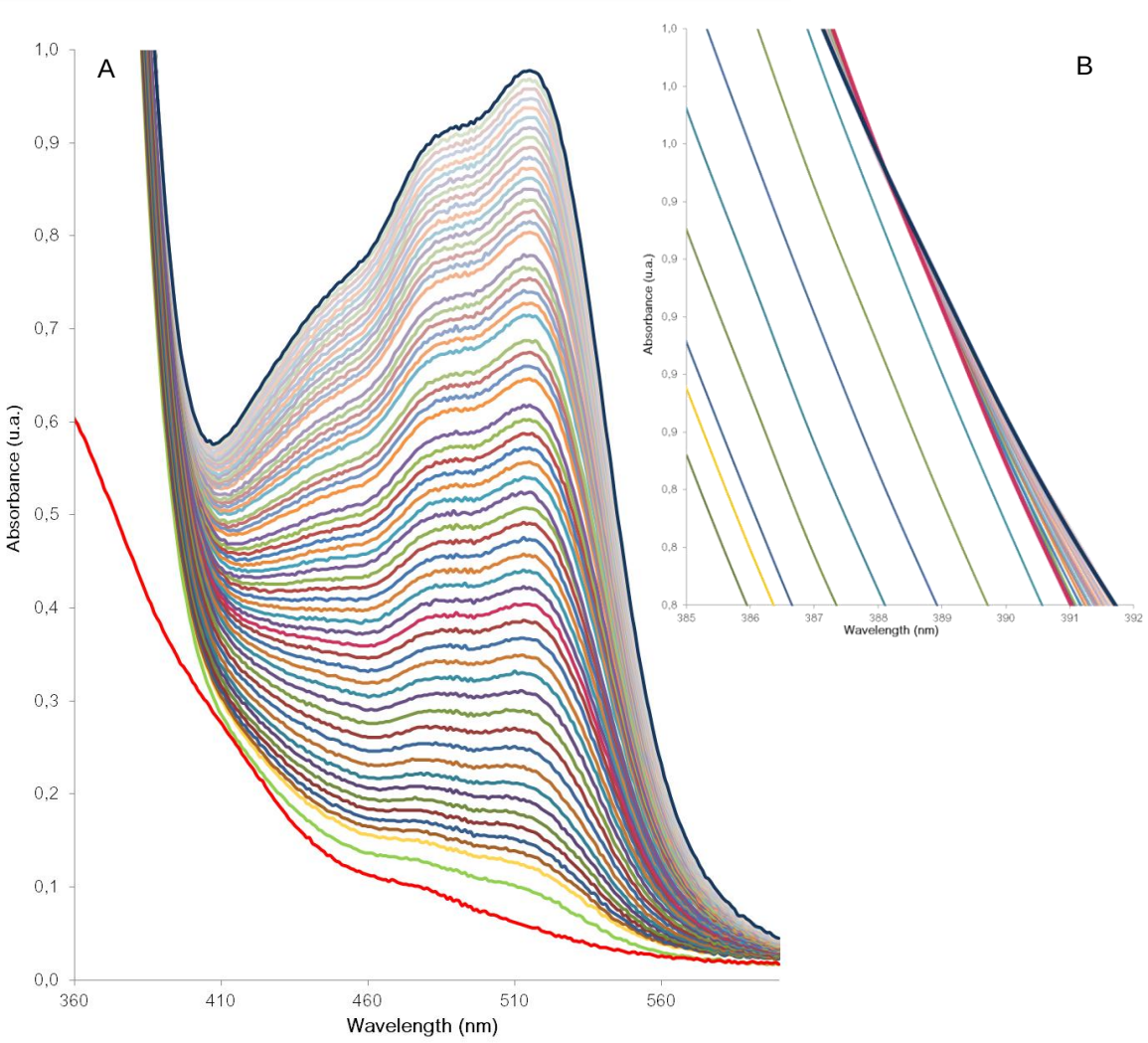

Figure 33 - Anaerobic iron release kinetic assay by Dps-NADH-WrbA system. **A)** The spectrum in red represents the phenanthroline (3.9 mM) reacted Dps (5.5 µM) mixture. Then was added NADH (3.9 mM) and recorded the spectrum marked at green. The yellow spectrum correspond to the 0.47 min of reaction, after added WrbA (66 µM). The following were recorded over time with Abs_{510nm} increasing. The blue spectrum correspond to 274.48 min of reaction. **B)** Close view of inflexion point. The pink and blue highlighted spectra correspond to 74.12 min and 274.48 min, respectively.

The spectrum to the mixture of Dps(wt) with WrbA(FMN) (x12 Dps), NADH (x5 Fe) and phenanthroline (x5 Fe) was acquired as a function of time (0.47 to 274.48 minutes). After adding WrbA, iron is released from the cavity of Dps and forms a complex with three molecules of phenanthroline. This complex ion has an absorption maximum at 510 nm.

In figure 33 is noted the increase of the peak at 510 nm over the reaction time. Due to the consumption of NADH, the absorbance at less than 400nm decreased slightly. In Fig 33-b is possible to verify the highlighted spectrum obtained in 74.12 and 274.48 min, that there is an inflection point at approximately 389 nm.

The same experience was repeated with DpsΔ15 and DpsQ14E. As mentioned in the previous section, the data presented were analyzed to obtain the rate constant of liberation of iron.

Figure 34 shows data obtained according to the equation 11. Unlike the results of Mössbauer, three Dps variants have slight deviations, which suggest that the differences observed in the previous point should really from experimental errors.

However, the kinetic constant, despite being very similar between the various Dps, are much lower than the calculated constants in Mössbauer experiments. In some way, the addition of phenanthroline could inhibit the process. More, the obtained curves do not show the same first order behavior observed in the Mössbauer experiments.

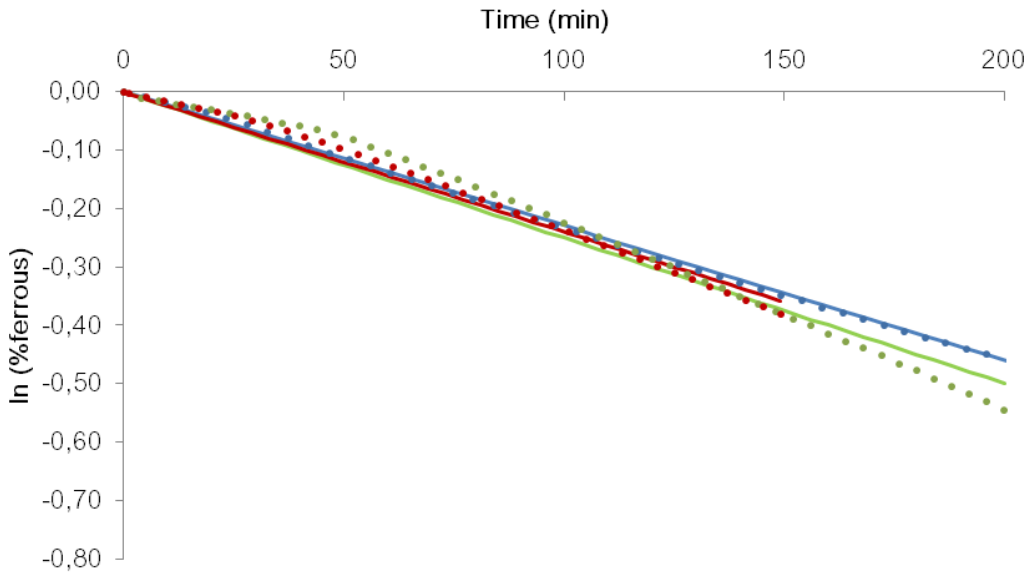

Figure 34- Kinetic observed for Dps wild-type (blue), Q14E (green) and Δ15 (red). The linear regression obtained for each data set was: **WT**: y= (-2.3±0.003) x 10^{-3} χ (R^2=0.999), **Q14E**: y=(-2.5 ±0.035) x10^{-3} χ (R^2=0.990), **Δ15**: y=(2.4 ± 0.027) x 10^{-3} χ (R^2=0.994)

To confirm this hypothesis, the experiment was repeated but the o-phenanthroline was added 100 min after addition of WrbA. The kinetics observed from that time was compared with the one previously obtained.

Comparison of the wild-type kinetic results obtained by UV-Visible spectroscopy based on the o-phenanthroline assay with the ones from the Mössbauer spectroscopy assay is represented in figure 35. Indeed, the kinetic constant observed is lower than the kinetic of Mössbauer. However, when the release occurs in the absence of phenanthroline, iron seems to approximately follow the same kinetics of wild-type during the first 100 min. From the moment in which the phenanthroline is added (100 min), the slope changes to a value similar to the UV-Visible spectroscopy based assay, which confirms an inhibition effect.

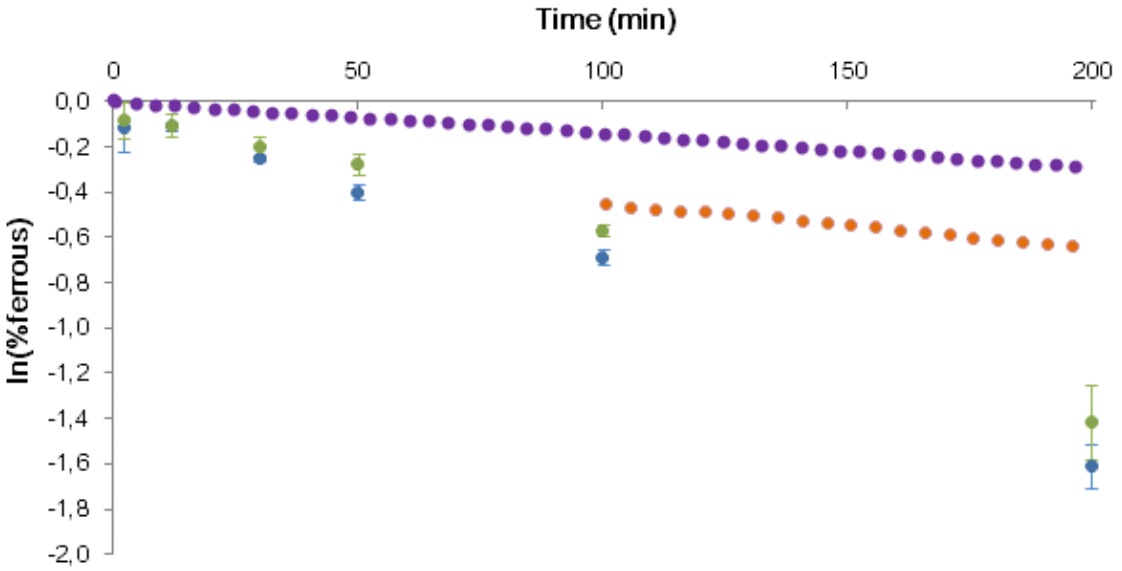

Figure 35- Phenanthroline kinetic data compared with Mössbauer results. The dots marked at orange are from wild-type kinetic recorded when phenanthroline is added 100 min after WrbA addition. Violet results correspond to the wild-type kinetic based on o-phenanthroline assay. Mossbauer result for WT, Q14E samples are marked at blue and green respectively.

There were also two types of controls prepared to verify that i) NADH, in the presence of phenanthroline, is unable to release iron by itself and ii) if WrbA needs NADH for the same purpose. In order to study this, were kept the same ratios of previous.

In the first control (the mixture of Dps (core) with NADH and phenanthroline - NADH control), the NADH revealed that is able to release iron since an absorbance rise at 510 nm after addition of NADH is observed (Figure 36). This is not a phenomenon observed in Mössbauer samples. The presence of phenanthroline might shift the equilibrium of the redox reaction; and, therefore, it is possible to help NADH driving the reduction reaction required for the iron release.

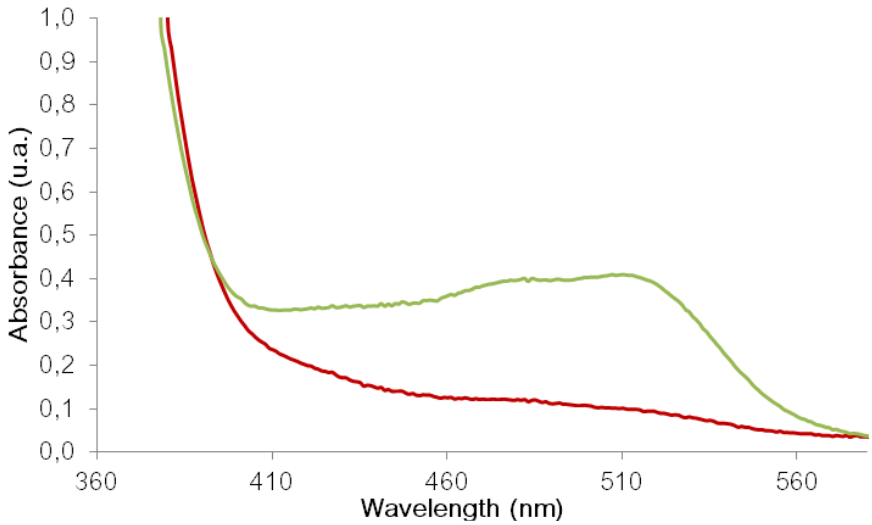

Figure 36- Spectra recorded 3.62 (red) and 462 (green) min after NADH was added to Dps(core) and phenanthroline.

By comparing the kinetics of Dps(wt) with the ones obtained in NADH control experiment, it was found that the release constant of the NADH/phenantroline dependent process is much lower (figure 37).

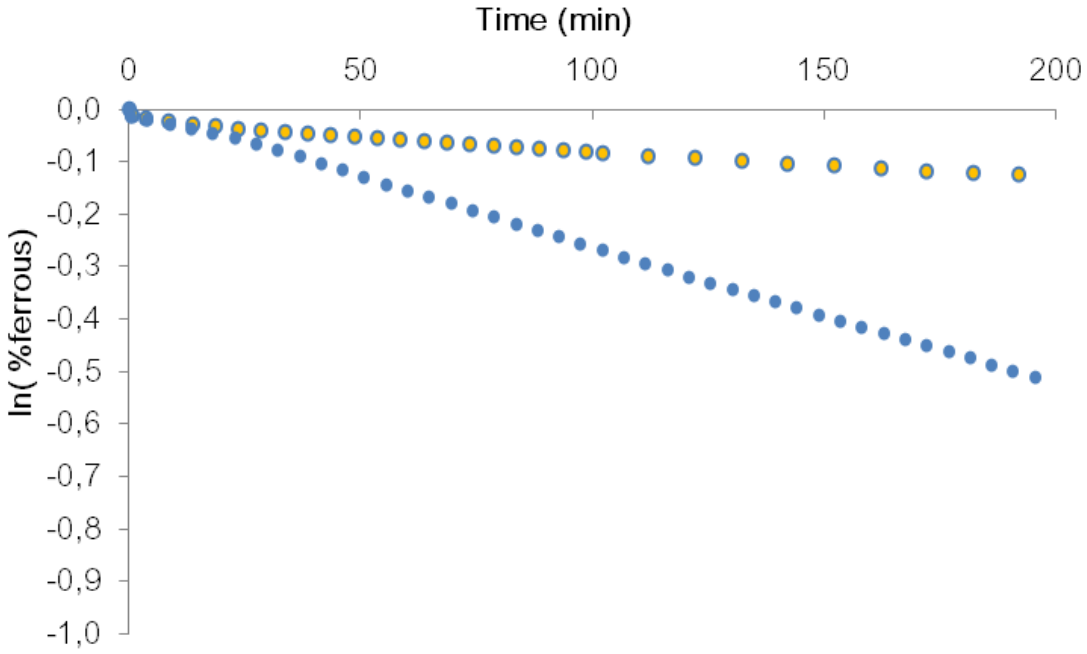

Figure 37- Kinetic of wild-type (blue) and NADH control samples (yellow).

In the case of Dps(core) mixture with Wrba (FMN) and phenanthroline (WrbA control), the iron release does not occurs over time. As such, if added NADH to the mixture, the absorbance at 510nm increased, which means that, without WrbA, NADH has no ability to cause the release of iron (Figure 38).

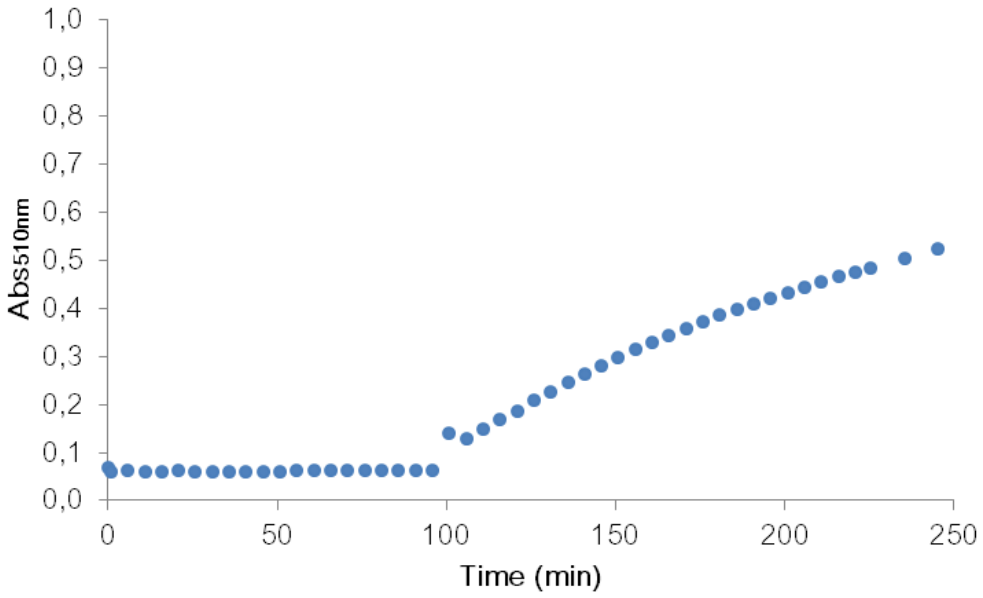

Figure 38- Absorbance recorded at 510 nm for WrbA control. At the 100 min WrbA was added and iron release occurs.

4.8 Docking Dps and ferroin/phenanthroline

The results presented above point to an inhibitory effect when phenanthroline is used. A possible explanation for this observation is that some of the amino acid residues relevant for the electron transfer complex are impaired. Studying the docking process between Dps and phenanthroline could give clues about the structural perspective of the process and help understanding if the formation of an electron transfer complex is being disturbed.

Using Autodock Vina software[120], A.Loupas performed the docking of phenanthroline and ferroin with Dps.[121] 90% of the obtained results show that the amino acids that interact with phenanthroline are N4, G75, K42, W149 and R152.

Figure 39 shows the results obtained, a possible docking between Dps and phenantroline (solution for which less docking energy is obtained).

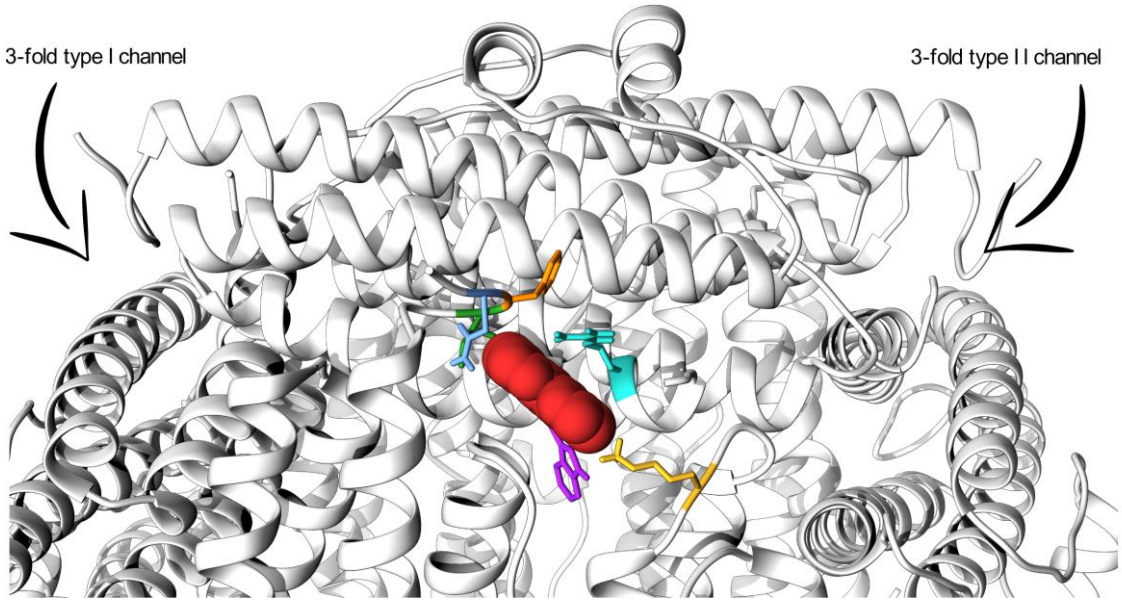

Figure 39- Best result for Dps and phenanthroline docking. The side-chain of the following amino acids interaction with phenanthroline (red): N4 (blue), F5 (orange), I6 (green), L42 (yellow), W149 (cyan) and R152 (purple)

In the case of docking with the ferroin, the most affected amino acids are E90, P92, E93. The result with the best energy is represented in figure 40. Combining this information with the Dps:WrbA docking results shows that the amino acids of the Dps:phenanthroline interaction are between the amino acids within 5 Å of Dps and WrbA interface.

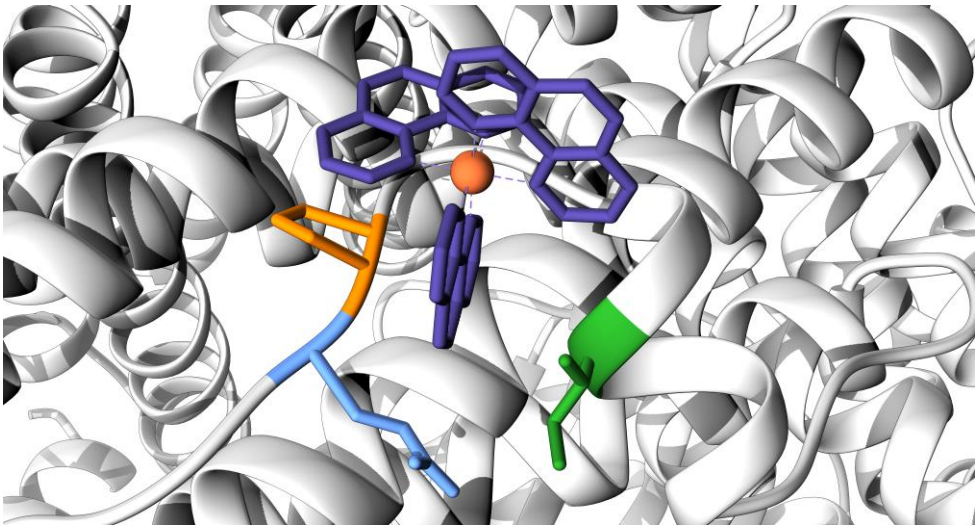

Figure 40- Best scored docking of Dps with ferroin (purple). The side-chain of the aminoacids who interact with ferroin are marked at orange (P92), blue (E93) and green (E90).

This bioinformatic result emphasizes that phenanthroline interacts in the same region as WrbA and can possibly prevent the proper amino acids side chains from participating in the electron transfer reaction.

Admitting that functional important residues are conserved across sequences, the amino acids that are most likely responsible for the interactions studied here should be conserved among Dps proteins.

Confsurf server was used to assign to each amino acid in the sequence Dps (sequence at annex 8.1) a conservation index (Figure 41).

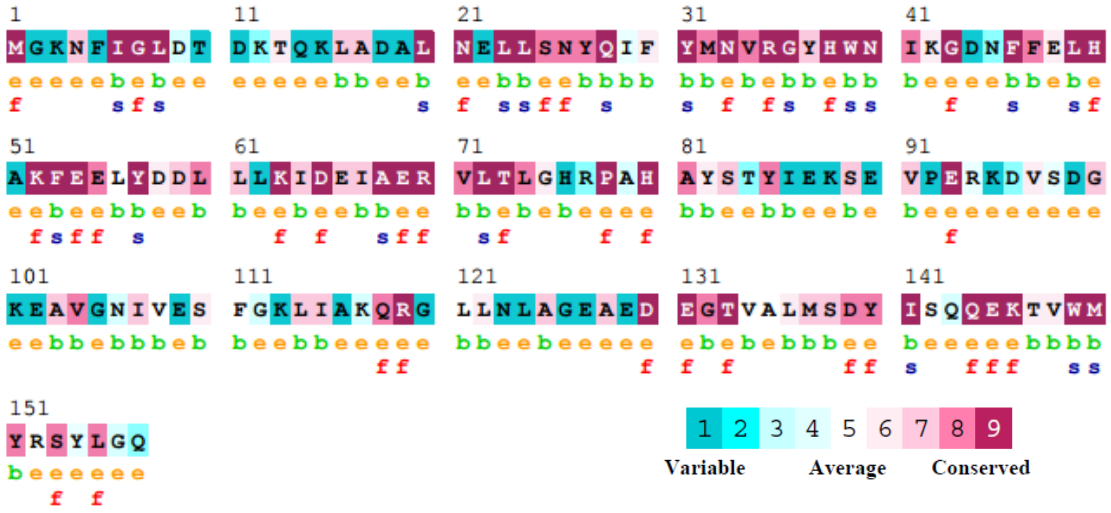

Figure 41- Confsurf results for Dps sequence**. e -** An exposed residue according to the neural-network algorithm; **b -** A buried residue according to the neural-network algorithm; **f -** A predicted functional residue (highly conserved and exposed); **s -** A predicted structural residue (highly conserved and buried).

The following table shows the results from the analysis regarding the conserved residues that have shown importance in all dockings. Some of the amino acids present were solution for more than one docking. The docking Dps:ferroin showed common amino acid with vdw+elec docking of Dps with model 5 of WrbA.

Table 12- Detailed information about conservation of some amino acids from docking results.

Amino acid	Type of docking	Conservation
N4	Dps/Phen	Not conserved
F5	Dps/WrbA	Not conserved. The next three amino acids has the highest index
K42	Dps/WrbA; Dps/Phen	Not conserved. The next amino acids has the highest index
G75	Dps/WrbA; Dps/Phen	Not conserved. The next two amino acids has the highest index
R77	Dps/WrbA	Not conserved. The next amino acids has the highest index
E90	Dps/Ferroin	Index 7 of conservation
P92	Dps/Ferroin	Not conserved
E93	Dps/Ferroin	Conserved
E102	Dps/WrbA	Not conserved
W149	Dps/Phen	Not conserved
R152	Dps/WrbA; Dps/Phen	Not conserved. The next amino acids has the highest index
G157	Dps/WrbA	Not conserved. The next amino acids has the highest index

Using another bioinformatics tool, it is possible to predict, based on the amino acid sequence, the effect of a point mutation. Amongst the amino acids that are specified in the above table, having or displaying conserved neighbors, it was found some high score for point mutation effect. The results for all Dps sequence are present in annex 8.9.

G43, L74, P78 and W149 have a high score when mutated by any amino acid. Two of these are neighbors of K43 and G75 for both Dps:phenanthroline and Dps:WrbA docking. The other two residues may also be relevant since Dps:phenanthroline docking area is the same of Dps:WrbA.

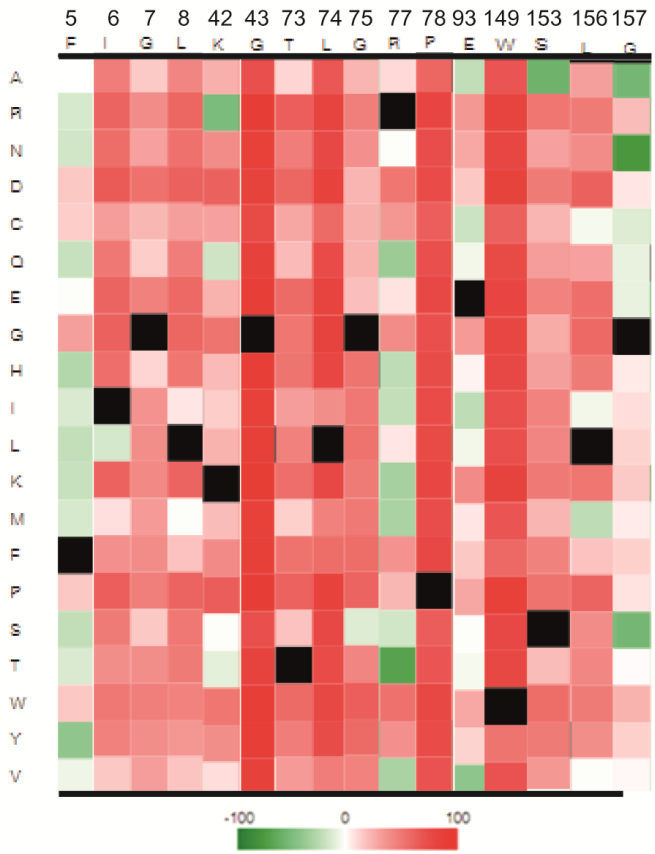

Figure 42- Effect of point mutation results of Predict Protein server. Each column corresponds to a Dps aminoacid. The columns are organized accordingly to the sequence of Dps protein.

5 . Conclusion and general overview of results

Dps wild-type protein was produced in *E.coli* BL21(DE3) cells with the over-expression vector Dps(wt)-pEt21c(+). After cell lysis, and harvested by various centrifugations, Dps was purified through HPLC chromatography using a DEAE-Sepharose, Superdex and Q-Resource column.

After the purification procedure the obtained protein was used to study the kinetics of iron release. For ferric iron to be reduced, Dps needs a redox partner, like WrbA, which mediates electron transfer from NADH. To accomplish its function, WrbA uses a FMN cofactor.

To rationalize obtained results and get a more detailed structural perspective of this system, WrbA structure was modeled by homology and *ab initio* servers. Robetta server was able to calculate the two best models (model 4 and model 5) that were used for a docking with Dps structure with ClusPro server.

ClusPro perform the docking accordingly to four different score functions. Analyzing the 5 best solution of each one, it was conclude that the F5, E102, R152, G157, K42 and R77 residues might have some relevance in the electronic transfer or in the WrbA:Dps interaction/complex formation. Since it is known that the N-terminal is also important for the DNA binding capacity of Dps, variants DpsΔ15 and DpsQ14E were also studied and kinetic parameters determined by the same procedure used for wild-type protein.

To determine kinetic parameters it was needed to acquire spectra for different reaction times. When reaction starts the ferric iron core is reduced and starts releasing ferrous iron in solution. Using high-temperature Mössbauer spectroscopy to probe the kinetic process results in the detection of a ferric iron quadrupole doublet (δ= 0.47-0.48 mm/s and ΔE_Q= 0.6-1.11 mm/s) that decreases over time, giving rise to high-spin ferrous iron quadrupole doublet (with approximately δ= 1.27 mm/s and ΔE_Q= 3.28 mm/s). Ferrous and Ferric contribution at each spectrum was analyzed and quantified with WMOSS© v. 2.51 (See Co.) software. The iron release for wild-type, Q14E and Δ15 variants follow a first-order kinetic, with a rate constant of 0.008 (±0.0002), 0.006 (±0.0002), 0.010 (±0.0003), respectively. Despite this, values might appear somehow different, they are similar within experimental error and very similar to the constant obtained by Almeida[68] with the same setup (0.011 (±0.0003) min^{-1}). So, the N-terminal shows no relevant function in iron release step.

Based on o-phenanthroline assay for iron quantification, a kinetic assay was developed to follow iron release in anaerobic conditions. The result showed that the three Dps variants have no significant difference regarding the kinetic profile obtained, but rate constants were significantly lower than those obtained by Mössbauer spectroscopy probed kinetic measurements. Phenanthroline might cause an inhibitor effect and in order to understand that effect, the kinetic assays were repeated in the absence of phenanthroline. Only after 100 min,

phenanthroline was added and UV-Visible spectrums were recorded over time. Such procedure allowed us to conclude that some inhibitor effect does occur when phenanthroline is present.

This last results show that one could devise an UV-Visible assay that is faster and less expensive than the one used for Mössbauer spectroscopy analysis. However, one should not use a continuous essay where phenanthroline is present in the reaction media. The use of this chelator should be restricted to the detection part of the assay which will have to be discontinuous in nature.

An electron transfer pathway blocking can cause the inhibitor effect caused by phenanthroline or ferroin. Again, taking a structural look into this system, A. Loupas[121], performed a docking Dps:phenanthroline and Dps:ferroin with AutoDock Vina software. 90% of Phenanthroline docking results show this molecule interact with N4, G75, K42, W149 and R152 amino acid of Dps. All this amino acids are also verified to be at less than 5Å of Cluspro predicted WrbA:Dps docking site (with the exception of model 5 vdw+elec docking results). For 50% of ferroin docking, the amino acids were the E90, P92, E92. These amino acids are within the vdw+elec docking result of WrbA model 5.

Finally, when we look at the conserved amino acid and the effect of point mutation of the referred residues and its vicinity, G43, L74, P78 e W149 appear to be good candidates of amino acid that participate and are important in the electron transfer pathway.

6 . Future prospects

So far there is still a long way to go to understand the iron release and electron transfer reaction. While is clear that WrbA mediates a specific electron transfer between a donor (NADH) and Dps, the mechanism of the macromolecular interactions is still not fully understood.

The development of a novel assay for kinetic studies which can use less biologic materials as well as being faster regarding data acquisition is important. Due to the observed inhibition one should consider to use a discontinuous based assay, or maybe the use of other chelators. There is some chelator molecules used in medical therapy that can be doubly interesting for this application, not only to provide a new inhibition free assay, but also to comprehend how effective they are in the therapeutically function.

Most importantly, from the docking results and experimental results, we can postulate some amino acids of Dps whose side-chain might be involve in electron transfer reaction. Similar to what was done in this work with DpsQ14E, DpsΔ15 and Dps(wt) new mutants can be produced and compared with wild-type.

In this case, using the docking results and additional bioinformatics information, mutation at W149 can be the priority to study. W149 was found to be of importance in the majority of the docking Dps:WrbA and Dps:phenanthroline complexes. Besides, is a conserved amino acid and has a high score for point mutation effect. The second option is to mutant G43, L74 or P78 amino acids. A P93 mutant should also provide significant information. This is a conserved amino acid that might be involved in Dps:WrbA (see vdw+ elec docking of WrbA model 5 with Dps) and in Dps:ferroin interaction.

7 . References

[1] W. Kaim, B. Schwederski, and A. Klein, "*Bioinorganic Chemistry - Inorganic Elements in the Chemistry of Life: An Introduction and Guide*." Wiley, 2013.

[2] J. Davidge and D. r. Williams, “Speciation dependent intake and uptake of essential elements,” in *Metal ions in biological Systems: Volume 41 Metal ions and their complexes in medication*, A. Sigel and H. Sigel, Eds. CRC Press, 2004.

[3] I. Bertini, H. B. Gray, S. Lippard, and J. Valentine, "*Bioinorganic Chemistry*." University Science Books, 1994.

[4] R. M. Roat-Malone, "Inorganic Chemistry Essentials", in *Bioinorganic chemistry: a short course*, John Wiley & Sons Inc., 2002.

[5] E. P. Widmaier, H. Raff, and K. T. Strang, “Neuronal signalling and the structure of the nervous system,” in *Vander’s human Physiology: the mechanism of body function*, 9th ed., McGraw-Hill Companies, 2004.

[6] I. Bertini and P. Turano, “Metal ions and proteins: binding, stability and folding,” in *Biological inorganic chemistry: Structure and reactivity*, University Science Books, 2007.

[7] T. J. Lyons and D. J. Eide, “Transport and storage of metal ions in biology,” in *Biological inorganic chemistry: Structure and reactivity*, University Science Books, 2007.

[8] A. L. Lehninger, D. L. Nelson, and M. M. Cox, “Protein function,” in *Lehninger Principles of Biochemistry*, 4th ed., W. H. Freeman, Ed. 2004.

[9] S. M. Williams, A. V. Chandran, M. S. Vijayabaskar, S. Roy, H. Balaram, S. Vishveshwara, M. Vijayan, and D. Chatterji, “A histidine aspartate ionic lock gates the iron passage in miniferritins from Mycobacterium smegmatis,” *J. Biol. Chem.*, vol. 289, pp. 11042–11058, 2014.

[10] N. E. Le Brun, A. Crow, M. E. P. Murphy, a G. Mauk, and G. R. Moore, “Iron core mineralisation in prokaryotic ferritins.,” *Biochim. Biophys. Acta*, vol. 1800, no. 8, pp. 732–44, Aug. 2010.

[11] S. C. Andrews, A. K. Robinson, and F. Rodriguez-Quiñones, “Bacterial iron homeostasis,” *FEMS Microbiol. Rev.*, vol. 27, no. 2–3, pp. 215–237, Jun. 2003.

[12] F. Bou-Abdallah, “The iron redox and hydrolysis chemistry of the ferritins.,” *Biochim. Biophys. Acta*, vol. 1800, no. 8, pp. 719–31, Aug. 2010.

[13] R. M. Roat-Malone, “Electronic and geometric structures of metals in biological systems,” in *Bioinorganic chemistry: a short course*, 2nd ed., John Wiley & Sons Inc., 2007, pp. 13–18.

[14] R. M. Roat-Malone, “Metals in biological systems: a survey,” in *Bioinorganic chemistry: a short course*, 2nd ed., John Wiley & Sons Inc., 2007, pp. 3–6.

[15] R. M. Roat-Malone, *Bioinorganic Chemistry: a short course*, 2nd ed. John Wiley & Sons Inc., 2007.

[16] I. Bertini, H. B. Gray, E. I. Stiefel, and J. Valentine, *Biological Inorganic Chemistry: Structure and Reactivity*. University Science Books, 2007.

[17] J. a Imlay, “Pathways of oxidative damage.,” *Annu. Rev. Microbiol.*, vol. 57, pp. 395–418, 2003.

[18] R. Chakraborty, V. Braun, K. Hantke, and P. Cornelis, "*Iron Uptake in Bacteria with Emphasis on E.coli and Pseudomonas*." 2013.

[19] K. Zeth, “Dps biomineralizing proteins: multifunctional architects of nature,” *Biochem. J.*, vol. 445, no. 3, pp. 297–311, 2012.

[20] J. Wang and K. Pantopoulos, “Regulation of cellular iron metabolism.,” *Biochem. J.*, vol. 434, no. 3, pp. 365–381, 2011.

[21] P. Arosio, R. Ingrassia, and P. Cavadini, “Ferritins: A family of molecules for iron storage, antioxidation and more,” *Biochim. Biophys. Acta (BBA)-Bioenergetics*, vol. 1790, pp. 589–599, 2008.

[22] L. E. Bevers and E. C. Theil, “Maxi- and mini-ferritins: minerals and protein nanocages.,” *Prog. Mol. Subcell. Biol.*, vol. 52, pp. 29–47, 2011.

[23] M. Mahmoudi, S. Sant, B. Wang, S. Laurent, and T. Sen, “Superparamagnetic iron oxide nanoparticles (SPIONs): development, surface modification and applications in chemotherapy.,” *Adv. Drug Deliv. Rev.*, vol. 63, no. 1–2, pp. 24–46, 2011.

[24] M. Bozzi, G. Mignogna, S. Stefanini, D. Barra, C. Longhi, P. Valenti, and E. Chiancone, “A novel non-heme iron-binding ferritin related to the DNA-binding proteins of the Dps family in Listeria innocua,” *J. Biol. Chem.*, vol. 272, no. 6, pp. 3259–3265, 1997.

[25] J. L. Smith, “The physiological role of ferritin-like compounds in bacteria.” *Crit. Rev. Microbiol.*, vol. 30, no. 3, pp. 173–185, 2004.

[26] P. Arosio, G. Adelman, and W. Drysdale, “On ferritin heterogeneity. Further evidence for heteropolymers.” *J. Biol. Chem.*, pp. 4451–4458, 1978.

[27] M. Almiron, A. Link, D. Furlong, and R. Kolter, “A novel DNA-binding protein with regulatory and protective roles in starved Escherichia coli.” *Genes Dev.*, pp. 2646–2654, 1992.

[28] A. Martinez and R. Kolter, “Protection of DNA during oxidative stress by the nonspecific DNA-binding protein Dps.” *J. Bacteriol.*, vol. 179, no. 16, pp. 5188–5194, 1997.

[29] R. Grant, D. Filman, and S. Finkel, “The crystal structure of Dps, a ferritin homolog that binds and protects DNA,” *Nat. Struct. …*, 1998.

[30] T. Haikarainen and A. C. Papageorgiou, “Dps-like proteins: structural and functional insights into a versatile protein family.” *Cell. Mol. Life Sci.*, vol. 67, no. 3, pp. 341–51, Feb. 2010.

[31] A. Ilari and S. Stefanini, “The dodecameric ferritin from Listeria innocua contains a novel intersubunit iron-binding site,” *Nat. Struct. …*, 2000.

[32] S. Franceschini, P. Ceci, F. Alaleona, E. Chiancone, and A. Ilari, “Antioxidant Dps protein from the thermophilic cyanobacterium Thermosynechococcus elongatus: An intrinsically stable cage-like structure endowed with enhanced stability,” *FEBS J.*, vol. 273, no. 21, pp. 4913–4928, 2006.

[33] J. T. Macedo, “Functional and structural studies of a mini-ferritin protein,” 2014.

[34] L. Ping, R. Büchler, A. Mithöfer, A. Svatoš, D. Spiteller, K. Dettner, S. Gmeiner, J. Piel, B. Schlott, and W. Boland, “A novel Dps-type protein from insect gut bacteria catalyses hydrolysis and synthesis of N-acyl amino acids,” *Environ. Microbiol.*, vol. 9, no. 6, pp. 1572–1583, 2007.

[35] S. Nair and S. E. Finkel, “Dps Protects Cells against Multiple Stresses during Stationary Phase Dps Protects Cells against Multiple Stresses during Stationary Phase,” *J Bacteriol*, vol. 186, no. 13, pp. 4192–8, 2004.

[36] C. J. Sund, E. R. Rocha, A. O. Tzinabos, W. G. Wells, J. M. Gee, M. A. Reott, D. P. O’Rourke, and C. J. Smith, “The Bacteroides fragilis transcriptome response to oxygen and H2O2: the role of OxyR and its effect on survival and virulence,” *Mol. Microbiol.*, vol. 67, no. 1, pp. 129–142, Nov. 2007.

[37] S. Gupta and D. Chatterji, “Bimodal protection of DNA by Mycobacterium smegmatis DNA-binding protein from stationary phase cells,” *J. Biol. Chem.*, vol. 278, no. 7, pp. 5235–5241, 2003.

[38] G. Zhao, P. Ceci, A. Ilari, L. Giangiacomo, T. M. Laue, E. Chiancone, and N. Dennis Chasteen, “Iron and hydrogen peroxide detoxification properties of DNA-binding protein from starved cells. A ferritin-like DNA-binding protein of Escherichia coli,” *J. Biol. Chem.*, vol. 277, no. 31, pp. 27689–27696, 2002.

[39] M. Su, S. Cavallo, S. Stefanini, E. Chiancone, N. D. Chasteen, L. Sapienza, and P. A. Moro, “Articles The So-Called Listeria innocua Ferritin Is a Dps Protein . Iron Incorporation, Detoxification, and DNA Protection Properties,” pp. 5572–5578, 2005.

[40] X. Yang, E. Chiancone, S. Stefanini, A. Ilari, and N. Dennis Chasteen, “Iron oxidation and hydrolysis of a novel ferritin from Listeria innocua,” *Biochem. J.*, no. 349, pp. 783–786, 2000.

[41] S. Wolf, D. Frenkiel, T. Arad, and S. Finkel, “DNA protection by stress-induced biocrystallization,” *Nature*, vol. 400, no. July, pp. 83–85, 1999.

[42] B. Ren, G. Tibbelin, T. Kajino, O. Asami, and R. Ladenstein, “The Multi-layered Structure of Dps with a Novel Di-nuclear Ferroxidase Center,” *J. Mol. Biol.*, vol. 329, no. 3, pp. 467–477, Jun. 2003.

[43] P. Ceci, S. Cellai, E. Falvo, C. Rivetti, G. L. Rossi, and E. Chiancone, “DNA condensation and self-aggregation of Escherichia coli Dps are coupled phenomena related to the properties of the N-terminus,” *Nucleic Acids Res.*, vol. 32, no. 19, pp. 5935–5944, 2004.

[44] T. J. Stillman, M. Upadhyay, V. a Norte, S. E. Sedelnikova, M. Carradus, S. Tzokov, P. a Bullough, C. a Shearman, M. J. Gasson, C. H. Williams, P. J. Artymiuk, and J. Green, “The crystal structures of Lactococcus lactis MG1363 Dps proteins reveal the presence of an N-terminal helix that is required for DNA binding.,” *Mol. Microbiol.*, vol. 57, no. 4, pp. 1101–12, Aug. 2005.

[45] A. R. Arnold and J. K. Barton, “DNA protection by the bacterial ferritin Dps via DNA charge transport,” *J. Am. Chem. Soc.*, vol. 135, no. 42, pp. 15726–15729, 2013.

[46] L. N. Calhoun and Y. M. Kwon, “Structure, function and regulation of the DNA-binding protein Dps and its role in acid and oxidative stress resistance in Escherichia coli: a review.,” *J. Appl. Microbiol.*, vol. 110, no. 2, pp. 375–86, Feb. 2011.

[47] M. Polidoro, D. De Biase, B. Montagnini, L. Guarrera, S. Cavallo, P. Valenti, S. Stefanini, and E. Chiancone, “The expression of the dodecameric ferritin in Listeria spp. is induced

by iron limitation and stationary growth phase," *Gene*, vol. 296, no. 1–2, pp. 121–128, 2002.

[48] J. Pesek, R. Büchler, R. Albrecht, W. Boland, and K. Zeth, "Structure and mechanism of iron translocation by a Dps protein from Microbacterium arborescens," *J. Biol. Chem.*, vol. 286, no. 40, pp. 34872–34882, 2011.

[49] S. Altuvia, M. Almiron, G. Huisman, R. Kolter, and G. Storz, "The dps promoter is activated by OxyR during growth and by IHF and sigma s in stationary phase," *Mol. Microbiol.*, vol. 13, no. 2, pp. 265–272, Jul. 1994.

[50] K. Stephani, D. Weichart, and R. Hengge, "Dynamic control of Dps protein levels by ClpXP and ClpAP proteases in Escherichia coli," *Mol. Microbiol.*, vol. 49, no. 6, pp. 1605–1614, 2003.

[51] D. C. Grainger, M. D. Goldberg, D. J. Lee, and S. J. W. Busby, "Selective repression by Fis and H-NS at the Escherichia coli dps promoter," *Mol. Microbiol.*, vol. 68, no. 6, pp. 1366–1377, 2008.

[52] G. Bellapadrona, S. Stefanini, C. Zamparelli, E. C. Theil, and E. Chiancone, "Iron translocation into and out of Listeria innocua Dps and size distribution of the protein-enclosed nanomineral are modulated by the electrostatic gradient at the 3-fold 'ferritin-like' pores," *J. Biol. Chem.*, vol. 284, no. 16, pp. 19101–19109, 2009.

[53] G. H. Gauss, P. Benas, B. Wiedenheft, M. Young, T. Douglas, and C. M. Lawrence, "Structure of the DPS-like protein from Sulfolobus solfataricus reveals a bacterioferritin-like dimetal binding site within a DPS-like dodecameric assembly," *Biochemistry*, vol. 45, no. 36, pp. 10815–10827, 2006.

[54] K. Zeth, S. Offermann, L.-O. Essen, and D. Oesterhelt, "Iron-oxo clusters biomineralizing on protein surfaces: structural analysis of Halobacterium salinarum DpsA in its low- and high-iron states.," *Proc. Natl. Acad. Sci. U. S. A.*, vol. 101, no. 38, pp. 13780–13785, 2004.

[55] P. Ceci, E. Chiancone, O. Kasyutich, G. Bellapadrona, L. Castelli, M. Fittipaldi, D. Gatteschi, C. Innocenti, and C. Sangregorio, "Synthesis of iron oxide nanoparticles in Listeria innocua Dps (DNA-binding protein from starved cells): a study with the wild-type protein and a catalytic centre mutant.," *Chemistry*, vol. 16, no. 2, pp. 709–17, Jan. 2010.

[56] A. Kauko, A. T. Pulliainen, S. Haataja, W. Meyer-Klaucke, J. Finne, and A. C. Papageorgiou, "Iron Incorporation in Streptococcus suis Dps-like Peroxide Resistance Protein Dpr Requires Mobility in the Ferroxidase Center and Leads to the Formation of a Ferrihydrite-like Core," *J. Mol. Biol.*, vol. 364, no. 1, pp. 97–109, 2006.

[57] E. C. Theil, H. Takagi, G. W. Small, L. He, A. . Tipton, and D. Danger, "The ferritin iron entry and exit problem," *Inorganica Chim. Acta*, vol. 297, no. 1–2, pp. 242–251, Jan. 2000.

[58] T. Jones, R. Spencer, and C. Walsh, "Mechanism and kinetics of iron release from ferritin by dihydroflavins and dihydroflavin analogues." *Biochemistry*, vol. 17, no. 19, pp. 4011–4017, 1978.

[59] G. D. Watt, D. Jacobs, and R. B. Frankel, "Redox reactivity of bacterial and mammalian ferritin: is reductant entry into the ferritin interior a necessary step for iron release?," *Proc. Natl. Acad. Sci. U. S. A.*, vol. 85, no. 20, pp. 7457–7461, 1988.

[60] R. R. Crichton, F. Roman, and F. Roland, "Iron mobilization from ferritin by chelating agents," *J. Inorg. Biochem.*, vol. 13, no. 4, pp. 305–316, Jan. 1980.

[61] M. Castruita, L. a Elmegreen, Y. Shaked, E. I. Stiefel, and F. M. M. Morel, “Comparison of the kinetics of iron release from a marine (Trichodesmium erythraeum) Dps protein and mammalian ferritin in the presence and absence of ligands,” *J. Inorg. Biochem.*, vol. 101, no. 11–12, pp. 1686–91, Nov. 2007.

[62] G. N. L. Jameson, R. F. Jameson, and W. Linert, “New insights into iron release from ferritin: direct observation of the neurotoxin 6-hydroxydopamine entering ferritin and reaching redox equilibrium with the iron core,” *Org. Biomol. Chem.*, vol. 2, no. 16, p. 2346, 2004.

[63] X. Yang, P. Arosio, and N. D. Chasteen, “Molecular diffusion into ferritin: pathways, temperature dependence, incubation time, and concentration effects,” *Biophys. J.*, vol. 78, no. 4, pp. 2049–2059, 2000.

[64] W. Jin, H. Takagi, B. Pancorbo, and E. C. Theil, “‘Opening’ the Ferritin Pore for Iron Release by Mutation of Conserved Amino Acids at Interhelix and Loop Sites,” *Biochemistry*, vol. 40, no. 25, pp. 7525–7532, Jun. 2001.

[65] S. Lacour and P. Landini, “S-Dependent Gene Expression at the Onset of Stationary Phase in Escherichia coli: Function of S-Dependent Genes and Identification of Their Promoter Sequences,” *J. Bacteriol.*, vol. 186, no. 21, pp. 7186–7195, Nov. 2004.

[66] J. Wolfova, I. K. Smatanova, J. Brynda, J. R. Mesters, M. Lapkouski, M. Kuty, A. Natalello, N. Chatterjee, S.-Y. Chern, E. Ebbel, A. Ricci, R. Grandori, R. Ettrich, and J. Carey, “Structural organization of WrbA in apo- and holoprotein crystals,” *Biochim. Biophys. Acta*, vol. 1794, no. 9, pp. 1288–98, Sep. 2009.

[67] I. Kishko, B. Harish, V. Zayats, D. Reha, B. Tenner, D. Beri, T. Gustavsson, R. Ettrich, and J. Carey, “Biphasic kinetic behavior of E. coli WrbA, an FMN-dependent NAD(P)H:quinone oxidoreductase,” *PLoS One*, vol. 7, no. 8, p. e43902, Jan. 2012.

[68] N. Alexandra, “Estudo da Libertação de Ferro em Miniferritinas”, Tese de Mestrado, FCT-UNL, 2014.

[69] “BL21 (DE3) Competent Cells MB00601 kit protocol.” pp. NZYtech– genes & enzymes,2013.

[70] “NZY5 Competent Cells MB00401 kit protocol.” pp. NZYtech– genes & enzymes, 2013.

[71] “NZYMiniprep MB0101 kit protocol.” pp. NZYtech– genes & enzymes,2015.

[72] A. Orry and R. Abagyan, “Homology Modeling,” vol. 857, p. 419, 2012.

[73] P. A. Bates, L. A. Kelley, R. M. MacCallum, and M. J. E. Sternberg, “Enhancement of protein modeling by human intervention in applying the automatic programs 3D-JIGSAW and 3D-PSSM,” *Proteins Struct. Funct. Genet.*, vol. 45, no. S5, pp. 39–46, 2001.

[74] B. Contreras-Moreira and P. A. Bates, “Domain Fishing: a first step in protein comparative modelling,” *Bioinformatics*, vol. 18, no. 8, pp. 1141–1142, Aug. 2002.

[75] P. A. Bates and M. J. E. Sternberg, “Model building by comparison at CASP3: Using expert knowledge and computer automation,” *Proteins*, vol. 37, no. 3, pp. 47–54, 1999.

[76] R. D. Finn, A. Bateman, J. Clements, P. Coggill, R. Y. Eberhardt, S. R. Eddy, A. Heger, K. Hetherington, L. Holm, J. Mistry, E. L. L. Sonnhammer, J. Tate, and M. Punta, “Pfam: the protein families database,” *Nucleic Acids Res.*, vol. 42, no. D1, pp. D222–D230, Jan. 2014.

[77] P. E. Bourne, “The distribution and query systems of the RCSB Protein Data Bank,” *Nucleic Acids Res.*, vol. 32, no. 90001, p. 223D–225, Jan. 2004.

[78] N. K. Fox, S. E. Brenner, and J.-M. Chandonia, “SCOPe: Structural Classification of Proteins--extended, integrating SCOP and ASTRAL data and classification of new structures,” *Nucleic Acids Res.*, vol. 42, no. D1, pp. D304–D309, Jan. 2014.

[79] J. Soding, “Protein homology detection by HMM-HMM comparison,” *Bioinformatics*, vol. 21, no. 7, pp. 951–960, Apr. 2005.

[80] S. F. Altschul, T. L. Madden, a a Schäffer, J. Zhang, Z. Zhang, W. Miller, and D. J. Lipman, “Gapped BLAST and PSI-BLAST: a new generation of protein database search programs.,” *Nucleic Acids Res.*, vol. 25, no. 17, pp. 3389–402, Sep. 1997.

[81] “Ongoing and future developments at the Universal Protein Resource,” *Nucleic Acids Res.*, vol. 39, no. Database, pp. D214–D219, Jan. 2011.

[82] C. P. Ponting, J. Schultz, F. Milpetz, and P. Bork, “SMART: identification and annotation of domains from signalling and extracellular protein sequences,” *Nucleic Acids Res.*, vol. 27, no. 1, pp. 229–232, Jan. 1999.

[83] J. Soding, A. Biegert, and A. N. Lupas, “The HHpred interactive server for protein homology detection and structure prediction,” *Nucleic Acids Res.*, vol. 33, no. Web Server, pp. W244–W248, Jul. 2005.

[84] D. T. Jones, “Protein secondary structure prediction based on position-specific scoring matrices,” *J. Mol. Biol.*, vol. 292, no. 2, pp. 195–202, Sep. 1999.

[85] N. Fernandez-Fuentes, B. K. Rai, C. J. Madrid-Aliste, J. Eduardo Fajardo, and A. Fiser, “Comparative protein structure modeling by combining multiple templates and optimizing sequence-to-structure alignments,” *Bioinformatics*, vol. 23, no. 19, pp. 2558–2565, Oct. 2007.

[86] N. Fernandez-Fuentes, C. J. Madrid-Aliste, B. K. Rai, J. E. Fajardo, and A. Fiser, “M4T: a comparative protein structure modeling server,” *Nucleic Acids Res.*, vol. 35, no. Web Server, pp. W363–W368, May 2007.

[87] D. Rykunov, E. Steinberger, C. J. Madrid-Aliste, and A. Fiser, “Improved scoring function for comparative modeling using the M4T method,” *J. Struct. Funct. Genomics*, vol. 10, no. 1, pp. 95–99, Mar. 2009.

[88] L. A. Kelley, S. Mezulis, C. M. Yates, M. N. Wass, and M. J. E. Sternberg, “The Phyre2 web portal for protein modeling, prediction and analysis,” *Nat. Protoc.*, vol. 10, no. 6, pp. 845–858, May 2015.

[89] Y. Song, F. DiMaio, R. Y.-R. Wang, D. Kim, C. Miles, T. Brunette, J. Thompson, and D. Baker, “High-Resolution Comparative Modeling with RosettaCM,” *Structure*, vol. 21, no. 10, pp. 1735–1742, Oct. 2013.

[90] D. E. Kim, D. Chivian, and D. Baker, “Protein structure prediction and analysis using the Robetta server,” *Nucleic Acids Res.*, vol. 32, no. Web Server, pp. W526–W531, Jul. 2004.

[91] S. Raman, R. Vernon, J. Thompson, M. Tyka, R. Sadreyev, J. Pei, D. Kim, E. Kellogg, F. DiMaio, O. Lange, L. Kinch, W. Sheffler, B.-H. Kim, R. Das, N. V. Grishin, and D. Baker, “Structure prediction for CASP8 with all-atom refinement using Rosetta,” *Proteins Struct. Funct. Bioinforma.*, vol. 77, no. S9, pp. 89–99, 2009.

[92] J. Soding, “Protein homology detection by HMM-HMM comparison,” *Bioinformatics*, vol. 21, no. 7, pp. 951–960, Apr. 2005.

[93] M. Källberg, H. Wang, S. Wang, J. Peng, Z. Wang, H. Lu, and J. Xu, “Template-based protein structure modeling using the RaptorX web server,” *Nat. Protoc.*, vol. 7, no. 8, pp. 1511–1522, Jul. 2012.

[94] Y. Yang, E. Faraggi, H. Zhao, and Y. Zhou, “Improving protein fold recognition and template-based modeling by employing probabilistic-based matching between predicted one-dimensional structural properties of query and corresponding native properties of templates,” *Bioinformatics*, vol. 27, no. 15, pp. 2076–2082, Aug. 2011.

[95] M. Biasini, S. Bienert, A. Waterhouse, K. Arnold, G. Studer, T. Schmidt, F. Kiefer, T. G. Cassarino, M. Bertoni, L. Bordoli, and T. Schwede, “SWISS-MODEL: modelling protein tertiary and quaternary structure using evolutionary information,” *Nucleic Acids Res.*, vol. 42, no. W1, pp. W252–W258, Jul. 2014.

[96] K. Arnold, L. Bordoli, J. Kopp, and T. Schwede, “The SWISS-MODEL workspace: a web-based environment for protein structure homology modelling,” *Bioinformatics*, vol. 22, no. 2, pp. 195–201, Jan. 2006.

[97] L. Bordoli, F. Kiefer, K. Arnold, P. Benkert, J. Battey, and T. Schwede, “Protein structure homology modeling using SWISS-MODEL workspace,” *Nat. Protoc.*, vol. 4, no. 1, pp. 1–13, Dec. 2008.

[98] M. Remmert, A. Biegert, A. Hauser, and J. Söding, “HHblits: lightning-fast iterative protein sequence searching by HMM-HMM alignment,” *Nat. Methods*, vol. 9, no. 2, pp. 173–175, Dec. 2011.

[99] N. Guex and M. C. Peitsch, “SWISS-MODEL and the Swiss-Pdb Viewer: An environment for comparative protein modeling,” *Electrophoresis*, vol. 18, no. 15, pp. 2714–2723, 1997.

[100] A. A. Vaguine, J. Richelle, and S. J. Wodak, “SFCHECK : a unified set of procedures for evaluating the quality of macromolecular structure-factor data and their agreement with the atomic model,” *Acta Crystallogr. Sect. D Biol. Crystallogr.*, vol. 55, no. 1, pp. 191–205, Jan. 1999.

[101] “Validation & Deposition Services,” *RCSB PDB*. [Online]. Available: http://validate.rcsb.org/.

[102] “The Structure Analysis and Verification Server version 4,” *UCLA-DOE LAB*. [Online]. Available: http://services.mbi.ucla.edu/SAVES/.

[103] R. A. Laskowski, M. W. MacArthur, D. S. Moss, and J. M. Thornton, “PROCHECK: a program to check the stereochemical quality of protein structures,” *J. Appl. Crystallogr.*, vol. 26, no. 2, pp. 283–291, Apr. 1993.

[104] R. W. W. Hooft, G. Vriend, C. Sander, and E. E. Abola, “Errors in protein structures,” *Nature*, vol. 381, no. 6580, pp. 272–272, May 1996.

[105] C. Colovos and T. O. Yeates, “Verification of protein structures: Patterns of nonbonded atomic interactions,” *Protein Sci.*, vol. 2, no. 9, pp. 1511–1519, Sep. 1993.

[106] R. Lüthy, J. U. Bowie, and D. Eisenberg, “Assessment of protein models with three-dimensional profiles,” *Nature*, vol. 356, no. 6364, pp. 83–85, Mar. 1992.

[107] J. Bowie, R. Luthy, and D. Eisenberg, “A method to identify protein sequences that fold into a known three-dimensional structure,” *Science (80-.).*, vol. 253, no. 5016, pp. 164–170, Jul. 1991.

[108] J. Pontius, J. Richelle, and S. J. Wodak, “Deviations from Standard Atomic Volumes as a Quality Measure for Protein Crystal Structures,” *J. Mol. Biol.*, vol. 264, no. 1, pp. 121–136, Nov. 1996.

[109] P. Benkert, M. Kunzli, and T. Schwede, “QMEAN server for protein model quality estimation,” *Nucleic Acids Res.*, vol. 37, no. Web Server, pp. W510–W514, Jul. 2009.

[110] P. Benkert, M. Biasini, and T. Schwede, “Toward the estimation of the absolute quality of individual protein structure models,” *Bioinformatics*, vol. 27, no. 3, pp. 343–350, Feb. 2011.

[111] E. F. Pettersen, T. D. Goddard, C. C. Huang, G. S. Couch, D. M. Greenblatt, E. C. Meng, and T. E. Ferrin, “UCSF Chimera?A visualization system for exploratory research and analysis,” *J. Comput. Chem.*, vol. 25, no. 13, pp. 1605–1612, Oct. 2004.

[112] J. Wang, W. Wang, P. A. Kollman, and D. A. Case, “Automatic atom type and bond type perception in molecular mechanical calculations,” *J. Mol. Graph. Model.*, vol. 25, no. 2, pp. 247–260, Oct. 2006.

[113] J. Wang, R. M. Wolf, J. W. Caldwell, P. A. Kollman, and D. A. Case, “Development and testing of a general amber force field,” *J. Comput. Chem.*, vol. 25, no. 9, pp. 1157–1174, Jul. 2004.

[114] D. Kozakov, D. Beglov, T. Bohnuud, S. E. Mottarella, B. Xia, D. R. Hall, and S. Vajda, “How good is automated protein docking?,” *Proteins Struct. Funct. Bioinforma.*, vol. 81, no. 12, pp. 2159–2166, Dec. 2013.

[115] D. Kozakov, R. Brenke, S. R. Comeau, and S. Vajda, “PIPER: An FFT-based protein docking program with pairwise potentials,” *Proteins Struct. Funct. Bioinforma.*, vol. 65, no. 2, pp. 392–406, Aug. 2006.

[116] S. R. Comeau, D. W. Gatchell, S. Vajda, and C. J. Camacho, “ClusPro: an automated docking and discrimination method for the prediction of protein complexes,” *Bioinformatics*, vol. 20, no. 1, pp. 45–50, Jan. 2004.

[117] S. R. Comeau, D. W. Gatchell, S. Vajda, and C. J. Camacho, “ClusPro: a fully automated algorithm for protein-protein docking,” *Nucleic Acids Res.*, vol. 32, no. Web Server, pp. W96–W99, Jul. 2004.

[118] “NZYDNA Ladder III MB04401.” pp. NZYtech– genes & enzymes, 2014.

[119] “Low Molecular Weight (LMW) Protein Marker MB08201.” pp. NZYtech– genes & enzymes ,2014.

[120] O. Trott and A. J. Olson, “AutoDock Vina: Improving the speed and accuracy of docking with a new scoring function, efficient optimization, and multithreading,” *J. Comput. Chem.*, vol. 31, no. 2, pp. 455–461, 2010.

[121] A. Loupas, “Research rotation II RaBBit (Radiation Biology and Biophysics phD program.” FCT-UNL, 2015.

[122] U. K. LAEMMLI, “Cleavage of Structural Proteins during the Assembly of the Head of Bacteriophage T4,” *Nature*, vol. 227, no. 5259, pp. 680–685, Aug. 1970.

8 . Annex

8.1 Dps protein sequence

The sequence of *P. nautica* Dps wild-type is the following:

MGKNFIGLDTDKTQKLADALNELLSNYQIFYMNVRGYHWNIKGDNFFELHAKFEELYDDLLLKID
EIAERVLTLGHRPAHAYSTYIEKSEVPERKDVSDGKEAVGNIVESFGLIAKQRGLLNLAGEAEDE
GTVALMSDYISQQEKTVWMYRSYLGQ

8.2 Transformation of competent cells

Genotype of competent cells:

E. coli BL21(DE3) with genotype F^{-} ompT gal dcm lon hsdSB(rB- mB-) λ(DE3 *lacI lacUV5-T7 gene 1 ind1 sam7 nin5])

E. coli NZ5γ with genotype fhuA2Δ(argF-lacZ)U169 phoA glnV44 Φ80 Δ(lacZ)M15 gyrA96 recA1 relA1 endA1 thi-1 hsdR17

Transformation of E. coli NZ5 BL21(DE3) Protocol[69], [70]

1. Thaw competent cells on ice. Gently mix cells;

2. To determine the transformation efficiency, add 2 µL (0.02 ng) of control plasmid DNA to one tube containing 100 µL competent cells. Gently tap tube to mix;

3. Add 5 to 10 µL of the plasmid DNA (0.2 to 50 ng DNA) to the competent cells. Gently tap tubes to mix;

5. Incubate cells on ice for 30 minutes;

6. Heat-shock cells for 40 seconds in a 42 °C water bath; do not shake;

7. Place on ice for 2 minutes;

8. Add 0.9 mL room temperature LB medium;

9. Shake at 225 rpm (37 °C) for 1 h;

10. Spread 50 to 150 µL of cells transformed with competent cells control plasmid on LB agar plates containing 100 µg/mL ampicillin;

11. Incubate overnight at 37 °C.

8.3 Nzytech plasmid DNA miniprep protocol[71]

1. Harvest bacterial cells: Pellet 1-5 mL of an *E. coli* LB culture for 30 s. Discard supernatant. Remove as much media as possible.;

2. Cell lysis: Re-suspend cell pellet in 500 µL Buffer A1 by vigorous vortexing. Add 500 µL of Buffer A2 and mix gently by inverting the tube for 6-8 times. Incubate at room temperature for a maximum of 4 min. Do not vortex. Add 600 µL Buffer A3. Mix gently by inverting the tube for 6-8 times;

3. Clarification of lysate: Centrifuge for 10 min at room temperature;

4. Bind DNA: Place Nzytech spin column in a 2 mL collecting tube and load the supernatant from step 3 onto the column. Centrifuge for 1 min at 11,000 xg. Discard flow-through;

5. Wash silica membrane: Add 500 µL of Buffer AY onto the column. Centrifuge for 1 min. Discard flow-through. Add 600 µL of Buffer A4. Centrifuge for 1 min. Discard flow-through;

6. Dry silica membrane: Re-insert the Nzytech spin column into the empty 2 mL collecting tube and centrifuge for 2 min;

7. Elute highly pure DNA: Place the dried Nzytech spin column into a clean 1.5 mL microcentrifuge tube and add 30 µL of Buffer AE. Incubate 1 min at room temperature. Centrifuge for 1 min. Repeat this step to increase the yield. Store the purified DNA at -20 °C.

8.4 Agarose gel electrophoresis for DNA analysis

First, dissolve 0.8% agarose (Nzytech) in 1% of TEA Buffer 1x (40 mM Tris, 20 mM acetate, pH 8.0, 1 mM EDTA) and pour to the gel tray introducing the combs. Let sit at room temperature for approximately 30 min, until completely solidified,

Place the agarose gel into the electrophoretic unit (Bio-rad Mini®PROTEAN Tetra System) and fill it with TEA buffer 1x until the gel is covered. Molecular weight marker (NZYDNA Ladder III, Nzytech – Figura 43) and DNA samples are prepared with 1:1 (in volume) sample buffer (Nzytech), and carefully loaded into the wells.

Connect the power source (Electrophoresis Power Supply – 301, GE Healthcare) to the electrodes and set 80 V for 1 h 30 min (time for dye line run 80% of the way down the gel).

After electrophoretic separation, the agarose gel is stained on SYBER Safe solution (Invitrogen) for 30-45 min. For gel visualization and recording a Gel Logic 1000, Imaging System (Kodak) with a transiluminator Safe Imager (Invitrogen) is used.

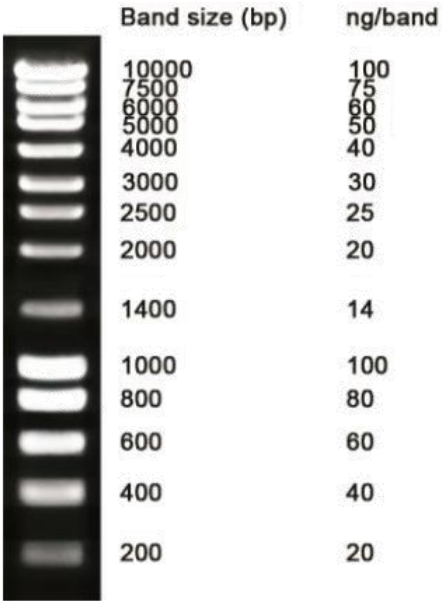

Figure 43 - NZYDNA Ladder III (Nzytech) molecular weight marker. 5 µL of marker were electrophoresed in a 1% (w/v) agarose gel. The gel was buffered with 1xTAE (v/v) and stained with GreenSafe Premium. [118]

8.5 SDS-PAGE for protein analysis

The polyacrylamide gels are prepared accordingly to the Laemmli method using solutions described in tables 15 and 16.[122]

First the resolving gel solution is poured into the stacking gels. After the resolving gel polymerization, butanol is removed and stacking gel is poured. The combs must be set for the wells formation and setup is set until the gel is polymerized.

The gel is removed from the support and set on the electrophoresis unit. Pour the running buffer and apply the Low Molecular weight marker (Figure 44) and protein sample to the wells. For start the running, fill the unit with running buffer, close it and connect the power source (Electrophoresis Power Supply – 301, GE Healthcare) to the electrodes. Set the voltage to 120 mV until the dye line pass the stacking gel and change for 90 mV.

At the end the gel is stained for 20 min and bleached overnight. The gel is photographed in a Gel Logic 1000 Imaging System.

Table 13 – Composition and preparation of buffers, staining and bleaching SDS-PAGE. solutions.

Solution	Composition	Quantity	Obs.
Running Buffer	Tris-Base 0.25 M, Glicine 1.92 M, SDS 10% H2O	30.3 g 144.1 g 10 g Until 1 L	pH 8.3 dilute 1:10 before use
Sample Buffer	Tris-HCl 0.5 M pH 6.8, SDS 10%, B- mercaptoetanol, Glicerol Bromofenol blue	5 mL 8 mL 1 mL 2 mL 4 mg	Total volume: 20 mL
Staining solution	Blue Comassie R-250 Glacial acid acetic Metanol H_2O	1 g 15 mL 90 mL Until 200 mL	
Bleached solution	Acid acetic Metanol H_2O	75 mL 450 mL Until 1L	

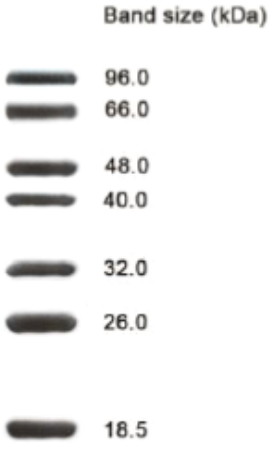

Figure 44- Electrophoretic profile of the low molecular weight (LMW) protein marker from Nzytech stained with Comassie Brilliant Blue. The gel was loaded with 5 µL of LMW standard per lane on a 14% Tris-glicine SDS-PAGE.[119]

Table 14 – Preparation of a 12.5% polyacrylamide gel for SDS-PAGE analysis.

Solutions	Staking gel 5% acrilamide	Loading gel 12.5% acrilamide
Tris-HCl 2.5 M, pH 8.8	-	0.75 mL
Tris-HCl 0.5 M, pH 6.8	0.45 mL	-
Acrlamide-bisacrilamide 30% (37.5:1)	0.3 mL	2.08 mL
SDS 10%	0.018 mL	0.05 mL
H20	0.94 mL	2.1 mL
PSA 10%	13.5 µL	38 µL
TEMED	2 µL	2.5 µL

8.6 WHATCHECK number code

1 Missing unit cell information
2 Missing symmetry information
3 Rounded coordinates detected
4 Valine nomenclature
5 Threonine nomenclature
6 Isoleucine nomenclature
7 Leucine nomenclature
8 Arginine nomenclature
9 Tyrosine convention problem
10 Phenylalanine convention problem
11 Aspartic acid torsion conventions
12 Glutamic acid torsion conventions
13 Heavy atom naming problem
14 Chirality
15 Improper dihedral angle distribution
16 Chain names
17 Weights checked
18 No missing atoms detected
19 OXT check
20 Extra C-terminal groups found
21 All bond lengths
22 Bond length variability
23 Directionality in bond lengths and X-ray cell

24 Unusual bond angles
25 Normal bond angle variability
26 Side chain planarity
27 Atoms connected to aromatic rings
28 PRO puckering amplitude
29 Unusual PRO puckering phases
30 Torsion angle evaluation shows unusual residues
31 Backbone torsion angle evaluation shows unusual conformations
32 Ramachandran Z-score
33 Omega angles too tightly restrained
34 chi-1/chi-2 angle correlation Z-score
35 #36 #37 #38 Ramachandran plot
39 Inside/Outside residue distribution normal
40 #41 #42 #43 Inside/Outside RMS Z-score plot
44 Secondary structure
45 Abnormally short interatomic distances
46 Second generation packing environment
47 No series of residues with abnormal new packing environment
48 Structural average packing Z-score OK
49 #50 #51 #52 Second generation quality Z-score plot
53 Backbone oxygen evaluation
54 Unusual rotamers
55 Unusual backbone conformations
56 Backbone conformation Z-score OK
57 Average B-factor problem
58 #59 #60 #61 # B-factor plot
62 HIS, ASN, GLN side chain flips
63 Histidine type assignments
64 Buried unsatisfied hydrogen bond donors
65 Buried unsatisfied hydrogen bond acceptors

8.7 Cluspro score functions

$E=0.40E_{rep}+-0.40E_{att}+600E_{elec}+1.00E_{DARS}$ (balanced)

$E=0.40E_{rep}+-0.40E_{att}+1200E_{elec}+1.00E_{DARS}$ (electrostatic-favored)

$E=0.40E_{rep}+-0.40E_{att}+600E_{elec}+2.00E_{DARS}$(hydrophobic-favored)

$E=0.40E_{rep}+-0.10E_{att}+600E_{elec}+0.00E_{DARS}$(vdw+elec)

E_{rep} - potential of repulsive energies; E_{att} - potential attractive energies; E_{elec} - electrostatical potential; E_{DARS} - (Decoys As the Reference State) potential

8.8 Mössbauer spectra results

Table 15- Percentage of ferric and ferrous specie calculated by WMOSS© v 1.51 (See co.) software for each Mossbauer spectra.

Time	Spectra	%Ferric	%Ferrous
0	WT0	0.998	0.002
	Q14E0	0.996	0.004
	15N0	1	0
2	WT2	0.895	0.105
	Q14E2	0.958	0.042
	15N2	0.922	0.078
12	WT12	0.897	0.103
	Q14E12	0.938	0.062
	15N12	0.902	0.098
30	WT30	0.779	0.221
	Q14E30	0.721	0.279
	15N30	0.820	0.180
50	WT50	0.672	0.328
	Q14E50	0.532	0.468
	15N50	0.758	0.242
100	WT100	0.504	0.496
	Q14E100	0.317	0.683
	15N100	0.568	0.432
200	WT200	0.200	0.800
	Q14E200	0.099	0.901
	15N200	0.243	0.757

8.9 Predict protein

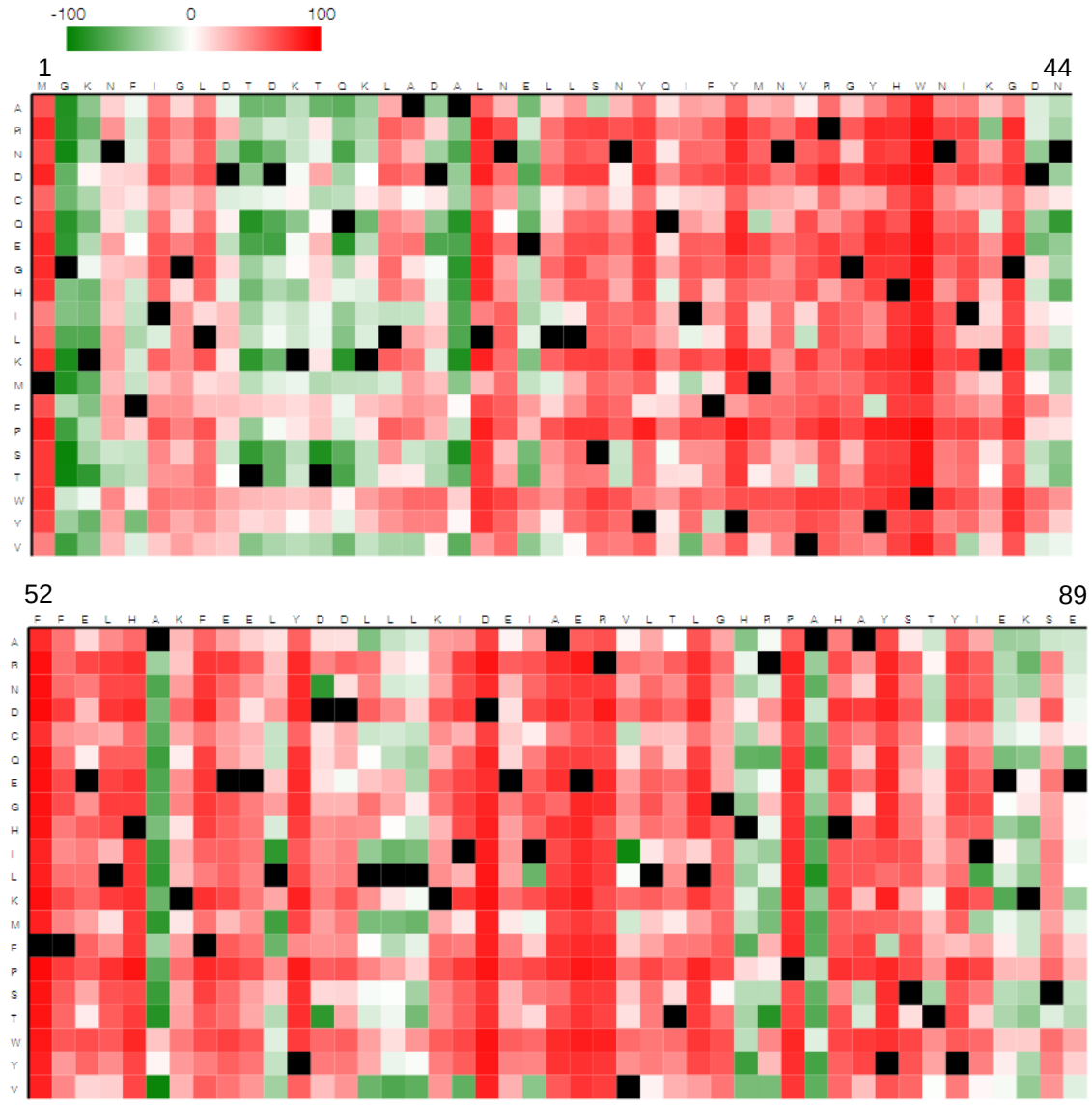

Figure 45- Predict protein server result for point mutation effect from aminoacid 1 to 89 of Dps sequence. Each column corresponds to a Dps aminoacid. The columns are organized accordingly to the sequence of Dps protein.

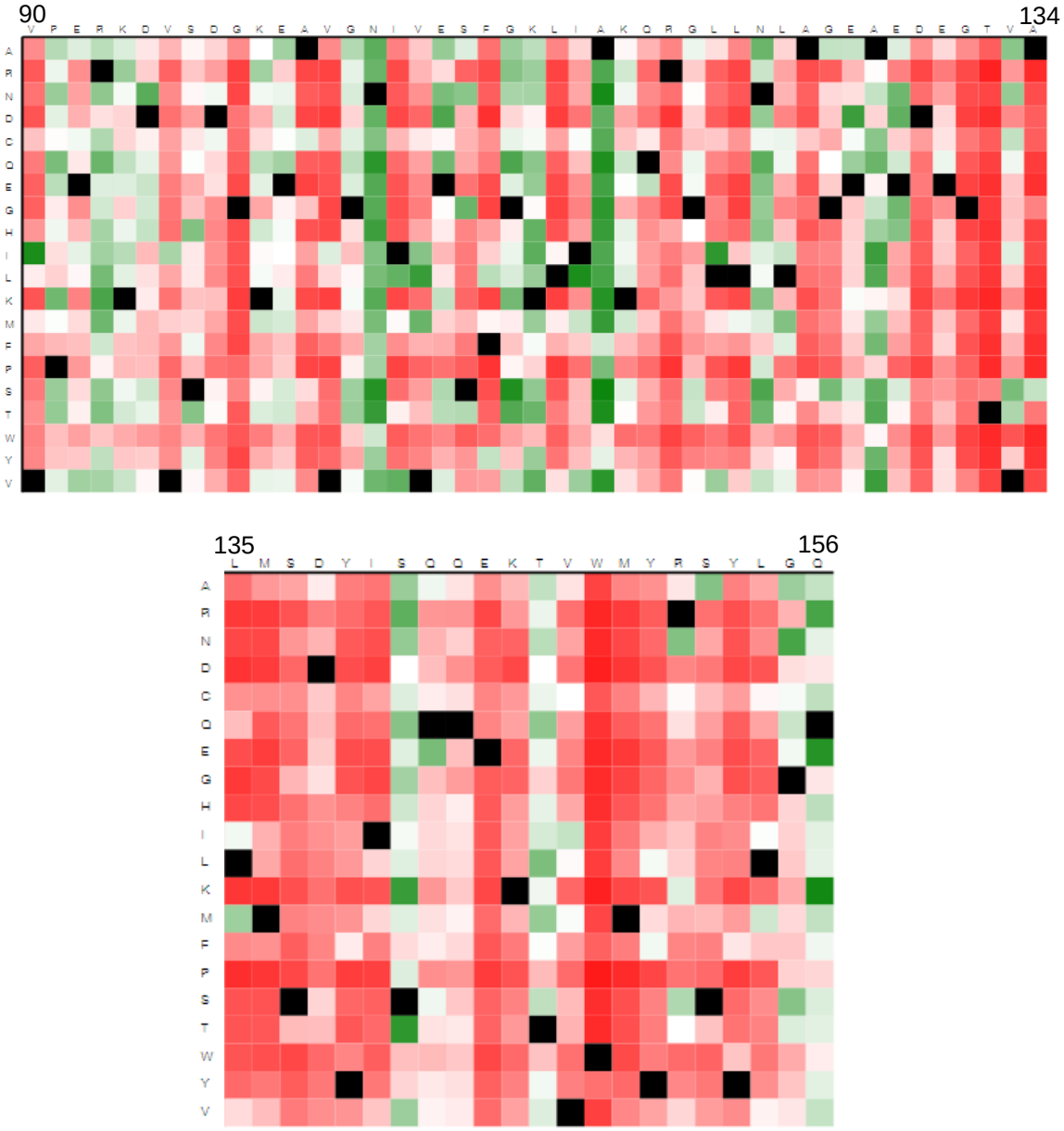

Figure 46- Predict protein server result for point mutation effect from aminoacid 90 to 156 of Dps sequence. Each column corresponds to a Dps aminoacid. The columns are organized accordingly to the sequence of Dps protein.